

COLORIMETRIC SENSOR ARRAYS:
DEVELOPMENT AND APPLICATION TO ART CONSERVATION

BY

MARIA KATHLEEN LAGASSE

DISSERTATION

Submitted in partial fulfillment of the requirements
for the degree of Doctor of Philosophy in Chemistry
in the Graduate College of the
University of Illinois at Urbana-Champaign, 2016

Urbana, Illinois

Doctoral Committee:

Professor Kenneth S. Suslick, Chair
Professor Alexander Scheeline
Professor Catherine J. Murphy
Professor Alison R. Fout

Abstract

This dissertation explores the optimization, development and application of cost-effective, compact colorimetric arrays, focusing specially on their use in the cultural heritage and art conservation communities. One of Society's most important cultural responsibilities is the preservation of the past for the future. The surest way to protect a cultural heritage material from damage is to control the environment in which it is displayed. While there are a number of monitoring techniques available, there are many limitations (e.g., cost, portability) or problems (e.g., lack of desired sensitivity, time consuming, need for laboratory personnel). The Suslick Group believes we have a technology that could become a valuable tool for museum professionals.

Chapter 1 provides a comprehensive review of destructive air pollutants in conservation environments and the existing methods to monitor and quantify them. This chapter serves to lay the groundwork for why low-cost, convenient colorimetric array technology is crucial. **Chapter 2** optimizes the performance of portable colorimetric arrays, establishing them as an invaluable technology for museums and art conservationists. **Chapter 3** provides a quantitative, side-by-side comparison of two standard colorimetric detection methods—RGB imaging and full reflectance spectrophotometry—in order to further improve the performance of these arrays. Finally, **Chapter 4** applies the concepts learned in this work and in past work from the Suslick group, to extend with new sensor chemistry and detection techniques, our already sensitive optoelectronic nose technology into one capable of detecting museum pollutants in a variety of environments. In addition, this chapter addresses a study that uses this technology, through an exciting collaboration with the Getty Conservation Institute and the Walt Disney Animation Research Library, to make trial experiments in the monitoring of artwork from the Walt Disney Animation Research Library exhibition in Beijing, “Drawn from Life: the Art of Disney Animation Studios”, in order to monitor pollutant exposure both during shipping and during exhibition.

Acknowledgments

As I come to the culmination of my doctoral thesis work I would be remiss if I didn't acknowledge those of you who have supported me through the various challenges an endeavor such as this throws at you.

I would like to begin with my advisor and Principal Investigator, Dr. Kenneth Suslick. When I began my career at the University of Illinois I was looking to grow my skills and to challenge myself. When I met Ken, I knew he was just the type of mentor to do that. The obvious things to thank him for are accepting me into his lab group, funding me so I could engage in research, and for fulfilling his general duties as an advisor. There are, however, things that go unseen that I believe have brought me to the place I am today. So for that I thank you. Thank you for challenging me to become a better scientist and, at times, letting me know that the path I was taking was wrong and to turn around immediately. In the times when I was in need of the advice of a man with great experience and expertise, you were there with words of guidance and wisdom. Also, when I needed encouragement and a laugh or two, well you didn't disappoint there either. For those unseen day to day interactions I am truly grateful.

Next, I would like to thank one of my other committee members who I spent a significant amount of time with collaborating on my first graduate level research project, Dr. Alexander Scheeline. I admit, in the beginning I was a bit overwhelmed and in need of a confidant who would say it like it was and set me straight if needed. Thank you for reassuring me that this program was made for me to succeed and not break me. Your advice, optimism and integrity are something to be admired. I would also like to thank my other committee members Dr. Alison Fout and Dr. Catherine Murphy for their commitment to my success and guidance through this process that is only outdone by their inspiration as women in chemistry.

There is not enough room on these pages to express my gratitude to the ones in my academic career that have molded and shaped me with their advice, discussions, and most importantly their friendship! I am truly lucky to call you colleagues. The great times and knowledge that you have afforded me will stay with me long into my career. Out of fear of missing someone I would just like to acknowledge the Suslick sensing group (Jackie, Rankin, Jon Askim, Zheng Li, Yinan Zhang, Frank Schwandt, Qifan Zhang, and Kimberly Lundberg).

As for the project that has not only been a great challenge but has brought me great joy and once in a lifetime experiences, I would like to thank my collaborators, Kristen McCormick from the Walt Disney Animation Research Library and Herant Khanjian and Michael Schilling from the Getty Conservation Institute. My time spent working with you and Ken on this project has been an invaluable asset to my growth as a scientist and awakened a passion in me for art conservation.

There is also a group of gentlemen who need a great deal of praise and they are the men from the Machine Shop: particularly Mike "Hodge" Harland and Tom Wilson. Your passion for your job and willingness to pass it on to me is an appreciated bit of expertise that for which you should have probably gotten hazard pay. Thank you to the wonderful women of the IMP office: Connie Knight, Beth Myler, Theresa Struss, Karen Watson, and Stacy Dudzinski. Aside from the consultation on the tremendous (and diverse) amount of knowledge you have all accrued; when I needed a break, some laughs or a sweet treat to get me through a long day, you were there!

To the Department of Education GAANN Fellowship, Department of Chemistry, J&M Witt Fellowship, your financial backing laid the foundation to allow me to be able to execute my research to date. I cannot in 1 million acknowledgements thank you enough times for your support.

Now, for those of you outside of the UIUC Chemistry community. I will start with my non-science friends (who knew you could have those). Your ability to get my mind off of science when I needed just a bit of a break was amazing and I thank you. To My Sisters on the U of I Hockey team thank you for the laughs, stress relief, and support through all of these crazy times. To my family, a list that would be longer than my thesis if my grandmother had anything to do with it, I'd just like to say that the support you've provided throughout my schooling has been above and beyond and I am happy to share this accomplishment with you. A very special thank you to my two biggest supporters, my Mother and father, Mark and Mary-Kay LaGasse. Your selflessness and support is the reason I am here today. I see the best of myself in you guys and there will never be enough words to say what your sacrifices signify in my life so I will simply say I am forever grateful. And lastly, I'd like to thank my fiancé Jon Durney. At the risk of sounding cliché, you have been my rock through all of this, willing to do anything to make my life even the tiniest bit easier. I don't think I could have completed this process without you.

Table of Contents

Chapter 1: Gaseous Pollutants in Museum Environments and Monitoring Methods	1
1.1 Introduction	1
1.2 Gaseous Pollutants in Museum Environments	2
1.3 Damage by Gaseous Pollutants to Museum Objects.....	6
1.4 Air Quality Monitoring Technologies.....	9
1.5 Summary and Outlook	20
1.6 References	21
Chapter 2: Colorimetric Sensor Arrays: Interplay of Geometry, Substrate, and Immobilization	35
2.1 Introduction	35
2.2 Experimental	37
2.3 Results and Discussion.....	44
2.4 Conclusions	52
2.5 References	53
Chapter 3: RGB versus Spectrophotometric Systems for Detection of Colorimetric Sensor Arrays.....	56
3.1 Introduction	56
3.2 Materials and Methods	60
3.3 Experimental Procedure	61
3.4 Data Processing and Analysis	63
3.5 Results and Discussion.....	64
3.6 Conclusions and Outlook	69
3.7 References	69
Chapter 4: Colorimetric Sensor Arrays: Development and Application to Art Conservation ..	72
4.1 Introduction	72
4.2 Equilibrium Real Time Imaging vs. Cumulative (Dosimetric) Sensor Arrays	73
4.3 Development of 1 st Generation Cumulative (Dosimetric) Sensor Array	76
4.4 Experimental	81
4.5 Field Testing of 1 st Generation Colorimetric Sensor Array	105
4.6 Conclusions and Outlook	120
4.7 References	121

Chapter 1:

Gaseous Pollutants in Museum Environments and Monitoring Methods

1.1 Introduction

One of Society's most important cultural responsibilities is the preservation of the past for the future.¹ The surest way to protect a cultural heritage material from damage is to control the environment in which it is displayed; both physical and chemical factors, such as light, temperature, relative humidity and so on, can have a profound impact on these objects' lifetime.²⁻³ The discussion of slowing the deterioration of museum materials through environmental control was formally initiated in a book written by Garry Thomson in 1978 titled *The Museum Environment* which presented current knowledge on the behavior of different materials under various conditions and provided suggested control measures based on the climate of the region.⁴⁻⁵ Thus, focus was shifted from restoration to prevention and the field of preventive conservation as it is known today was born.⁶

The intention of preventive conservation is to extend an object's lifetime by studying environmental conditions (micro-climate, microbiology and chemical pollution) around a work of art. Only within the last 40 years, has research in this area begun to concentrate on the effects of environmental pollutants on the materials used in works of art. The likely reasons for this are, in most cases, it is difficult to attribute deterioration to any specific factor over another and the processes used to study the effects of aging (i.e., in accelerated environments) can be biased.³ However, with the emergence of new studies in preventive conservation that reveal the deteriorative effects of low levels of specific pollutants and improved, more sensitive, and portable detection methods, excluding or reducing these agents in the museum environments has become an important focus in the field. In order to continue this progress, it is necessary to develop cost effective techniques for continuous control and monitoring of pollutants for a large number of locations and microenvironments (e.g., every display case in a museum) at the low levels needed to minimize the effects of aging.

1.2 Gaseous Pollutants in Museum Environments

Air pollution is not just a public health or global climate concern but a cultural heritage one as well. A review written by Thomson in 1965⁷ was the first of its kind to specifically target conservation chemists in a discussion about the fundamentals of air pollution and atmospheric chemistry as it affects museum materials.⁸ Pollutants relevant to cultural heritage can be broadly grouped into two categories: (1) outdoor generated pollutants and (2) indoor generated pollutants.⁹ **Figure 1.1** gives a general overview of relevant indoor and outdoor pollutants and their emission sources.

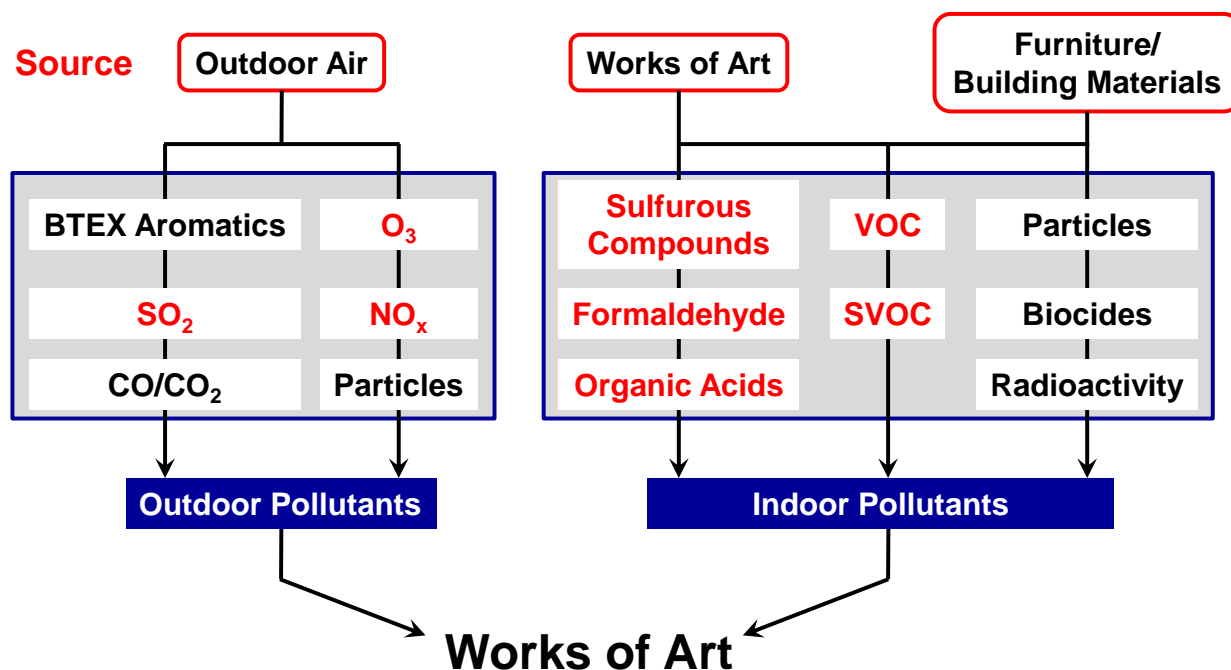


Figure 1.1 General overview of relevant indoor and outdoor pollutants and their emission sources (SVOC: semi-volatile organic compounds, BTEX: benzene, toluene, ethylbenzene, xylenes). Adapted from Schieweck (2005).¹⁰

The content of outdoor air is dependent on a number of factors including climate, geography, number and type of industries and vehicles, fuels used and so on. The environment in naturally ventilated buildings (oftentimes seen with historical buildings) can be strongly affected by local climatic conditions causing indoor concentrations to come close to outdoor levels.¹¹⁻¹³ For this reason, when possible, many cultural heritage institutions employ heating, ventilation

and air conditioning (HVAC) systems proven capable of reducing indoor levels to as low as 5% of the outdoor concentration levels.¹⁴ However, HVAC systems themselves can sometimes do more harm than good with the production of air motions that cause heat and vapor variations which can increase the deposition rate of gaseous and particulate pollutants thus affecting bio deterioration.^{2,4} These issues can be intensified with the increase of human traffic throughout the museum so that a more powerful HVAC system is required which can agitate the microclimate and increase indoor pollution and particulate matter (i.e., dust, cloth fibers and spores).

Pollutants generated indoors arise from a number of sources including paints, boards, carpets, and cleaning and heating processes with some of the most important sources being those with the greatest surface area (i.e., floor coverings, sealants, varnishes, wallpaper).⁶ Works of art themselves can even be a source for these harmful pollutants⁵ or have the capacity to absorb these pollutants (shown with textiles, wallboard, artwork) that upon heating can then become a potential source for the pollutants they've trapped.⁸⁻⁹

The destruction pollutants are capable of inflicting depends on a number of factors including the nature of the source materials, the efficiency of air exchange systems, the material composition of the pieces being stored and/or displayed, and where the at-risk piece(s) are relative to the pollutant source. There are two types of environments in museums: (1) macroenvironments (i.e., galleries, storage areas) that typically contain several cubic meters of air and (2) microenvironments (i.e., storage cabinets, display cases) that contain less than a cubic meter of air. Several museums,¹¹⁻¹⁵ including the Getty Conservation Institute,¹⁶⁻¹⁷ have done investigations on air quality throughout the museum environment; it has been found that macroenvironments contain the lowest pollutant level, likely due to improved ventilation, high air circulation and dilution effects. Microenvironments on the other hand have limited air exchange allowing pollutants to build up over time (**Figure 1.2**), which can become especially problematic when museum enclosures are made with inappropriate materials.¹⁸ Several groups have even worked with modeling to simulate these effects in the various environments throughout the museum.¹⁹⁻²¹

There are a number of challenges associated with establishing target guidelines for pollutant exposure of pieces of art. One of the biggest challenges is the presence of synergistic effects where the risk of damage from a mixture of pollutants may not simply be the additive effect of the materials risk to each pollutant and can depend on a number of factors including

reactivity of the pollutants present with each other, relative humidity (RH) and light, and even the history of the artifact.²²⁻²⁶ This makes the establishment of all-encompassing exposure standards nearly impossible and recommendations for acceptable levels are constantly in flux. While there are a number of standards and methods used to define these limits (e.g., acceptable risk concentration, background level, dosage),²⁶⁻²⁸ the more widely accepted set of standards are based on results from studies conducted by Tétreault that establish some threshold standards based on both theoretical and experimental data.²⁹ This system sets Low-Observable Adverse Effects Levels (LOAEL), an adaptation of a system used in the pharmaceutical and pesticide industry, which sets No Observable Adverse Effects Levels (NOAEL). This system classifies pollutants based on the susceptibility of materials (setting lower limits for “sensitive” materials or those that are at a higher risk from a particular pollutant) and the length of exposure. While this system of standards is a starting point, there is still room to improve as more sensitive analytical procedures appropriate for museum applications continue to be developed.

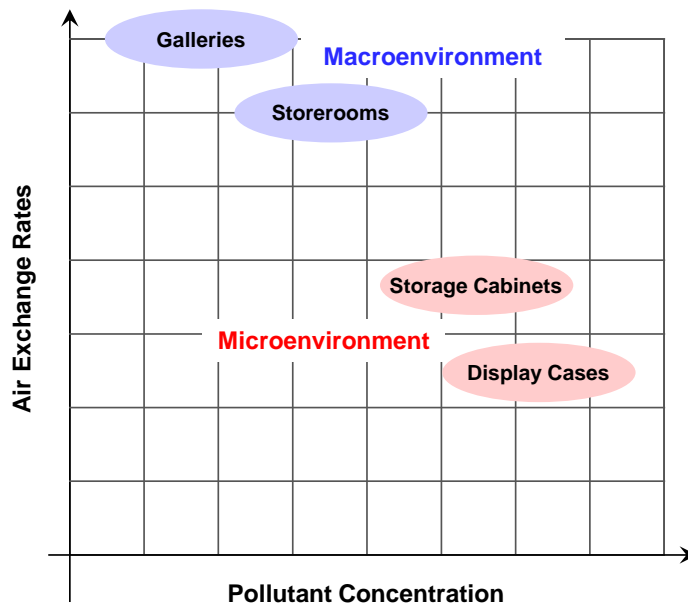


Figure 1.2 Diagram representing the relationship between air exchange in macroenvironments (i.e., galleries and storerooms) and microenvironments (i.e., storage cabinets and display cases) present in a museum. Environments with higher air exchange rates (i.e., macroenvironments) effectively reduce accumulation of pollutants.¹⁷

Table 1.1 presents the most important pollutants found inside museums together with their suggested concentration limits for cultural materials versus humans. Clear from this table,

permissible exposure levels for cultural heritage objects are often well below those acceptable for humans. In fact, the acceptable pollutant concentration limits for sensitive artwork are generally at or below the few ppb regime; for many pollutants, this is only ~1% of the permissible exposure limits (NIOSH PEL required for humans). This is because, unlike humans exposed to damaging pollutants, art objects have no possibility of internal healing; in addition, individuals have a finite lifetime, whereas the desired life of cultural artifacts is indefinite. Alternatively, there are a number of pollutants that are important to human health concerns (e.g., carbon monoxide, lighter noble and trace gases, heavy metals) that have no adverse effects on cultural heritage materials. In fact, most volatile organic chemicals (VOCs) do not damage collections.

Table 1.1 Important pollutants found inside museums and suggested concentration limits for cultural heritage materials and humans.^{17, 30}

Major Pollutants	Suggested Limits^a for Sensitive Materials (ppb)	Suggested Limits for other Collection Materials (ppb)	Permissible Exposure Limits for Humans (ppb)
NO ₂	0.05-2.6	2-10	5,000
O ₃	<0.5	0.5-5	1,000
SO ₂	0.04-0.4	0.4-2	5,000
H ₂ S	<0.1	<0.1	20,000
acetic acid	<5	40-280	10,000
formic acid	<5	5-20	5,000
formaldehyde	<0.1-5	10-20	750
acetaldehyde	<1-20		200,000

^a Sensitive materials are those that are at risk from the particular gaseous pollutant.

At a low degree of air pollution, the direct effect of pollutants on materials with historical or cultural value are rather limited, but over longer periods, more severe effects such as surface alteration, color change or even weakening of the material may occur. Therefore it is important that vulnerable materials are kept under controlled conditions free from air pollution.

1.3 Damage by Gaseous Pollutants to Museum Objects

Documentation of exhibit conditions altering objects on display can be traced back to the 19th century with reports from Loftus St. George Byne (1899)³¹ describing corrosion of shell specimens, Russell Abney and Church (1856-1888)³²⁻³³ regarding the action of light on water colors, and A. Richardson (1888)³⁴ on the interplay of light and moisture on the decomposition of pigments. Since then there have been a large number of well documented cases with recent attention paid to cultural material damage at pollutant levels typically found in museum environments.^{17, 27, 35}

The means by which an object can be harmed in a museum environment are highly varied and oftentimes complex, with much about the mechanism of the deterioration and corrosion process left to discover. However, certain materials are at greater risk in the presence of a given pollutant or class of pollutants over others (**Table 1.2**). This section will deal with the damaging action of the main museum pollutants described in **Table 1.1**. **Figure 1.3** provides images that illustrate the kind of damage that can result. There are, however, a variety of other pollutants that can inflict damage on materials as well (e.g., hydrogen peroxide discoloration of photographic materials, alkaline aerosol discoloration and soiling of paintings and organic coatings, ammonia tarnishing of metals).

The gaseous pollutants that provide the greatest risk are acidic pollutants (i.e., acetic acid, formic acid) or those that can be converted to their acidic analogs under ambient temperature and humidity (i.e., formaldehyde,³⁶⁻³⁸ acetaldehyde,³⁹ nitrogen dioxide and sulfur dioxide, which hydrolyze to nitric and sulfuric acid in the presence of moisture^{7, 40}). Acidic substances are corrosive and can affect the surface of materials such as metals (**Figure 1.3a**) and calcareous stone (**Figure 1.3d**). In addition, they can cause hydrolysis in cellulose materials (**Figure 1.3e**): a process of decomposition by moisture, which induces the breakage of molecular chains (loss of strength) and eventually the disintegration of the affected material.⁴¹

Table 1.2 Main museum pollutant sources and effects on cultural heritage materials.³⁵

Major Pollutants	Outdoor	Indoor	Materials at Risk	Damage Observed
Nitrogen Dioxide (NO₂)	lightning, automotive/engine sources, fuel combustion for energy and industry	gas heating/cooking, cellulose nitrate degradation, pyroxylin-coated bookbinding cloth degradation	metals, photographic materials, dyes, textiles	fading, color change (textile dyes, reduced tensile strength, soiling (textiles))
Ozone (O₃)	light, high temperature	electrical equipment, electrostatic particle filters, physical wear	metals (e.g., Silver), rubber, photographic and other paper-based materials, textiles, dye-based colorants	corrosion (metals), cracking (rubber, plastics), embrittlement (paper, textiles), fading (dyes), color change
Sulfur dioxide (SO₂)	combustion fossil fuels*, moisture, sunlight, air, salt, microorganisms	acidic materials introduced in manufacturing, physical wear, washing	metals, stone, leather, paper-based materials, textiles, paints, organic coatings, photographic materials	tarnish/corrosion (metals), discoloration, soiling (paintings, organic coatings); embrittlement (paper), microblemishes, 'sulfiding' (photographic materials); reduced tensile strength, soiling (textiles);
Hydrogen Sulfide (H₂S)	bioeffluents (i.e., volcanoes, marine algae), combustion fossil fuels*, moisture, sunlight, air, salt	construction materials, wool and other textiles, dyes; vulcanized rubber degradation	metals (e.g., silver, copper, bronze), paints, photographic materials	tarnish/corrosion (metals), discoloration, soiling (paintings); microblemishes, 'sulfiding' (photographic materials)
Acetic Acid (CH₃COOH)		construction materials, degradation cellulose acetate	metals (especially lead), calcareous materials, mineralogical specimens, paper, textiles, pigments	tarnish/corrosion, salt formation, embrittlement, fading
Formic Acid (HCOOH)	oxidation of formaldehyde	oxidation of formaldehyde, drying oil paints, alkyd resin paints, wood products	metals (i.e., lead, zinc, copper alloys), calcareous materials, mineralogical specimens	tarnish/corrosion, salt formation
Formaldehyde (HCOH)		construction materials, textiles, surface finishes, paints, coatings and adhesives	proteins	denaturing/cross-linking?

Oxidants (i.e., ozone, nitrogen dioxide and peroxyacetyl nitrate-PAN) are also a problem in museum environments.⁴²⁻⁴⁴ Not only are they capable of oxidative cleavage of double bonds present in the carbon chains of most organic materials, which results in fading of dyes and pigments, but they also form acids in organic materials. Once formed, these acids cause cross-links in the molecular structure of the materials, making them brittle. Pyrite decay (“fossil disease”), where the sulfide containing pyrite present in many fossil materials is oxidized to sulfur dioxide, is another concern as it results in yellow and white efflorescence, crazing, and sometimes total destruction (**Figure 1.3c**).⁴⁵

Sulfurous compounds in both their reduced (hydrogen sulfide, carbonyl sulfide) and oxidized (sulfur dioxide) state are particularly hazardous to metals, leading to tarnishing and black sulfide copper corrosion which has the appearance of mold, among other things (**Figure 1.3b**).⁴⁶⁻⁴⁷ Sulfur dioxide and subsequently sulfuric acid has been implicated in the fading and color conversion of dyes, pigments and colorants. The synergistic action of light and sulfur dioxide has been found to degrade textile fibers and, in the presence of water and nitrogen dioxide, can cause serious damage to un-buffered paper.⁴⁸⁻⁴⁹

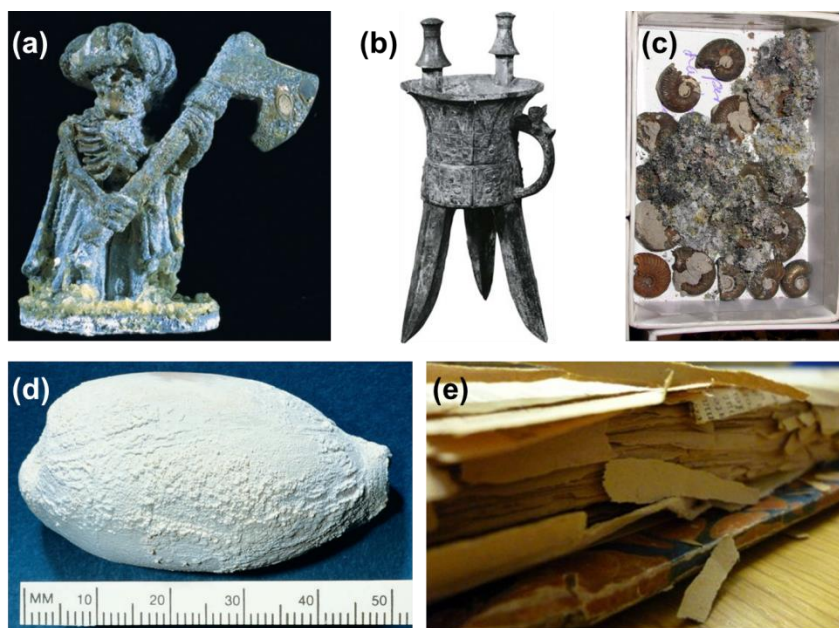


Figure 1.3 (a) Miniature lead statue of a warrior covered in white basic lead carbonate corrosion product representative of acetic acid pollution.¹⁷ (b) Bronze object from the Shang Dynasty showing signs of black sulfide copper corrosion.⁵⁰ (c) Card box of small fossilized Jurassic ammonites covered in grey and yellow powder characteristic of pyrite decay.⁵¹ (d) Shell with distinctive bumps of Byne’s disease.¹⁷ (e) Volume of British regional papers deteriorated by the environment.⁵²

Quantifying the level of ‘damage’ when it comes to heritage science is somewhat more ambiguous than in other fields. The fact is, not all ‘change’ in heritage materials can be considered ‘damage’ as the value of this change must play a role in the decision whether a given change constitutes damage (e.g., copper roofs turning green can add dignity to a building, a bullet hole in an 18th century admiral’s jacket caused by musket fire adds to historic value).⁵³ Damage functions are often discussed as a means of quantifying unacceptable change (where there is a permanent and noticeable loss in value or potential) to heritage materials and to decouple the impact of the numerous agents of change on a given material in an effort to prioritize remediation needs.⁵⁴ However, in an effort to decouple change from damage it is useful to split damage functions into a value function and a ‘dose-response function’. Value functions are empirically deduced depending on factors such as whether an object can be handled or transported safely (where an accumulation of damage can become a higher priority) or the type of object, value, stakeholder group or collection involved. Dose-response functions are experimentally deduced and take into account the action of agents of change or stressors (e.g., pollutants, light, relative humidity) on a given object.

It is in this multi-parametric dose-response function where this field is lacking. While monitoring of the environment (at least temperature and relative humidity) is performed routinely, monitoring the dosage of other stressors (i.e., pollutants, particulate matter) is not. As discussed earlier, damage to an object can result from synergistic effects so a damage function is of little use if information on the dose experienced by an object or site is not linked with the damage sustained by the same object. In order to use these damage functions more broadly in the field of heritage science and better assist in the development of environment-based guidelines and standards, it’s necessary to establish methods for continuous monitoring of individual objects in a variety of environments in an effort to provide the dosimetric information necessary to build these functions. **Section 1.4** will address the technology currently available for monitoring dosage of gaseous pollutants in museum environments.

1.4 Air Quality Monitoring Technologies

There are a number of important considerations that need to be made when determining the mitigation strategy necessary for a given situation. First, is the identity of pollutants and their

sources and second, is the sensitivity of the material involved to the pollutants present. As discussed in **Section 1.2**, certain materials are at greater risk in the presence of some pollutants over others (i.e., organic materials in the presence of oxidants, metals in the presence of sulfides). Therefore, it is necessary to have methods to not only test the environment in which these objects are stored but also the materials used to house them (important in pinpointing the source of the problematic contaminant). Materials that give off even low levels of a contaminant can be problematic because these contaminants can build up over time in closed microenvironments. This sometimes requires analytical methods with long sampling times which can make it difficult to produce reliable results.

Environmental testing methods can be divided into two general categories: active and passive. Active sampling, sometimes called dynamic sampling, relies on the use of a pump or aspirator to pull a known volume of gas over a known sampling time through a properly designed container filled with solid or liquid sorbent where trapped analytes can be later released and determined. While these devices tend to be very sensitive and precise, they also require sophisticated analytical methods (i.e., GC-MS^{10, 55-56}, HPLC⁵⁷⁻⁵⁸, FTIR⁵⁹, SPME⁶⁰), a power source, and can be costly. Passive sampling, which relies on the principles of mass transport where air is allowed to diffuse through a gas layer or permeate through a semipermeable membrane to a trapping medium, is often the more economical choice, especially when long sampling time is required for a large number of environments.⁶¹ While active sampling may be necessary in some more sophisticated situations and remains the primary method by which other methods are validated, passive sampling has seen significant advances since the 1970s and is oftentimes the more appropriate economical choice.

1.4.1 Passive Monitoring Systems

There are two classes of passive sampling devices (PSDs): (1) laboratory analyzed, where sample collection uses a passive device that is sent to a laboratory to be analyzed, and (2) direct reading, where the sample is collected on adsorbents and the results are indicated, usually by a color change, on the detector.¹⁷ While direct reading devices provide almost instantaneous results, they are not always as informative as laboratory-analyzed devices, whose results typically take one to three weeks to receive. The advantages of laboratory analyzed systems,

however, are greater accuracy, precision and specificity. Both device types can be either qualitative (indicate potential risk) or quantitative (provide actual pollutant concentrations).

Table 1.3 gives a summary of the advantages and disadvantages of each type of PSD.

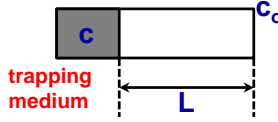
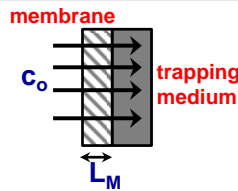
Table 1.3 Summary of advantages and disadvantage of the different passive sampling devices.¹⁷

Device Type	Advantages	Disadvantages
Direct-Reading PSD	Lower expense per unit Easy to use No analysis required Immediate results	High detection limits Lower accuracy Subject to interferences
Laboratory-analyzed PSD	High accuracy High precision Pollutant specific Low detection limits	Higher cost per unit Complexity of use Results not immediate (weeks)
Qualitative PSD	Indicates overall corrosivity of the environment	Nonspecific: reacts with classes of pollutants, not necessarily individual gases
Quantitative PSD	Pollutant specific	Complex methodology

1.4.2 Principles for Passive Sampling

PSDs can be as simple as a reactive metal coupon or pH indicator paper or as complex as a specially designed enclosure with an active surface or trap behind a diffusion barrier. In all cases, diffusion is the mechanism by which gaseous pollutants travel to the active surface. Without the use of a pump, as is used in active devices, sampling can be as much as three orders of magnitude slower with pollutant transport to the active surface governed by Fick's 1st law of diffusion.⁶¹ A detailed description of the operation of passive samplers can be found in the available literature;⁶¹⁻⁶³ a brief summary is compiled in **Table 1.4**.

Table 1.4 Summary of principles of operation for diffusive and permeation passive samplers.⁶¹

	Diffusive passive sampler	Permeation passive sampler
Phenomenon used for mass transport of analytes	Diffusion	Permeation
Principle of operation		
Equation for rate of transport of analyte to trapping medium (U)	$U = \frac{DA}{L}(C_0 - C)$	$U = SA \frac{(\rho_1 - \rho_2)}{L_M}$
Equation for amount of analyte retained in trapping medium (M) for given exposure time (t)	$M = \frac{DA}{L} C_0 t$	$M = \frac{SA(\rho_1 - \rho_2)}{L_M} C_0 t$
Expression for rate of collection of analyte from air	$\frac{DA}{L} = (SR)$	$k = \frac{L_M}{SA(\rho_1 - \rho_2)}$
Equation for analyte concentration in air during the sampler exposure (C)	$C = \frac{(SR)M}{t}$	$C = \frac{kM}{t}$

c: analyte concentration in trapping medium (mol/cm); **c_o:** ambient concentration of analyte (mol/cm);
L: length of diffusion zone (cm); **L_M:** membrane thickness (cm); **D:** diffusion coefficient (cm²/min);
A: cross section of diffusion zone (cm²); **S:** analyte permeability coefficient dependent on membrane material (cm²/min); **(ρ₁-ρ₂):** difference in partial pressure of the analyte on both sides of the membrane;
SR: sampling rate (cm³/min); **k:** calibration constant (cm³/min)

One difficulty with the development of PSDs is that calibration of these devices can be rather cumbersome. Typically two approaches, theoretical and experimental, are used. The theoretical approach is based on literature findings of the diffusion or permeability coefficient of the analyte and Henry's law constant (in the case of permeation sampling), and the accurate determination of geometrical parameters of the sampler. The experimental approach requires the experimental determination of sampling rate and calibration constants based on the exposure of the sampler to standard gas mixtures in exposure chambers at different temperatures. The latter method suffers from the lack of standards for how exposure experiments are performed.

The choice of an appropriate trapping medium is an important one as there are a number of factors based on physicochemical interactions (i.e., strength of interactions between trapping medium and analyte, sorption and release of analytes for final determination) and practicality (i.e., cost, ease of use) that influence the samplers efficiency.⁶¹ There are a variety of trapping media out there, some react chemically with the pollutant to form a new compound that is measured to determine the concentration of the original pollutants while others are used to selectively trap particular pollutants to be later released by solvent extraction or thermal

desorption to be analyzed by analytical techniques such as GC-MS or HPLC. For a more in depth description of trapping media used for these types of analyses see the literature.⁶³⁻⁶⁵

In general, passive samplers operate in one of two different accumulation regimes (**Figure 1.4**). The first type, termed linear uptake passive samplers, work in the kinetic or time-integrative uptake region where uptake of the analyte is linearly proportional to the difference in chemical potential of the contaminant in the receiving phase. In this type of passive sampling it is assumed that the rate of mass transfer or sampling rate remains constant throughout the duration of sampling and the relationship between the concentration of target analytes in the sample matrix and the amount of analyte extracted is linear. The second, called equilibrium passive samplers, work in the equilibrium uptake region and are described by a partition coefficient between the receiving phase and the sample matrix.⁶⁶

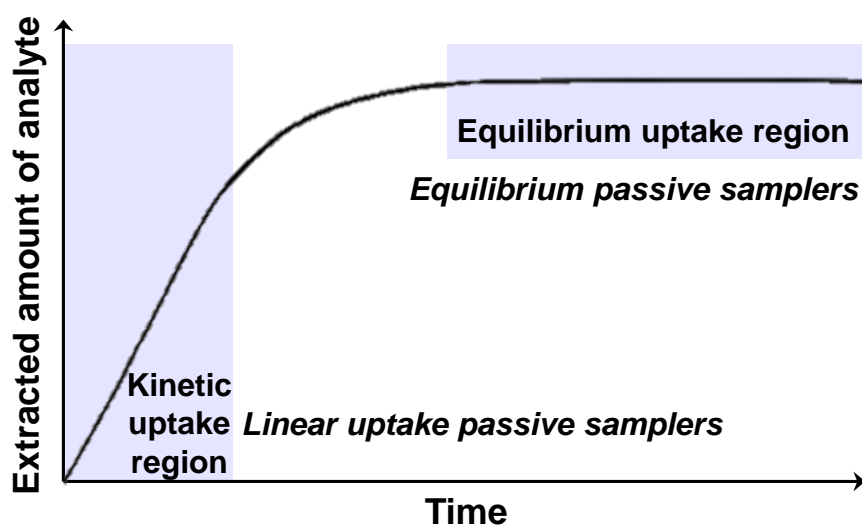


Figure 1.4 Analyte mass uptake profile in passive sampling devices (PSDs). Two different accumulation regimes (i.e., kinetic uptake and equilibrium uptake region) of PSDs can be distinguished. Reproduced with permission of Springer⁶⁶

Linear uptake passive samplers are the primary sampler type used in the cultural heritage sciences. The concentration output for these samplers is given as a time-weighted average (TWA) and is therefore a function of the amount of pollutant measured, sampling rate and exposure time. This value gives a snapshot of total pollutant exposure over a given period of time and will not be able to distinguish cyclic fluctuations within that time period. Readings can be volumetric measurements (ppm or ppb) or gravimetric measurements ($\text{mg}\cdot\text{m}^{-3}$ or $\mu\text{g}\cdot\text{m}^{-3}$).

Volumetric units (popular in U.S. manufactured products) are temperature and pressure dependent, whereas gravimetric units (popular in products from the European Union) are not.

1.4.3 Direct-reading PSDs: Qualitative

These passive devices are simply an active surface, which is usually nonspecific, that reacts with pollutants in the environment. While not ideal, even the collection's housing (e.g., screws, hinges) can act as qualitative indicators of conditions in a microenvironment. These devices are useful as prescreening tools to identify an area with high pollutant concentration that needs further monitoring. This screening capability allows curators to save more sophisticated and expensive devices for those instances that truly require it.

One popular device, simply called a coupon, uses a small square of standardized material representative of the collection at risk that can be examined for the markers of deterioration (e.g., basic lead carbonate present as a white powder on a lead coupon). It is important that these materials be more susceptible to damage than the objects in the collection, so that damage is seen on the coupon before it occurs in the object. While the use of a polished metal foil (i.e., silver, copper and lead) is typical, other materials such as paper, shell or glass can be used as well.⁶⁷ These coupons can be mounted on a support and discreetly placed in a microenvironment (e.g., display case) and monitored periodically (**Figure 1.5a**) or used under accelerated conditions to screen materials to be used with collections (Oddy test).⁶⁸⁻⁶⁹ Results of this test allow for general deductions regarding the pollutants present in an environment depending on the type of metal used. For instance, copper corrosion is often associated with chlorides, sulfides and acidic pollutants such as nitrogen dioxide and sulfur dioxide, while silver reacts with reduced sulfides (i.e., carbonyl sulfide and hydrogen sulfide), and lead reacts with organic carbonyl pollutants and other acidic pollutants. The rate of corrosion of these coupons can be indicative of the severity of the air quality problem but is very subjective and can only be used to indicate whether an environment is low, moderate, or high risk. If desired, scrapings from the surface of the metal can be sent to a laboratory to be analyzed to determine the composition of the corrosion products.

Dye-coated test strips, like a universal pH paper, are also a very popular low cost pre-screening tool for the presence of acids. There are semi-quantitative versions of these tests

available (i.e., ozone test sticks) where color change is proportional to pollutant concentration and can be compared to a reference scale for a semi-quantitative reading of pollutant concentration (**Figure 1.5b**). There are also commercially available (i.e., A-D Strips)⁷⁰ test strips and other variations have been investigated in the literature.⁷¹⁻⁷³

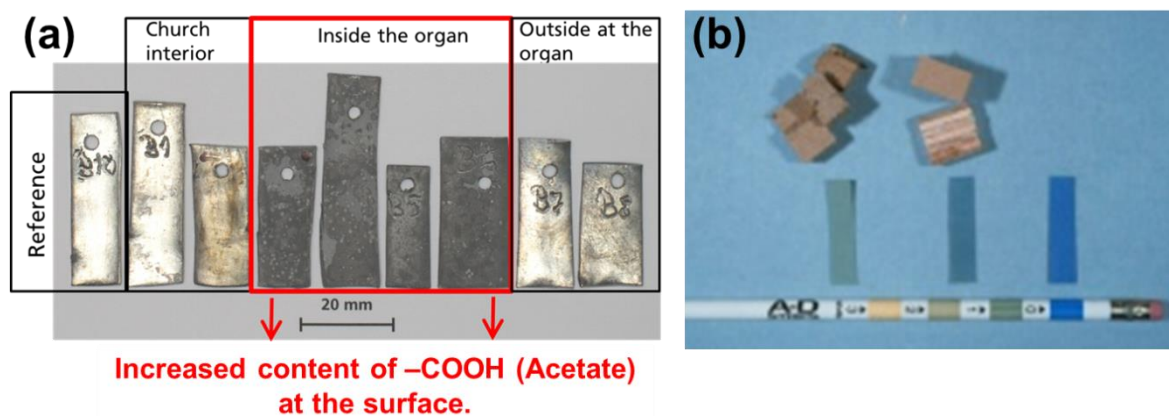


Figure 1.5 (a) Results from corrosion test using lead coupons to determine climatic conditions inside a church and organ where lead organ pipes showed signs of extensive corrosion. It was determined that corrosion resulted from acetic acid emitted from wood and adhesive materials used in organ construction materials, changes in heating conditions, and humidity.⁷⁴ **(b)** Results from acid testing on wood samples using A-D test strips and reference scale.⁷⁵

1.4.4 Direct-reading PSDs: Quantitative

Quantitative direct-reading devices, just as their name suggests, indicate the presence of a specific pollutant and the amount or concentration present. A color change, proportional to the pollutant's concentration, is used as an indicator. This color can then be compared to a reference scale from the manufacturer.

One example, colorimetric diffusion tubes, consist of glass tubes (**Figure 1.6a**) filled with reagent that changes color upon reacting with a specific pollutant; these tubes are labeled with calibrated graduations along the length of the tube that are used to indicate concentration in ppm·hr. The concentration can be calculated by dividing the reading at the line where color change ends by the sampling time (in hours). While the reagents used in these tubes are chosen to react with a specific pollutant they oftentimes react with classes of pollutants and are, therefore, susceptible to interference from pollutants within the same class of compounds (e.g., a tube used for formaldehyde detections will change color in the presence of other aldehydes). In

addition to susceptibility to interferences, they have relatively high detection limits (80-1200 ppb), and only give a semi-quantitative reading. These tubes can be found commercially through companies such as Draeger and Gastec™.

Badges (**Figure 1.6b&c**) are another example that involves open-face sampling (i.e., without a diffusion barrier). These are typically used in a work environment to indicate exposure of personnel to harmful volatiles but methods for converting this technology for use in a museum environment have been explored.⁷⁶ However, for general use, these sensors indicate exposure levels above 100 ppb for a specific pollutant and require some airflow in order to achieve accurate results.⁷⁷

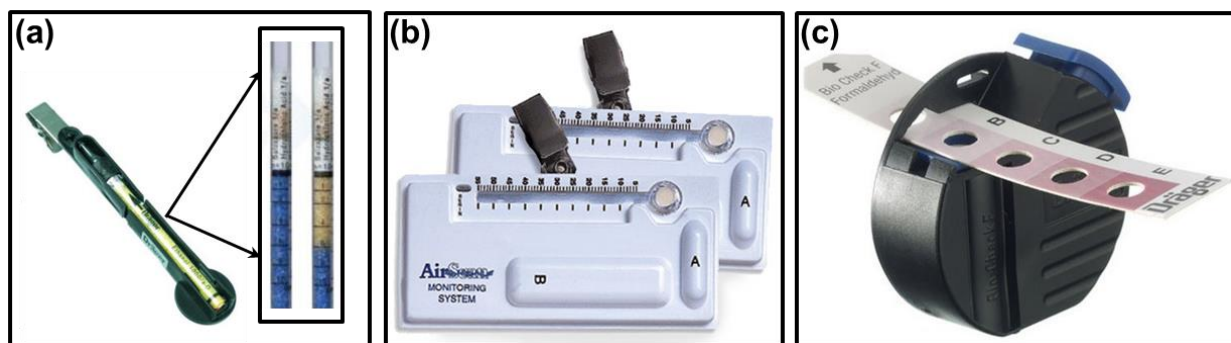


Figure 1.6 (a) Draeger long-term color diffusion tube consisting of a glass tube filled with reagent that changes color upon reacting with a specific pollutant; these tubes are labeled with calibrated graduations along the length of the tube used to indicate concentration in ppm-hr (detection range: varies depending on pollutant).⁷⁸ (b) Airscan badges for monitoring pollutant levels given as a time-weighted average (detection range: varies depending on pollutant).⁷⁹ (c) Draeger bio-check enzyme-based formaldehyde test kit. An ampule is broken to expose to active ingredients and color change indicates formaldehyde level (detection range: 0.05-0.1 ppm).⁸⁰

Another newer generation of sensors, called impact sensors, are intended especially for evaluating the cooperative effects of environmental agents and to simulate some specific phenomenon (e.g., discoloration, corrosion) an object on display may undergo.⁸¹ In general, these sensors incorporate a sacrificial material that reacts similarly to the collection to be surveyed and, upon reaction with the environment, give an easily measurable change in a specific property. This measured change represents, semi-quantitatively, the overall impact of the environment by a given agent (or agents). In a way these sensors are a more complex version of the qualitative direct-reading coupons but, combined with an analytical device, removes the human element from the measurement and improves sensitivity. Impact sensors can be extremely

helpful in identifying the presence of complex deterioration phenomena (i.e., synergistic effects) or risk situations that might require more detailed investigation. This category of sensors is highly varied and uses a large number of analytical techniques and materials to measure a variety of environmental stressors such as light, humidity, and pollutants. A thorough review of these sensors can be found in the literature;⁸¹ a few select devices are described below.

The first is a corrosion sensor based on an electric resistance technique (**Figure 1.7**).⁸²⁻⁸⁴ This sensor, developed in the framework of the EC CORRLOG Project, consists of a thin metallic track of the material of interest (e.g., silver, copper, nickel) deposited on a non-conductive substrate. Each metal track consists of a shielded area (reference) and an exposed area; the change in resistance between these two areas is used to measure corrosion rates in selected environments. This change in electrical resistance results from changes in metal thickness due to corrosion, so track thickness determines both sensitivity and service life of the device: while thinner tracks have higher sensitivity, this also means the device will have a shorter service life. The corrosion depth (CD) can be calculated from the equation below:

$$CD = t_{sens,i} \left[\frac{R_{ref}(T)R_{sens,i}(T_i)}{R_{sens}(T)R_{ref,i}(T_i)} \right]$$

where $t_{sens,i}$ is the initial (i) thickness, R_{ref} is the resistance measurement of the shielded (reference) track, R_{sens} is the resistance measurement of the exposed track and T is temperature.



Figure 1.7 AirCorr corrosion monitoring system equipped with 50 nm thick silver and copper metal tracks. The device output gives corrosion loss (CD) in metal thickness and when these values are plotted versus time, the slope of the curve corresponds to corrosion rate.⁸²

The second device is based on piezoelectric quartz crystals (PQC) coated with materials of artistic interest (egg tempera, resin mastic varnishes).⁸⁵⁻⁸⁷ The working principle of PQC sensors is that its oscillation frequency depends on the mass of the coatings, and thus frequency is shifted after a modification in the film due to ageing and interaction with pollutants. This relationship is described by Sauerbrey's equation:

$$\Delta f = -\frac{2f_o^2}{A\sqrt{\rho_q\mu_q}}\Delta m$$

where f_o is the resonant frequency (Hz), A is the crystal area between the two electrodes (cm²), ρ_q is the density of quartz (2.648 g/cm³), μ_q is the shear modulus of quartz (2.947 x 10¹¹ g/cm s²) and Δm is the change in mass (g).

1.4.5 Laboratory-analyzed PSDs: Qualitative

Given the cost for a qualitative result, these types of devices are only used under special circumstances. As mentioned in **Section 1.4.3**, a metal coupon can be sent to a laboratory to get a more specific idea of the composition of pollutant exposure and there are some commercially available coupons intended for this specific purpose (i.e., Purafil Environmental Reactivity Coupons).

1.4.6 Laboratory-analyzed PSDs: Quantitative

There are a large number of quantitative passive sampling devices that require laboratory analysis, many of them adapted from their intended use in industrial applications to museum monitoring. Many of these devices require longer exposure times or have high detection limits since permissible exposure limits for museum objects are significantly lower than those required for humans. In general, these devices fall into two categories: open-path (Palmer) diffusion tubes and badges.

Open-path (Palmer) diffusion tubes (**Figure 1.8**) are based on a housing design developed in the 1970s by Palmer *et al.*⁸⁸ and variations on this design have been developed since then.⁸⁹ The basic Palmer sampler is made up of a 7.1 cm long tube made of Teflon or an

acrylic plastic, two airtight caps at each end (one to be removed immediately prior to sampling) and an active surface (e.g., chemically treated cellulose pad or stainless steel mesh). The static air in this tube acts as the diffusion barrier and the ratio of length to outer diameter (usually 1 cm) is critical in controlling the rate of diffusion. Due to the longer axial diffusion path and smaller cross sectional diffusion area, as compared to badge-type samplers, the uptake rate tends to be lower making them suitable for long-term exposure (i.e., months).⁹⁰ However, this extended sampling time also makes these tubes vulnerable to reaction product degradation and environmental effects such as air velocity, temperature, and humidity. While there are commercial tubes available that were originally intended for industrial use (i.e., Gradko Air Monitoring tubes, SKC 526 Series Formaldehyde Passive Sampler for Indoor Air Sampling), there has been some progress in the development of open-path diffusion tubes specifically for the conservation field.⁹¹ These samplers, however, are only able to detect reduced sulfides and organic acids at low concentrations (ppt and ppb, respectively).

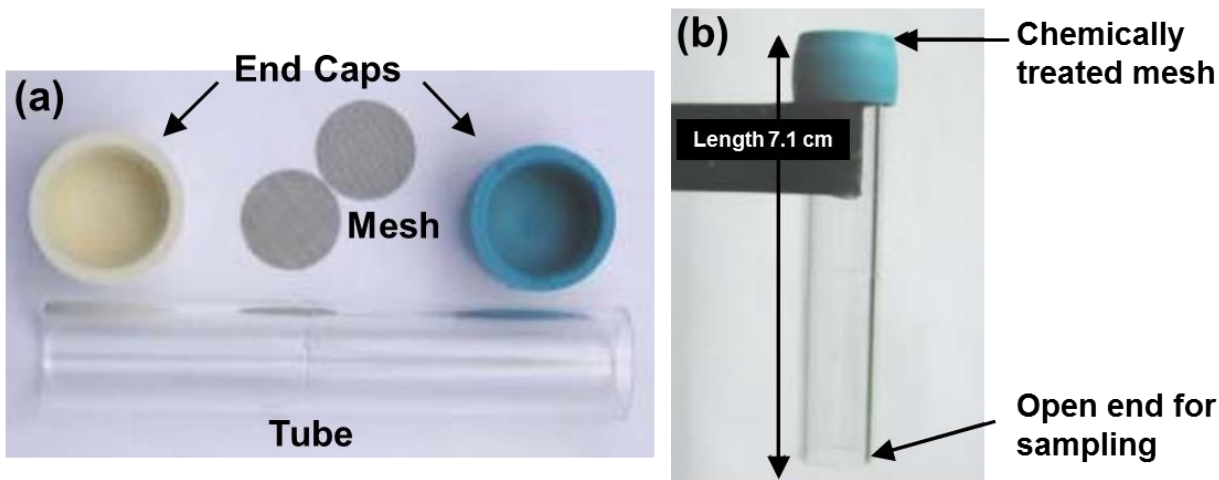


Figure 1.8 (a) Components of a typical Palme's diffusion tube. The basic Palmes sampler is made up of a 7.1 cm long tube made of Teflon or an acrylic plastic, two airtight caps at each end and an active surface (e.g., chemically treated cellulose pad or stainless steel mesh).⁹² **(b)** Palmes diffusion tube setup for sampling. The closed end contains the active surface and the open end, positioned facing downward, is for sampling.⁹²

Like quantitative direct-reading badges, quantitative badges that require laboratory analysis are meant to be personal monitors clipped to clothing. Typically, the active surface of these badges is enclosed in a plastic or Teflon housing with a diffusion barrier 1 mm to 1 cm

above the active surface. The badge-type samplers tend to have a higher uptake rate, over the diffusion tubes, due to the shorter diffusion path and larger diffusion area making them better suited for short term exposure.

1.5 Summary and Outlook

There are a number of agents of deterioration present in the museum environment that can wreak havoc on the priceless objects on display. It is at the interface of science and cultural heritage that advancements can be made to ensure a long lifetime for these objects. As this introduction has shown, the field of preventive conservation has made significant advancements in understanding the behavior of materials in the presence of environmental stressors and has made significant progress in the development of technologies to monitor these stressors so that proper mitigation strategies can be put into place.

This work will serve as an introduction to the cultural heritage community; a small, low cost colorimetric array technology that would be of inestimable value to museum professionals. **Chapter 2** will examine the factors that affect the performance of this technology (i.e., sensor geometry, immobilization method, and substrate) in an effort to optimize performance. **Chapter 3** examines two colorimetric detection methods (i.e., RGB imaging and full reflectance spectrophotometry) used to measure changes in the optical sensors of the array to serve as a quantitative comparison between the capabilities (i.e., limit of detection, signal to noise) of the two methods. **Chapter 4** presents a collaborative effort between the University of Illinois, the Getty Conservation Institute, and the Disney Animation Research Library (ARL) to develop a version of this technology suitable for monitoring museum pollutants and apply it as a passive sampling device for measuring air quality surrounding 8 pieces from Disney's animation archives during their journey from the Disney ARL to exhibitions in Beijing and then in Shanghai until their return 4 months later. The powerful potential of this technology to provide a portable, quantitative and cost effective method for monitoring low levels of pollutants in a large number of locations and microenvironments will also be discussed.

1.6 References

1. Whitmore, P. M.; Foundation, N. S., *Conservation Science Research: Activities, Needs, and Funding Opportunities ; a Report to the National Science Foundation*. 2005.
2. Camuffo, D.; Van Grieken, R.; Busse, H.-J.; Sturaro, G.; Valentino, A.; Bernardi, A.; Blades, N.; Shooter, D.; Gysels, K.; Deutsch, F.; Wieser, M.; Kim, O.; Ulrych, U., Environmental monitoring in four European museums. *Atmospheric Environment* **2001**, *35*, Supplement 1, S127-S140.
3. Brimblecombe, P., The balance of environmental factors attacking artifacts. *Durability and change: the science, responsibility and cost of sustaining cultural heritage*. Wiley, Chichester **1994**, 67-79.
4. Spolnik, Z.; Bencs, L.; Worobiec, A.; Kontozova, V.; van Grieken, R., Application of EDXRF and Thin Window EPMA for the Investigation of the Influence of Hot Air Heating on the Generation and Deposition of Particulate Matter. *Microchimica Acta* **2005**, *149* (1/2), 79-85.
5. Matsumura, M.; Eastop, D.; Gill, K., Monitoring emissions from cellulose nitrate and cellulose acetate costume accessories: An evaluation of ph indicator dyes on paper, cotton tape and cotton threads. *The Conservator* **2002**, *26* (1), 57-69.
6. Mølhave, L., Indoor air pollution due to organic gases and vapours of solvents in building materials. *Environment International* **1982**, *8* (1), 117-127.
7. Thomson, G., Air pollution—a review for conservation chemists. *Studies in Conservation* **1965**, *10* (4), 147-167.
8. McAusland, J., Conservation and storage: prints, drawings and water-colours. *Manual of Curatorship: A Guide to Museum Practice* **2015**, 259.
9. Desauziers, V.; Bourdin, D.; Mocho, P.; Plaisance, H., Innovative tools and modeling methodology for impact prediction and assessment of the contribution of materials on indoor air quality. *Heritage Science* **2015**, *3* (1), 1-8.
10. Schieweck, A.; Lohrengel, B.; Siwinski, N.; Genning, C.; Salthammer, T., Organic and inorganic pollutants in storage rooms of the Lower Saxony State Museum Hanover, Germany. *Atmospheric Environment* **2005**, *39* (33), 6098-6108.
11. Schieweck, A.; Salthammer, T., Indoor air quality in passive-type museum showcases. *Journal of Cultural Heritage* **2011**, *12* (2), 205-213.

12. Krupińska, B.; Worobiec, A.; Rotondo, G. G.; Novaković, V.; Kontozova, V.; Ro, C.-U.; Van Grieken, R.; De Wael, K., Assessment of the air quality (NO₂, SO₂, O₃ and particulate matter) in the Plantin-Moretus Museum/Print Room in Antwerp, Belgium, in different seasons of the year. *Microchemical Journal* **2012**, *102*, 49-53.
13. Brimblecombe, P.; Blades, N.; Camuffo, D.; Sturaro, G.; Valentino, A.; Gysels, K.; Grieken, R.; Busse, H. J.; Kim, O.; Ulrych, U., The indoor environment of a modern museum building, the Sainsbury Centre for Visual Arts, Norwich, UK. *Indoor air* **1999**, *9* (3), 146-164.
14. Eremin, K.; Wilthew, P., Monitoring concentrations of organic gases within the National Museums of Scotland. *SSCR Journal* **1998**, *9* (1), 15-19.
15. Krupińska, B.; Van Grieken, R.; De Wael, K., Air quality monitoring in a museum for preventive conservation: Results of a three-year study in the Plantin-Moretus Museum in Antwerp, Belgium. *Microchemical Journal* **2013**, *110*, 350-360.
16. Grzywacz, C. M.; Tennent, N. H., Pollution monitoring in storage and display cabinets: carbonyl pollutant levels in relation to artifact deterioration. *Studies in Conservation* **1994**, *39* (sup2), 164-170.
17. Grzywacz, C. M., *Monitoring for gaseous pollutants in museum environments*. Getty Publications: 2006.
18. Tétreault, J.; Stamatopoulou, E., Determination of concentrations of acetic acid emitted from wood coatings in enclosures. *Studies in Conservation* **1997**, *42* (3), 141-156.
19. Cao, L. N.; Cao, J.; Lee, S.; Zhang, Y.; Tie, X., Numerical simulation of the micro environment in the Han Yang Mausoleum museum. *Aerosol and Air Quality Research* **2012**, *12*, 544-552.
20. Popovici, C.-G.; Hudişteanu, V. S., Numerical Simulation of HVAC System Functionality in a Sociocultural Building. *Procedia Technology* **2016**, *22*, 535-542.
21. Ryhl-Svendsen, M., Indoor air pollution in museums: prediction models and control strategies. *Studies in Conservation* **2006**, *51* (sup1), 27-41.
22. Katsanos, N.; De Santis, F.; Cordoba, A.; Roubani-Kalantzopoulou, F.; Pasella, D., Corrosive effects from the deposition of gaseous pollutants on surfaces of cultural and artistic value inside museums. *Journal of hazardous materials* **1999**, *64* (1), 21-36.
23. Bradley, S.; Thickett, D. In *The pollution problem in perspective*, Triennial meeting (12th), Lyon, 29 August-3 September 1999: preprints. Vol. 1, James & James: 1999; pp 8-13.

24. Johansson, L.-G., Synergistic effects of air pollutants on the atmospheric corrosion of metals and calcareous stones. *Marine Chemistry* **1990**, *30*, 113-122.
25. Klumpp, E.; Heitmann, H.; Schwuger, M., Synergistic effects between cationic surfactants and organic pollutants on clay minerals. *Colloids and Surfaces A: Physicochemical and Engineering Aspects* **1993**, *78*, 93-98.
26. Svensson, J. E.; Johansson, L. G., The synergistic effect of hydrogen sulfide and nitrogen dioxide on the atmospheric corrosion of zinc. *Journal of the Electrochemical Society* **1996**, *143* (1), 51-58.
27. Thomson, G., *The museum environment*. Elsevier: 2013.
28. Purafil, I., *Environmental Control for Museums, Libraries, and Archival Storage Areas*. Purafil, Inc.: Doraville, GA, 2004.
29. Tétreault, J., *Airborne pollutants in museums, galleries, and archives: risk assessment, control strategies, and preservation management*. Canadian Conservation Institute: 2003.
30. Lauwerys, R. R.; Hoet, P., *Industrial chemical exposure: guidelines for biological monitoring*. CRC Press: 2001.
31. Byne, L. S. G., The corrosion of shells in cabinets. *Journal of conchology* **1899**, *9* (6), 172-178 253-254.
32. Russell, W. J.; de Wiveleslie Abney, W., *Report to the Science and Art Department of the Committee of Council on Education on the Action of Light on Water Colours: Presented to Both Houses of Parliament by Command of Her Majesty*. HM Stationery Office: 1888.
33. Church, A. H., The Chemistry of Paints and Painting. In *The Chemistry of Paints and Painting*, Fourth Edition ed.; Seeley, Service&Co.: London, 1889; p 388.
34. Richardson, A., On the action of light on water colours. *British Association for the Advancement of Science. Report* **1888**, *58*, 641-642.
35. Hatchfield, P. B., *Pollutants in the museum environment: practical strategies for problem solving, exhibition and storage*. Archetype Publications: 2002.
36. Hatchfield, P.; Carpenter, J., Formaldehyde: How great is the danger to museum collections? **1987**.
37. Raychaudhuri, M. R.; Brimblecombe, P., Formaldehyde oxidation and lead corrosion. *Studies in Conservation* **2000**, *45* (4), 226-232.

38. Striegel, M. F., The effects of gas phase formaldehyde on selected inorganic materials found in museums. In *Objects Specialty Group Postprints 1991, Albuquerque, New Mexico*, American Institute for Conservation of Historic and Artistic Works: 1992; Vol. 1, pp 1-12.
39. Fenech, A.; Strlič, M.; Cigić, I. K.; Levart, A.; Gibson, L. T.; de Bruin, G.; Ntanos, K.; Kolar, J.; Cassar, M., Volatile aldehydes in libraries and archives. *Atmospheric Environment* **2010**, *44* (17), 2067-2073.
40. Salmon, L. G.; Cass, G. R., The fading of artists' colorants by exposure to atmospheric nitric acid. *Studies in Conservation* **1993**, *38* (2), 73-91.
41. Puls, J.; Wilson, S. A.; Hölter, D., Degradation of Cellulose Acetate-Based Materials: A Review. *Journal of Polymers and the Environment* **2010**, *19* (1), 152-165.
42. Druzik, J. R., Ozone: The intractable problem. *Los Angeles Times* **1985**.
43. Cass, G. R.; Nazaroff, W. W.; Tiller, C.; Whitmore, P. M., Protection of works of art from damage due to atmospheric ozone. *Atmospheric Environment. Part A. General Topics* **1991**, *25* (2), 441-451.
44. Graedel, T. E.; McGill, R., Degradation of materials in the atmosphere. *Environmental science & technology* **1986**, *20* (11), 1093-1100.
45. Oddy, W. A., The conservation of pyritic stone antiquities. *Studies in Conservation* **1977**, *22* (2), 68-72.
46. Brimblecombe, P.; Shooter, D.; Kaur, A., Wool and reduced sulphur gases in museum air. *Studies in Conservation* **1992**, *37* (1), 53-60.
47. Hjelm-Hansen, N., Cleaning and stabilization of sulphide-corroded bronzes. *Studies in Conservation* **1984**, *29* (1), 17-20.
48. Zeronian, S. H.; Alger, K. W.; Omaye, S. T., Reaction of Fabrics made from Synthetic Fibers to Air Contaminated with nitrogen dioxide, ozone, or sulfur dioxide. In *Proceedings of the Second International Clean Air Congress*, Beery, W. T., Ed. Academic Press: 1971; pp 468-476.
49. Havermans, J. B. G. A., *Environmental influences on the deterioration of paper*. TU Delft, Delft University of Technology: 1995.
50. Butts, A. copper processing *Encyclopedia Britannica. Encyclopedia Britannica Online*. [Online], 2016. <http://www.britannica.com/technology/copper-processing>.
51. Larkin, N. R., Pyrite Decay: cause and effect, prevention and cure. *NatSCA News* **2011**, *21*, 35-43.

52. Duffy, C., Read all about it #1 - What's in the Papers? In *Collection Care Blog*, 2013.
53. Ashley-Smith, J., *Risk assessment for object conservation*. Routledge: 2013.
54. Strlič, M.; Thickett, D.; Taylor, J.; Cassar, M., Damage functions in heritage science. *Studies in Conservation* **2013**, 58 (2), 80-87.
55. Schieweck, A.; Delius, W.; Siwinski, N.; Vogtenrath, W.; Genning, C.; Salthammer, T., Occurrence of organic and inorganic biocides in the museum environment. *Atmospheric Environment* **2007**, 41 (15), 3266-3275.
56. McGath, M.; McCarthy, B.; Bosworth, J. In *Environmental monitoring of volatile organic compounds using silica gel, zeolite and activated charcoal*, MRS Proceedings, Cambridge Univ Press: 2015; pp mrsf13-1656-pp05-02.
57. Schieweck, A.; Bock, M.-C., Emissions from low-VOC and zero-VOC paints—Valuable alternatives to conventional formulations also for use in sensitive environments? *Building and Environment* **2015**, 85, 243-252.
58. Riggin, R. M.; Winberry, W.; Murphy, N. *Compendium of methods for the determination of toxic organic compounds in ambient air*; Engineering-Science, Inc., Cary, NC (USA): 1988.
59. Shearer, J. C.; Peters, D. C.; Hoepfner, G.; Newton, T., FTIR in the service of art conservation. *Analytical Chemistry* **1983**, 55 (8), 874A-880A.
60. Ryhl-Svendsen, M.; Glastrup, J., Acetic acid and formic acid concentrations in the museum environment measured by SPME-GC/MS. *Atmospheric Environment* **2002**, 36 (24), 3909-3916.
61. Partyka, M.; Zabiegała, B.; Namięśnik, J.; Przyjazny, A., Application of passive samplers in monitoring of organic constituents of air. *Critical Reviews in Analytical Chemistry* **2007**, 37 (1), 51-78.
62. Górecki, T.; Namięśnik, J., Passive sampling. *TrAC Trends in Analytical Chemistry* **2002**, 21 (4), 276-291.
63. Marć, M.; Tobiszewski, M.; Zabiegała, B.; de la Guardia, M.; Namięśnik, J., Current air quality analytics and monitoring: A review. *Analytica chimica acta* **2015**, 853, 116-126.
64. Kozdroń-Zabiegata, B.; Namięśnik, J.; Przyjazny, A., Use of passive dosimeters for evaluation of the quality of indoor and outdoor air. *Indoor and Built Environment* **1995**, 4 (3-4), 189-203.
65. Tuduri, L.; Millet, M.; Briand, O.; Montury, M., Passive air sampling of semi-volatile organic compounds. *TrAC Trends in Analytical Chemistry* **2012**, 31, 38-49.

66. Zabiegała, B.; Kot-Wasik, A.; Urbanowicz, M.; Namieśnik, J., Passive sampling as a tool for obtaining reliable analytical information in environmental quality monitoring. *Analytical and Bioanalytical Chemistry* **2009**, 396 (1), 273-296.
67. Brokerhof, A. W.; Van Bommel, M. In *Deterioration of calcareous materials by acetic acid vapour: a model study*, ICOM committee for conservation, 11th triennial meeting in Edinburgh, Scotland, 1-6 September 1996: Preprints, James & James (Science Publishers) Ltd.: 1996; pp 769-775.
68. Robinet, L.; Thickett, D., A New Methodology for Accelerated Corrosion Testing. *Studies in Conservation* **2003**, 48 (4), 263-268.
69. Oddy, W., An unsuspected danger in display. *Museums Journal* **1973**, 73 (1), 27-28.
70. Nicholson, C.; O'Loughlin, E. M., The use of AD strips for screening conservation and exhibit materials. **1996**.
71. Bacci, M.; Picollo, M.; Porcinai, S.; Radicati, B., Evaluation of the museum environmental risk by means of tempera-painted dosimeters. *Thermochimica Acta* **2000**, 365 (1), 25-34.
72. Bacci, M.; Cucci, C.; Dupont, A.-L.; Lavédrine, B.; Picollo, M.; Porcinai, S., Disposable indicators for monitoring lighting conditions in museums. *Environmental science & technology* **2003**, 37 (24), 5687-5694.
73. Hofmann, C.; Hartl, A.; Ahn, K.; Faerber, I.; Henniges, U.; Potthast, A., Studies on the Conservation of Verdigris on Paper. *Restaurator. International Journal for the Preservation of Library and Archival Material* **2015**, 36 (2), 147-182.
74. Fraunhofer Insititute for Manufacturing Technology and Advanced Materials IFAM (Combating) Corrosion of historic organ pipes. http://www.ifam.fraunhofer.de/en/Spin-Offs/Surface_Technology/organ_pipes.html (accessed March 10, 2016).
75. Museum of Fine Arts Boston A-D Strips. http://cameo.mfa.org/wiki/A-D_strips (accessed March 10, 2016).
76. Grzywacz, C. M.; Stulik, D. C., Passive monitors for the detection of pollutants in museum environments. In *Objects Specialty Group Postprints 1991, Albuquerque, New Mexico*, American Institute for Conservation of Historic and Artistic Works: 1992; Vol. 1, pp 33-41.
77. Gibson, L.; Cooksey, B.; Littlejohn, D.; Tennent, N., Determination of experimental diffusion coefficients of acetic acid and formic acid vapours in air using a passive sampler. *Analytica chimica acta* **1997**, 341 (1), 1-10.

78. Lubeck. Draeger Long-Term Diffusion Tubes *Draeger-Tubes & CMS-Handbook* [Online],2016.http://www.draeger.com/sites/assets/PublishingImages/Master/Oil_and_Gas/Upstream/9092086-Tubes-e-low.pdf (accessed 29 May 2016).
79. Products, A. Airscan Monitoring Badges *Andersen Products* [Online], 2016. <http://anpro.com/accessories/AN93/> (accessed 29 May 2016).
80. Draeger. Draeger Bio-Check Formaldehyde *Draeger Product Description* [Online], 2016. http://www.draeger.com/Sites/enus_us/Pages/Chemical-Industry/Draeger-Bio-Check-Formaldehyde.aspx (accessed 29 May 2016).
81. Bacci, M.; Cucci, C.; Mencaglia, A. A.; Mignani, A. G., Innovative sensors for environmental monitoring in museums. *Sensors* **2008**, 8 (3), 1984-2005.
82. Kouril, M.; Prosek, T.; Scheffel, B.; Degres, Y., Corrosion monitoring in archives by the electrical resistance technique. *Journal of Cultural Heritage* **2014**, 15 (2), 99-103.
83. Prosek, T.; Kouril, M.; Dubus, M.; Taube, M.; Hubert, V.; Scheffel, B.; Degres, Y.; Jouannic, M.; Thierry, D., Real-time monitoring of indoor air corrosivity in cultural heritage institutions with metallic electrical resistance sensors. *Studies in Conservation* **2013**, 58 (2), 117-128.
84. Prosek, T.; Le Bozec, N.; Thierry, D., Application of automated corrosion sensors for monitoring the rate of corrosion during accelerated corrosion tests. *Materials and Corrosion* **2014**, 65 (5), 448-456.
85. Cavicchioli, A.; Neves, C. A.; Paiva, R. I.; de Faria, D. L. A., An upgraded automatic piezoelectric quartz crystal dosimeter for environmental monitoring in indoor cultural heritage conservation areas. *Sensors and Actuators B: Chemical* **2014**, 190, 1014-1023.
86. Sturdy, L.; Casadio, F.; Kokkori, M.; Muir, K.; Shull, K. R., Quartz crystal rheometry: A quantitative technique for studying curing and aging in artists' paints. *Polymer Degradation and Stability* **2014**, 107, 348-355.
87. Odlyha, M.; Theodorakopoulos, C.; Thickett, D.; Ryhl-Svendsen, M.; Slater, J.; Campana, R. In *Dosimeters for indoor microclimate monitoring for cultural heritage*, Museum Microclimates Proc. Conference Copenhagen 19-23 Nov, National Museum of Denmark: Copenhagen: 2007; pp 73-79.
88. Palmes, E.; Gunnison, A.; DiMattio, J.; Tomczyk, C., Personal sampler for nitrogen dioxide. *The American Industrial Hygiene Association Journal* **1976**, 37 (10), 570-577.
89. Campbell, G.; Stedman, J.; Stevenson, K., A survey of nitrogen dioxide concentrations in the United Kingdom using diffusion tubes, July–December 1991. *Atmospheric Environment* **1994**, 28 (3), 477-486.

90. Vardoulakis, S.; Lumbreras, J.; Solazzo, E., Comparative evaluation of nitrogen oxides and ozone passive diffusion tubes for exposure studies. *Atmospheric Environment* **2009**, *43* (16), 2509-2517.
91. Gibson, L. T.; Cooksey, B. G.; Littlejohn, D.; Tennent, N. H., A diffusion tube sampler for the determination of acetic acid and formic acid vapours in museum cabinets. *Analytica chimica acta* **1997**, *341* (1), 11-19.
92. Targa, J.; Loader, A., Diffusion tubes for ambient NO₂ monitoring: practical guidance for laboratories and users. *Report to Defra and the Devolved Administrations. AEA Energy & Environment, Harwell* **2008**.
93. Askim, J. R.; Mahmoudi, M.; Suslick, K. S., Optical sensor arrays for chemical sensing: the optoelectronic nose. *Chemical Society Reviews* **2013**, *42* (22), 8649-8682.
94. Diehl, K. L.; Anslyn, E. V., Array sensing using optical methods for detection of chemical and biological hazards. *Chemical Society Reviews* **2013**, *42* (22), 8596-8611.
95. Guillermo, O.; Moreno-Bondi, M. C.; Garcia-Fresnadillo, D.; Marazuela, M. D., The interplay of indicator, support and analyte in optical sensor layers. In *Frontiers in Chemical Sensors*, Springer: 2005; pp 189-225.
96. Lim, S. H.; Feng, L.; Kemling, J. W.; Musto, C. J.; Suslick, K. S., An optoelectronic nose for the detection of toxic gases. *Nature chemistry* **2009**, *1* (7), 562-567.
97. Zhu, Z.; Garcia-Gancedo, L.; Flewitt, A. J.; Xie, H.; Moussy, F.; Milne, W. I., A critical review of glucose biosensors based on carbon nanomaterials: carbon nanotubes and graphene. *Sensors* **2012**, *12* (5), 5996-6022.
98. Jerónimo, P. C.; Araújo, A. N.; Montenegro, M. C. B., Optical sensors and biosensors based on sol-gel films. *Talanta* **2007**, *72* (1), 13-27.
99. Rottman, C.; Grader, G.; De Hazan, Y.; Melchior, S.; Avnir, D., Surfactant-induced modification of dopants reactivity in sol-gel matrixes. *Journal of the American Chemical Society* **1999**, *121* (37), 8533-8543.
100. Costa-Fernández, J.; Sanz-Medel, A., Air moisture sensing materials based on the room temperature phosphorescence quenching of immobilized mercurochrome. *Analytica chimica acta* **2000**, *407* (1), 61-69.
101. Suslick, K. S.; Bailey, D. P.; Ingison, C. K.; Janzen, M.; Kosal, M. E.; McNamara III, W. B.; Rakow, N. A.; Sen, A.; Weaver, J. J.; Wilson, J. B., Seeing smells: development of an optoelectronic nose. *Quimica Nova* **2007**, *30* (3), 677-681.
102. Suslick, K. S.; Rakow, N. A.; Sen, A., Colorimetric sensor arrays for molecular recognition. *Tetrahedron* **2004**, *60* (49), 11133-11138.

103. Rakow, N. A.; Suslick, K. S., A colorimetric sensor array for odour visualization. *Nature* **2000**, *406* (6797), 710-713.
104. Suslick, K. S., An optoelectronic nose: "seeing" smells by means of colorimetric sensor arrays. *MRS bulletin* **2004**, *29* (10), 720-725.
105. Salinas, Y.; Ros-Lis, J. V.; Vivancos, J.-L.; Martínez-Máñez, R.; Aucejo, S.; Herranz, N.; Lorente, I.; Garcia, E., A chromogenic sensor array for boiled marinated turkey freshness monitoring. *Sensors and Actuators B: Chemical* **2014**, *190*, 326-333.
106. Soga, T.; Jimbo, Y.; Suzuki, K.; Citterio, D., Inkjet-printed paper-based colorimetric sensor array for the discrimination of volatile primary amines. *Analytical chemistry* **2013**, *85* (19), 8973-8978.
107. Torsi, L.; Magliulo, M.; Manoli, K.; Palazzo, G., Organic field-effect transistor sensors: a tutorial review. *Chemical Society Reviews* **2013**, *42* (22), 8612-8628.
108. Grinthal, A.; Aizenberg, J., Adaptive all the way down: building responsive materials from hierarchies of chemomechanical feedback. *Chemical Society Reviews* **2013**, *42* (17), 7072-7085.
109. Tamayo, J.; Kosaka, P. M.; Ruz, J. J.; San Paulo, Á.; Calleja, M., Biosensors based on nanomechanical systems. *Chemical Society Reviews* **2013**, *42* (3), 1287-1311.
110. Janzen, M. C.; Ponder, J. B.; Bailey, D. P.; Ingison, C. K.; Suslick, K. S., Colorimetric sensor arrays for volatile organic compounds. *Analytical chemistry* **2006**, *78* (11), 3591-3600.
111. Kemling, J. W.; Qavi, A. J.; Bailey, R. C.; Suslick, K. S., Nanostructured substrates for optical sensing. *The journal of physical chemistry letters* **2011**, *2* (22), 2934-2944.
112. MacCraith, B.; McDonagh, C.; O'Keeffe, G.; McEvoy, A.; Butler, T.; Sheridan, F., Sol-gel coatings for optical chemical sensors and biosensors. *Sensors and Actuators B: Chemical* **1995**, *29* (1), 51-57.
113. Steinberg, I. M.; Lobnik, A.; Wolfbeis, O. S., Characterisation of an optical sensor membrane based on the metal ion indicator Pyrocatechol Violet. *Sensors and Actuators B: Chemical* **2003**, *90* (1), 230-235.
114. Lukowiak, A.; Streck, W., Sensing abilities of materials prepared by sol-gel technology. *Journal of sol-gel science and technology* **2009**, *50* (2), 201-215.
115. Podbielska, H.; Ulatowska-Jarza, A.; Müller, G.; Eichler, H. J., Sol-Gels for Optical Sensors. In *Optical Chemical Sensors*, Springer: 2006; pp 353-385.

116. Kemling, J. W.; Suslick, K. S., Nanoscale porosity in pigments for chemical sensing. *Nanoscale* **2011**, *3* (5), 1971-1973.
117. Lim, S. H.; Kemling, J. W.; Feng, L.; Suslick, K. S., A colorimetric sensor array of porous pigments. *Analyst* **2009**, *134* (12), 2453-2457.
118. Feng, L.; Musto, C. J.; Kemling, J. W.; Lim, S. H.; Suslick, K. S., A colorimetric sensor array for identification of toxic gases below permissible exposure limits. *Chem. Commun.* **2010**, *46* (12), 2037-2039.
119. Levitsky, I.; Krivoshlykov, S. G.; Grate, J. W., Rational design of a Nile Red/polymer composite film for fluorescence sensing of organophosphonate vapors using hydrogen bond acidic polymers. *Analytical chemistry* **2001**, *73* (14), 3441-3448.
120. Johnson, R. D.; Bachas, L. G., Ionophore-based ion-selective potentiometric and optical sensors. *Analytical and bioanalytical chemistry* **2003**, *376* (3), 328-341.
121. Feng, L.; Musto, C. J.; Kemling, J. W.; Lim, S. H.; Zhong, W.; Suslick, K. S., Colorimetric sensor array for determination and identification of toxic industrial chemicals. *Analytical chemistry* **2010**, *82* (22), 9433-9440.
122. Suslick, B. A.; Feng, L.; Suslick, K. S., Discrimination of complex mixtures by a colorimetric sensor array: coffee aromas. *Analytical chemistry* **2010**, *82* (5), 2067-2073.
123. Zhang, C.; Bailey, D. P.; Suslick, K. S., Colorimetric sensor arrays for the analysis of beers: a feasibility study. *Journal of agricultural and food chemistry* **2006**, *54* (14), 4925-4931.
124. Zhang, C.; Suslick, K. S., Colorimetric sensor array for soft drink analysis. *Journal of agricultural and food chemistry* **2007**, *55* (2), 237-242.
125. Carey, J. R.; Suslick, K. S.; Hulkower, K. I.; Imlay, J. A.; Imlay, K. R.; Ingison, C. K.; Ponder, J. B.; Sen, A.; Wittrig, A. E., Rapid identification of bacteria with a disposable colorimetric sensing array. *Journal of the American Chemical Society* **2011**, *133* (19), 7571-7576.
126. Janata, J., *Principles of chemical sensors*. Springer Science & Business Media: 2010.
127. Stetter, J. R.; Li, J., Amperometric Gas Sensors A Review. *Chemical Reviews* **2008**, *108* (2), 352-366.
128. Ahmed, M. U.; Hossain, M. M.; Tamiya, E., Electrochemical Biosensors for Medical and Food Applications. *Electroanalysis* **2008**, *20* (6), 616-626.
129. Barsony, I.; Dücső, C.; Fürjes, P., Thermometric gas sensing. In *Solid State Gas Sensing*, Springer: 2009; pp 1-24.

130. Gründler, P.; Janata, J., Chemical sensors: an introduction for scientists and engineers. *Physics Today* **2008**, *61* (3), 56.
131. Jerónimo, P. C. A.; Araújo, A. N.; Conceição B.S.M. Montenegro, M., Optical sensors and biosensors based on sol–gel films. *Talanta* **2007**, *72* (1), 13-27.
132. Nassau, K., The physics and chemistry of color: the fifteen causes of color. *The Physics and Chemistry of Color: The Fifteen Causes of Color, 2nd Edition*, by Kurt Nassau, pp. 496. ISBN 0-471-39106-9. Wiley-VCH, July 2001. **2001**, *1*.
133. Scheeline, A., Cell Phone Spectrometry: Science in Your Pocket? *TrAC Trends in Analytical Chemistry* **2016**.
134. Sharma, G.; Trussell, H. J., Digital color imaging. *Image Processing, IEEE Transactions on* **1997**, *6* (7), 901-932.
135. Shen, H.-L.; Xin, J. H., Spectral characterization of a color scanner by adaptive estimation. *JOSA A* **2004**, *21* (7), 1125-1130.
136. Ohta, N.; Robertson, A., *Colorimetry: fundamentals and applications*. John Wiley & Sons: 2006.
137. Fairchild, M. D.; Rosen, M. R.; Johnson, G. M., Spectral and metamerism color imaging. *RIT-MCSL Technical Report* **2001**.
138. Zhou, J.; Glotzbach, J. In *Image pipeline tuning for digital cameras*, Consumer Electronics, 2007. ISCE 2007. IEEE International Symposium on, IEEE: 2007; pp 1-4.
139. Huang, B.-C.; Fuh, C.-S. In *Image pipeline algorithms for standard mobile imaging architecture sensors*, 18th IPPR Conference on Computer Vision, Graphics and Image Processing (CVGIP 2005), 2005.
140. Hong, J. I.; Chang, B.-Y., Development of the smartphone-based colorimetry for multi-analyte sensing arrays. *Lab on a Chip* **2014**, *14* (10), 1725-1732.
141. Guan, L.; Tian, J.; Cao, R.; Li, M.; Cai, Z.; Shen, W., Barcode-like paper sensor for smartphone diagnostics: An application of blood typing. *Analytical chemistry* **2014**, *86* (22), 11362-11367.
142. Jia, M.-Y.; Wu, Q.-S.; Li, H.; Zhang, Y.; Guan, Y.-F.; Feng, L., The calibration of cellphone camera-based colorimetric sensor array and its application in the determination of glucose in urine. *Biosensors and Bioelectronics* **2015**, *74*, 1029-1037.
143. Meng, X.; Schultz, C. W.; Cui, C.; Li, X.; Yu, H.-Z., On-site chip-based colorimetric quantitation of organophosphorus pesticides using an office scanner. *Sensors and Actuators B: Chemical* **2015**, *215*, 577-583.

144. Debus, B.; Kirsanov, D.; Yaroshenko, I.; Sidorova, A.; Piven, A.; Legin, A., Two low-cost digital camera-based platforms for quantitative creatinine analysis in urine. *Analytica chimica acta* **2015**, *895*, 71-79.
145. Yuan, K.; Wu, Y.; Wang, C.; Jin, S., Spectrophotometric colorimeter based on LED light source and method for realizing the same. US Patent 9,243,953: 2016.
146. Chen, X.; Zhou, Y.; Peng, X.; Yoon, J., Fluorescent and colorimetric probes for detection of thiols. *Chemical Society Reviews* **2010**, *39* (6), 2120-2135.
147. Suzuki, Y.; Nakano, N.; Suzuki, K., Portable sick house syndrome gas monitoring system based on novel colorimetric reagents for the highly selective and sensitive detection of formaldehyde. *Environmental science & technology* **2003**, *37* (24), 5695-5700.
148. Germain, M. E.; Knapp, M. J., Optical explosives detection: from color changes to fluorescence turn-on. *Chemical Society Reviews* **2009**, *38* (9), 2543-2555.
149. Feng, L.; Musto, C. J.; Kemling, J. W.; Lim, S. H.; Suslick, K. S., A colorimetric sensor array for identification of toxic gases below permissible exposure limits. *Chemical Communications* **2010**, *46* (12), 2037-2039.
150. Sadaoka, Y.; Sakai, Y.; Yamada, M., Optical properties of sulfonephthalein dyes entrapped within polymer matrices for quantification of ammonia vapour and humidity in air. *Journal of Materials Chemistry* **1993**, *3* (8), 877-881.
151. Cheng, K. L.; Ueno, K.; Imamura, T., *CRC handbook of organic analytical reagents*. Crc Press: 1992.
152. Ingle Jr, J.; Crouch, S., Evaluation of precision of quantitative molecular absorption spectrometric measurements. *Analytical chemistry* **1972**, *44* (8), 1375-1386.
153. Rothman, L.; Crouch, S.; Ingle Jr, J., Theoretical and experimental investigation of factors affecting precision in molecular absorption spectrophotometry. *Analytical chemistry* **1975**, *47* (8), 1226-1233.
154. Askim, J. R.; Li, Z.; LaGasse, M. K.; Rankin, J. M.; Suslick, K. S., An optoelectronic nose for identification of explosives. *Chemical Science* **2016**, *7* (1), 199-206.
155. Askim, J. R.; Suslick, K. S., Hand-Held Reader for Colorimetric Sensor Arrays. *Analytical chemistry* **2015**, *87* (15), 7810-7816.
156. Kireyko, A.; Veselova, I.; Shekhovtsova, T., Mechanisms of peroxidase oxidation of o-dianisidine, 3, 3', 5, 5'-tetramethylbenzidine, and o-phenylenediamine in the presence of sodium dodecyl sulfate. *Russian Journal of Bioorganic Chemistry* **2006**, *32* (1), 71-77.

157. Pankratov, A. N.; Shchavlev, A. E., Semiempirical quantum chemical PM3 computations and evaluations of redox potentials, basicities, and dipole moments of the diphenylamine series as analytical reagents. *Canadian Journal of Chemistry* **1999**, *77* (12), 2053-2058.
158. Josephy, P. D., Oxidative activation of benzidine and its derivatives by peroxidases. *Environmental health perspectives* **1985**, *64*, 171.
159. Oldfield, L. F.; Bockris, J. O. M., Reversible Oxidation-Reduction Reactions of Aromatic Amines. *The Journal of Physical Chemistry* **1951**, *55* (7), 1255-1274.
160. Alexy, M.; Hanko, M.; Rentmeister, S.; Heinze, J., Disposable optochemical sensor chip for nitrogen dioxide detection based on oxidation of N, N'-diphenyl-1, 4-phenylenediamine. *Sensors and Actuators B: Chemical* **2006**, *114* (2), 916-927.
161. Meskath, S.; Urban, G.; Heinze, J., A new optochemical chlorine gas sensor based on the application of amphiphilic co-networks as matrices. *Sensors and Actuators B: Chemical* **2011**, *151* (2), 327-332.
162. Meskath, S.; Urban, G.; Heinze, J., Nanophase separated amphiphilic polymer co-networks as efficient matrices for optical sensors: Rapid and sensitive detection of NO₂. *Sensors and Actuators B: Chemical* **2013**, *186*, 367-373.
163. Druzik, C. M.; Grosjean, D.; Van Neste, A.; Parmar, S. S., Sampling of Atmospheric Carbonyls with Small DNPH-Coated C18 Cartridges and Liquid Chromatography Analysis with Diode Array Detection. *International Journal of Environmental Analytical Chemistry* **1990**, *38* (4), 495-512.
164. Gibson, L.; Kerr, W.; Nordon, A.; Reglinski, J.; Robertson, C.; Turnbull, L.; Watt, C.; Cheung, A.; Johnstone, W., On-site determination of formaldehyde: A low cost measurement device for museum environments. *Analytica chimica acta* **2008**, *623* (1), 109-116.
165. Robins, J. H.; Abrams, G. D.; Pincock, J. A., The structure of Schiff reagent aldehyde adducts and the mechanism of the Schiff reaction as determined by nuclear magnetic resonance spectroscopy. *Canadian Journal of Chemistry* **1980**, *58* (4), 339-347.
166. Haynes, W. M., *CRC handbook of chemistry and physics*. CRC press: 2014.
167. Craig, P. J.; Bartlett, P. D., The role of hydrogen sulphide in environmental transport of mercury. *Nature* **1978**, *275* (5681), 635-637.
168. Allain, L. R.; Sorasaenee, K.; Xue, Z., Doped Thin-Film Sensors via a Sol-Gel Process for High-Acidity Determination. *Analytical chemistry* **1997**, *69* (15), 3076-3080.
169. Koncki, R.; Wolfbeis, O. S., Composite films of Prussian Blue and N-substituted polypyrroles: fabrication and application to optical determination of pH. *Analytical chemistry* **1998**, *70* (13), 2544-2550.

170. Haswell, S., *Practical guide to chemometrics*. CRC Press: 1992.
171. Johnson, R. A.; Wichern, D. W., *Applied multivariate statistical analysis*. Prentice hall Englewood Cliffs, NJ: 1992; Vol. 4.
172. Hair, J. F.; Black, W. C.; Babin, B. J.; Anderson, R. E.; Tatham, R. L., *Multivariate data analysis*. Pearson Prentice Hall Upper Saddle River, NJ: 2006; Vol. 6.

Chapter 2:

Colorimetric Sensor Arrays: Interplay of Geometry, Substrate and Immobilization

This chapter is taken in large part from the following reference:

LaGasse, M.K; Rankin, J.M.; Askim, J.R.; Suslick, K.S., Colorimetric Sensor Arrays: Interplay of Geometry, Substrate and Immobilization. *Sens. Actuators B.* **2014**, *197*, 116-122.

2.1 Introduction

The effectiveness of a colorimetric sensor array is influenced by not only the choice of chemoresponsive dyes, but also the choice of solid support, flow path geometry, and immobilization method.¹⁻³ These secondary factors can have a profound impact on the sensor's selectivity, sensitivity, dynamic range, response time, and thermal- and photo-stability.⁴⁻⁸ While there are many variations in formulations of colorimetric sensors reported, a comprehensive comparison among the choices of these parameters has not been available.

Colorimetric sensor arrays utilize cross-responsive, chemically responsive dyes to generate a composite, olfactory-like response unique to a given odorant that can be quantified by digital imaging.^{1, 2, 4, 9-14} The colors of such dyes are affected by a wide range of intermolecular interactions between analyte and dye, including Brønsted and Lewis acid–base, hydrogen bonding, dipolar, and π – π interactions. In contrast, other array technologies rely on the weakest and least specific interactions between sensor and analyte (i.e., van der Waals and physical absorptions).^{1, 2, 15-17} While colorimetric sensor arrays have proven a powerful approach toward detection and differentiation of chemically diverse analytes, one encounters the problem of optimizing the inclusion of a large number of chemically diverse dyes into the sensor array without compromising desired functionality. Therefore, understanding the interplay of factors such as solid support and immobilization method on sensor response is central to improvements in the field.

Available solid supports for colorimetric sensor arrays are abundant in number, nature, and structure. The necessary properties of a solid support include optical transparency or high reflectivity, homogeneous structure, and general chemical compatibility.³ For vapor sensing, an accessible substrate microstructure and high surface area enhance analyte diffusion to and high

loading of the chromophore; hydrophobicity of the substrate will also help to reduce the effects of ambient humidity.^{9, 10, 18, 19} Organic polymer supports, such as cellulose derivatives or polyvinylidene difluoride, have been common substrates for many recent optical sensors because they satisfy many of these criteria and are, in general, commercially available with several types of microstructures. Inorganic substrates, such as glass, fused silica, or silica gel, are also widely used; while they are dimensionally stable (resistant to swelling) and chemically inert, they may also have limited surface area and porosity.

Dye immobilization can be used to protect colorants in humid environments, mediate the transfer of dyes onto a solid support, prevent leaching into the sample medium, enhance the modulation of the optical properties, and improve analyte diffusion to reaction centers.^{6, 20, 21} Two common immobilization materials are organically modified silanes (ormosils) and semi-liquid films of plasticizers or polymers. Ormosils can be tailored through the appropriate choice of sol-gel precursors and provide matrices with a range of hydrophobicity, nanoporosity, and surface area.²²⁻²⁶ Plasticizers and polymers serve to solubilize the dye, facilitate analyte access to the reactive chromophores where analyte-colorant interaction occurs, and can act as selective sorbents, enhancing analyte selectivity.^{27, 28} Semi-liquid formulations have a similar range of potential polarities as ormosil matrices, but lack hierarchical porosity and high surface area.

We have previously described colorimetric sensor arrays^{1, 9, 10} that can successfully differentiate among volatile organic compounds,¹⁸ toxic industrial chemicals (TICs),^{4, 26, 29} beverages,³⁰⁻³² and bacteria.³³ We have successfully employed both impermeable films (e.g., polyethylene terephthalate, PET) and permeable membranes (e.g., polyvinylidene difluoride, PVDF) as substrates, and used ormosils, polymers and plasticizers for dye immobilization. In this work, we explore the effect of array geometry, substrate, and immobilization method on sensor response. The response homogeneity, time, and magnitude of a new one-dimensional (linear) array configuration are compared to that of the previously reported two-dimensional (6×6) array configuration.⁴ Additionally, we have chosen to examine six substrate materials: two impermeable (i.e., glass slides and PET), two paper (i.e., printer paper and chromatography paper with large pore silica gel (SG81)), and two porous polymer membranes (i.e., polypropylene (PP) and PVDF). To explore the effect of immobilization methods on dye reactivity, we compare the response of eight dyes immobilized either in previously optimized ormosil or as optimized plasticizer formulations. We report here a semi-quantitative evaluation

of the influence of these secondary factors on colorimetric sensor array response, quality, consistency, and sensitivity.

2.2 Experimental

2.2.1 Materials

All reagents were of analytical grade and used without any further purification. Certified, premixed gas tanks were obtained from Matheson Tri-Gas through S.J. Smith. Substrates used included pre-cleaned glass slides (Gold Seal; thickness: 0.93–1.05 mm, size: 3 × 1"), PET (McMaster-Carr; thickness: 0.004 ± 0.0004 in.), SG81 chromatography paper (Whatman), multi-use paper (GP Spectrum), PP membrane (Sterlitech Corporation; thickness: 130–170 μm, pore size: 0.22 μm) and PVDF membrane (VWR Scientific, Batavia, IL; thickness: 165 μm, pore size: 0.45 μm).

2.2.2 Formulation Preparation

Sol–gel solutions were prepared according to previous methods.^{4, 24, 25} Briefly, sol–gel formulations were prepared by acid-catalyzed hydrolysis of solutions containing commercially-available silane precursors and low concentrations of surfactant dissolved in low volatility solvents. The surfactant acts to reduce capillary stress and improve print quality and the low volatility solvents act as porogens on the nanometer scale. The plasticizer formulation was prepared by adding tetraethylene glycol (10 wt%) to 2-methoxyethanol and stirring overnight.¹⁸ The sol–gel or tetraethylene glycol solutions were added to chemoresponsive indicators (**Table 2.1**) and mixed thoroughly by shaking. If appropriate, 1 M solutions of *t*-butylammonium hydroxide (TBAH) or *p*-toluenesulfonic acid (TsOH) in water were added immediately before printing.

Table 2.1 List of chemically responsive colorants.

Spot #	Name	Amount of Dye Added (mg/mL)	
		Ormosil	Plasticizer
1	5,10,15,20-tetraphenylporphyrinatozinc(II)		
2	5,10,15,20-tetrakis(2,4,6-trimethylphenyl)porphyrinatozinc(II)		
3	5,10,15,20-tetrakis(pentafluorophenyl)porphyrinatozinc(II)		
4	5,10,15,20-tetrakis(2,4,6-trimethylphenyl)porphyrinatocobalt(II)		
5	5,10,15,20-tetraphenylporphyrinatocadmium(II)		
6	5,10,15,20-tetraphenylporphyrinatoschromium(III) chloride		
7	Bromophenol Blue + TBAH		
8	Methyl Red + TBAH	4.0	1.8
9	Chlorophenol Red + TBAH	4.0	2.0
10	Nitrazine Yellow + TBAH	4.0	2.0
11	Bromothymol Blue + TBAH	4.0	10.0
12	Thymol Blue + TBAH		
13	<i>m</i> -Cresol Purple + TBAH		
14	Zn(OAc) ₂ + <i>m</i> -Cresol Purple + TBAH		
15	HgCl ₂ + Bromophenol Blue + TBAH		
16	HgCl ₂ + Bromocresol Green + TBAH		
17	Pb(OAc) ₂		
18	1-[4-[[4-(dimethylamino)phenyl]azo]phenyl]-2,2,2-trifluoroethanone + TsOH		
19	α -Naphthol Red + TsOH		
20	Tetraiodophenolsulfonephthalein		
21	Fluorescein	2.0	2.0
22	Bromocresol Green	4.0	20
23	Methyl Red		
24	Bromocresol Purple		
25	Bromophenol Red	4.0	3.5
26	Rosolic Acid		
27	Bromopyrogallol Red		
28	Pyrocatechol Violet		
29	Nile Red	0.5	0.4
30	Disperse Orange #25		
31	4-(4-Nitrobenzyl)pyridine + N-Benzylaniline		
32	4-[2-[4-(dimethylamino)phenyl]ethenyl]-2,6-dimethylpyrylium		
33	LiNO ₃ + Cresol Red		
34	Acridine Orange Base		
35	AgNO ₃ + Bromophenol Blue		
36	AgNO ₃ + Bromocresol Green		

Spot numbering from left to right in linear arrays.

Bold: colorants used in the comparison of the plasticizer vs. ormosil linear arrays.

TBAH: tetrabutylammonium hydroxide.

TsOH: p-toluenesulfonic acid.

2.2.3 Array Printing

Formulations with chemoresponsive dyes were loaded into a Teflon ink well containing either a 6×6 or a 3×12 pattern of $\sim 50 \mu\text{L}$ holes. An ArrayIt NanoPrint LM60 Microarray Printer (ArrayIt Corporation, Sunnyvale, CA) holding an array of floating slotted pins (delivering $\sim 100 \text{ nL}$ each) was used to robotically print arrays by dipping into the ink well and transferring to the substrate. For 6×6 arrays, all 36 spots were printed in one pass; linear arrays were printed in three passes, 12 at a time, in an interleaved linear pattern. Before use, ormosil arrays were stored in a nitrogen filled glove bag for three days and plasticizer arrays were stored first under vacuum at room temperature for 24 h and then in a nitrogen filled glove bag for two days.

2.2.4 Experimental Procedure

Gas mixtures were prepared according to previous methods.²⁹ Briefly, MKS mass flow controllers were used to achieve gas streams with the desired concentration (50 ppm NH_3 or 100 ppm SO_2), flow (500 sccm) and relative humidity (50% RH) by mixing the appropriate amount of stock gas with wet (100% RH) and dry (0% RH) nitrogen gas. A MKS multigas analyzer (model 2030) was used in-line to verify gas concentrations. A diagram of the setup is shown in **Figure 2.1**.

During each trial, arrays were exposed to a control stream (50% RH N_2) for 3 min followed by 4 min of an analyte stream and imaged using a Canon EOS 5D Mark II digital camera with a 100 mm macro lens. Using an imaging system (**Figure 2.2**) fabricated by the University of Illinois School of Chemical Sciences Machine Shop the camera was held at a fixed position (16 cm above above the array holder) and high definition video (30 fps) was captured throughout the entirety of the trial. Inconsistencies in lighting were minimized with the use of white LED strips (“natural white”, SuperBrightLEDs.com) mounted at the top of the holder in a position that avoided reflections off the surface of the array holder (5 cm off center). At the start of each trial, the opening of the imaging system was covered with black felt to isolate the system from ambient lighting.

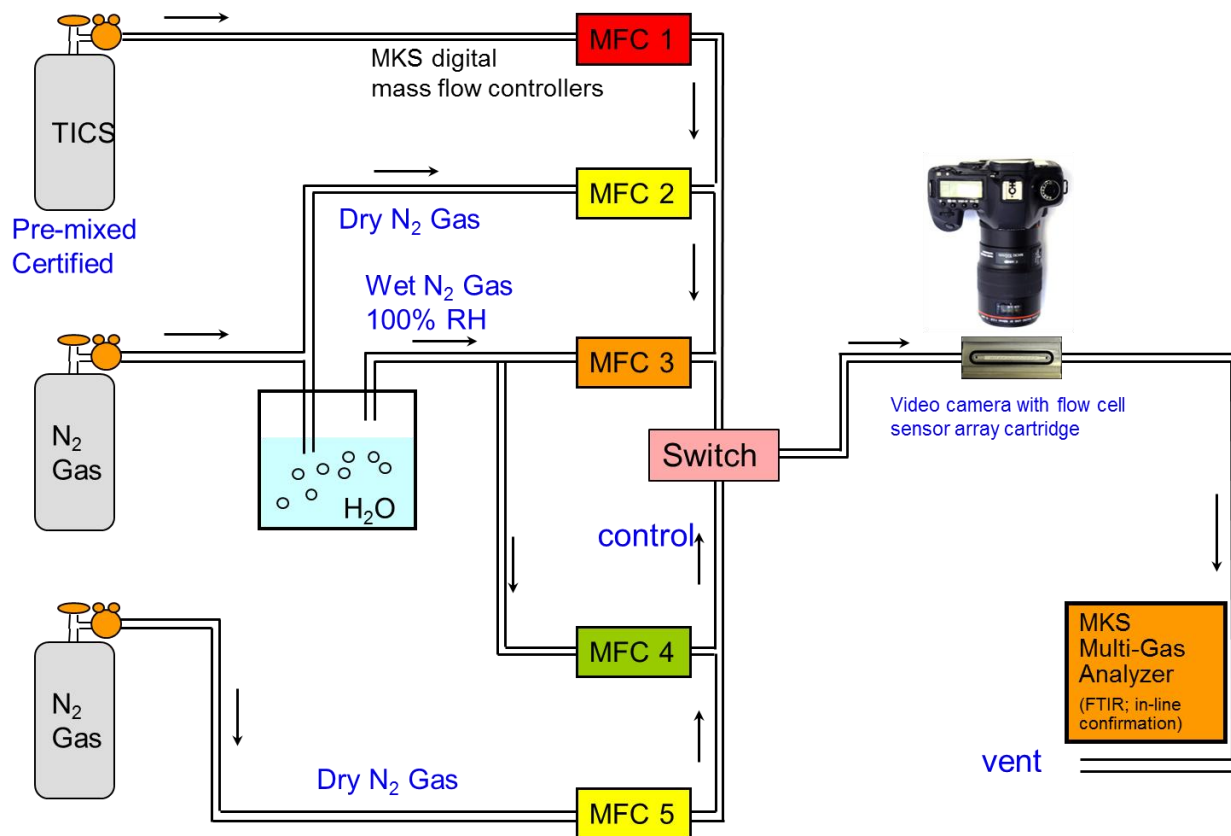


Figure 2.1 Gas mixing rig used for exposure of colorimetric sensor arrays. The box labeled “switch” is a three-way solenoid valve, which allows for venting and rapid exchange of the control to analyte lines.

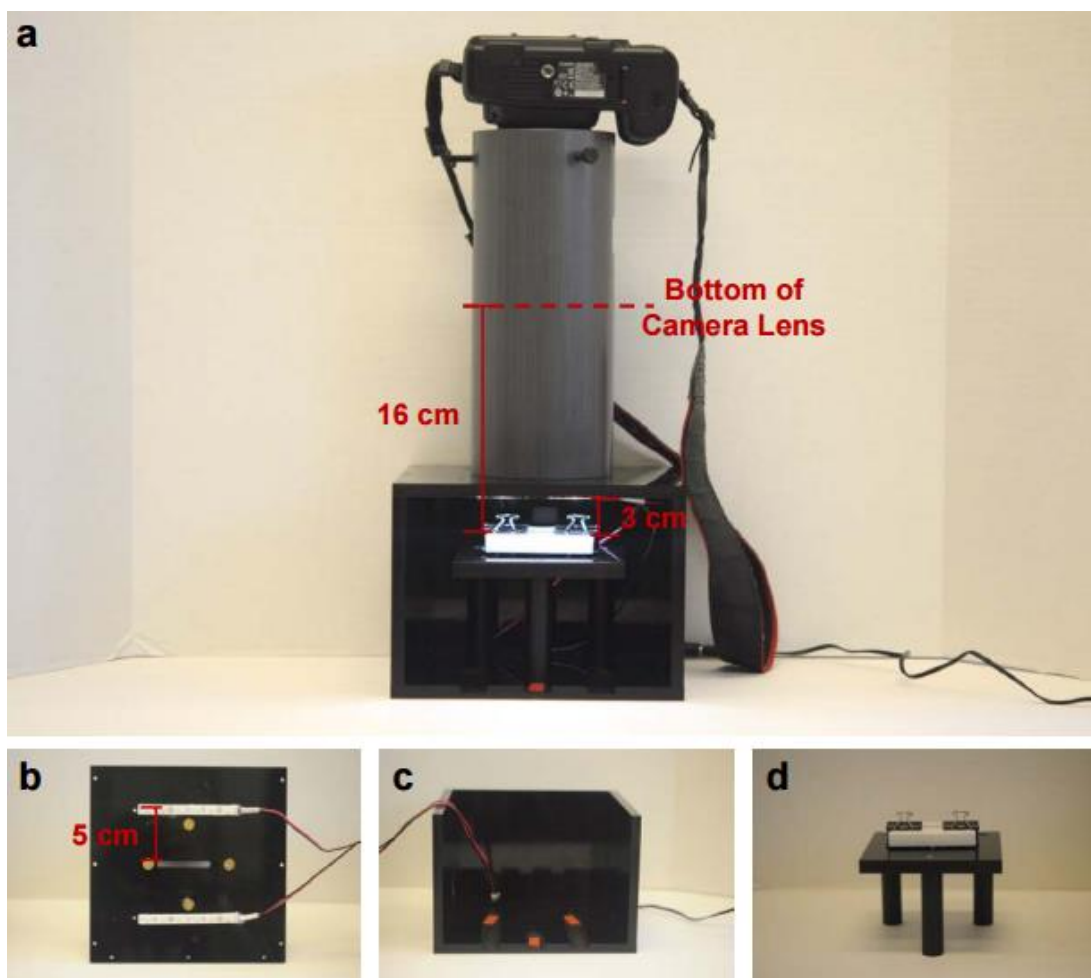


Figure 2.2 Photographs of (a) imaging system used to reduce inconsistencies in lighting, movement and focus. (b) White LED strips (“natural white”, SuperBrightLEDs.com) mounted at the top of the holder at 5 cm from oval aperture to avoid reflections off the surface of the glass slide. (c) Grooved base of the holder to allow for precise placement of (d) platform used to hold the array holder in the center of the imaging window.

6×6 arrays were placed within an injection molded disposable cartridge (dimensions of $22 \times 22 \times 4$ mm), as used in previous studies (**Figure 2.3a**). Linear arrays were tested within flow cells machined from Teflon (**Figure 2.3b**) or aluminum (**Figure 2.3c**) with channel dimensions of $1.6 \times 0.5 \times 57$ mm and $3 \times 0.6 \times 57$ mm, respectively. In both designs, an O-ring is placed in a groove around the channel and compressed by a glass slide to create a leak-free seal. Reflective substrates (PP, PVDF, SG81 and paper) were placed on the bottom of the aluminum holder channel and secured with silicone grease if necessary. Translucent substrates (glass slides and PET) were printed or secured to the glass slide and placed within the flow path of the Teflon holder.

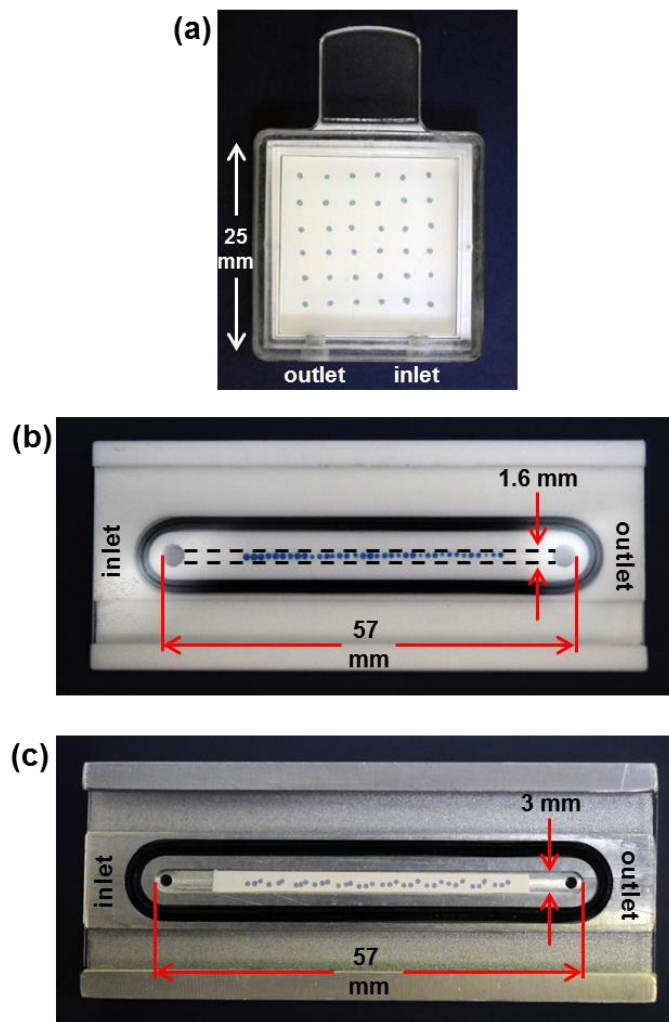


Figure 2.3 Photographs of (a) 6×6 injection molded disposable cartridge (dimensions of $22 \times 22 \times 4$ mm), as used in previous studies. Linear (b) Teflon (channel dimensions of $1.6 \times 0.5 \times 57$ mm) and (c) aluminum (channel dimensions of $3 \times 0.6 \times 57$ mm) holder with o-ring placed in a groove around the channel and compressed by a glass slide to create a leak-free seal.

To compare the linear and 6×6 array geometries, arrays of 36 identical spots of bromocresol green immobilized in an ormosil, were printed on PVDF in either a linear or 6×6 pattern. Arrays were exposed to NH_3 and run in quintuplicate. Substrate comparison was performed using arrays of 36 TICs responsive ormosil spots (**Table 2.1**) printed on each substrate. Arrays were exposed to either NH_3 (all substrates) or SO_2 (PP and PVDF) and run in septuplicate. To compare dye immobilization materials, arrays of select dyes were printed using either ormosil or plasticizer formulations and exposed to NH_3 or SO_2 as described previously. These experiments were run in septuplicate.

2.2.5 Image Processing and Data Analysis

GOM Media Player software was used to extract one still frame per second from video captured at 1920×1080 resolution (full HD). Images were processed using a customized software package, Spotfinder (iSense), which averaged the red, green and blue (*RGB*) values of an eight-pixel diameter area in the spot center. ΔRGB values were obtained by taking the difference of the *RGB* values from the before-exposure (i.e., after 3 min of nitrogen flow) and after-exposure images (i.e., after 4 min of analyte flow). This defines a 108-dimensional vector, i.e., 36 ΔRGB values, with each dimension ranging from -255 to $+255$ for eight-bit color imaging. The array response at a given timepoint is depicted pictorially using difference maps, an image generated from the ΔRGB absolute values for each spot in the array.

The ΔRGB values at a given timepoint can be combined into a Euclidean distance, defined by the equation $ED_t = (\Delta R_1^2 + \Delta G_1^2 + \Delta B_1^2 + \Delta R_2^2 + \dots + \Delta B_n^2)^{1/2}$, where n is the number of spots under consideration and t is the time. To generate a response profile for a given analyte, the average Euclidean distance (\overline{ED} for $n = 36$) at a given timepoint is plotted with respect to time. From this data, response time (defined here as the time necessary to reach 90% of the maximum ED) and relative standard deviation (RSD) is calculated. A map of the flow path at a given timepoint was generated by subtracting the \overline{ED} value of the least responsive spot from the \overline{ED} value of each spot in the array ($n = 1$). The ormosil and plasticizer formulations were compared using the equation: $(\overline{ED}_{plasticizer} - \overline{ED}_{ormosil}) / (\overline{ED}_{plasticizer} + \overline{ED}_{ormosil})$.

2.2.6 Scanning Electron Microscopy

Scanning electron micrographs were obtained on a JEOL 7000F instrument operating at 15 kV with a medium probe current and a working distance of 10 mm. Samples were mounted to the holder via carbon tape and sputter coated with approximately 10 nm of Au/Pd prior to analysis to prevent surface charging.

2.3 Results and Discussion

2.3.1 Geometry Comparison

The flow path analysis of a 6×6 vs. a linear array holder is shown in **Figure 2.4**. For the 6×6 array holder, the gas stream follows a U-shaped path traversing from the inlet, along the back wall, to the outlet. In contrast, a relatively homogeneous flow path is observed with the linear array holder. The inhomogeneous flow path in the 6×6 array holder contributes to a lower overall response, higher RSD, longer response time and less uniform array response (i.e., range of spot ED values) (**Table 2.2**). Spots in the 6×6 array that show the highest variation in color change are in locations where small differences in array position between trials brings the spot into or out of the analyte stream (**Figure 2.5**).

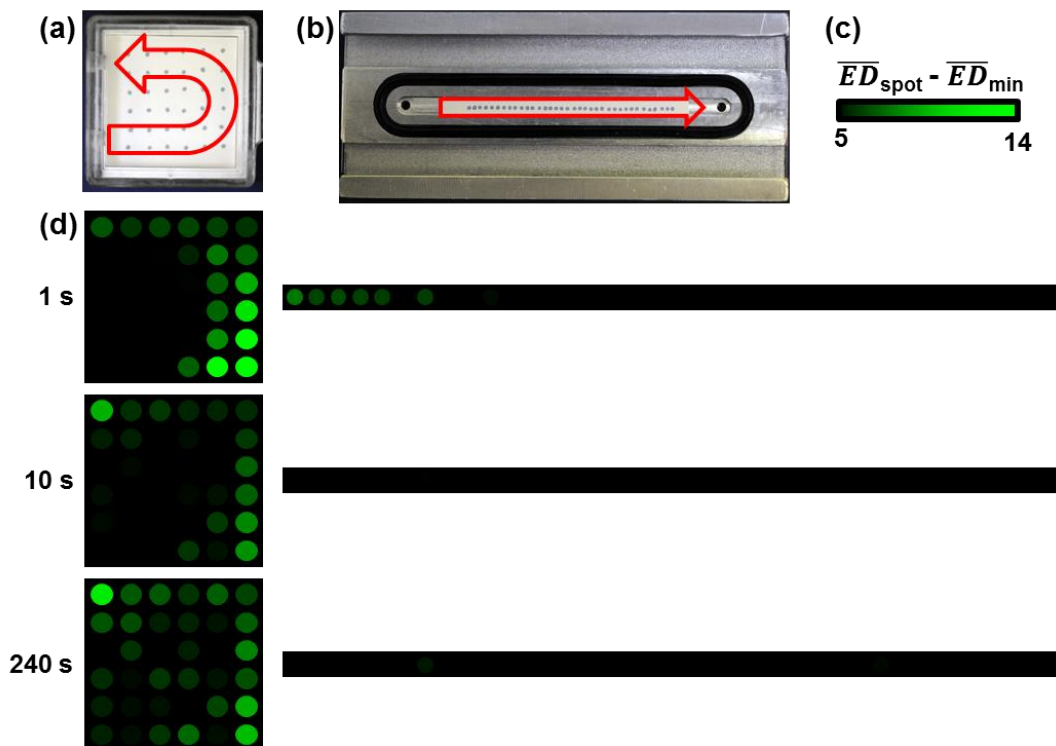


Figure 2.4 Analysis of flow path for square vs. linear arrays. **(a)** Photograph of the 6×6 square array in cartridge showing the gas flow path. **(b)** Photograph of the linear array in holder showing the gas flow path. **(c)** Color coding of the spot to spot variation of sensor response (where \overline{ED}_{spot} is the Euclidean distance from the ΔRGB values of each spot, and \overline{ED}_{min} is the Euclidean distance of the sensor spot with the minimum change in color.) **(d)** Graphic depiction of gas flow inhomogeneity for 6×6 square vs. linear arrays at 1 s, 10 s, and 240 s upon exposure to NH_3 at PEL (50 ppm).

Table 2.2 Comparison of 6 × 6 and linear arrays exposed to ammonia at PEL (50 ppm).

	6 x 6	Linear
Average Euclidean distance (ED) ^a of 36 sensors	571	621
Relative standard deviation ^a (%)	3.1	0.79
Average time for 90% of total response after equilibration (s)	31	23
Range in ED ^{a,b} at 10 s	30.8	15.3

^a From quintuplicate trials after 240 s analyte exposure.

^b Maximum ED minus minimum ED among all sensors after 10 s exposure.

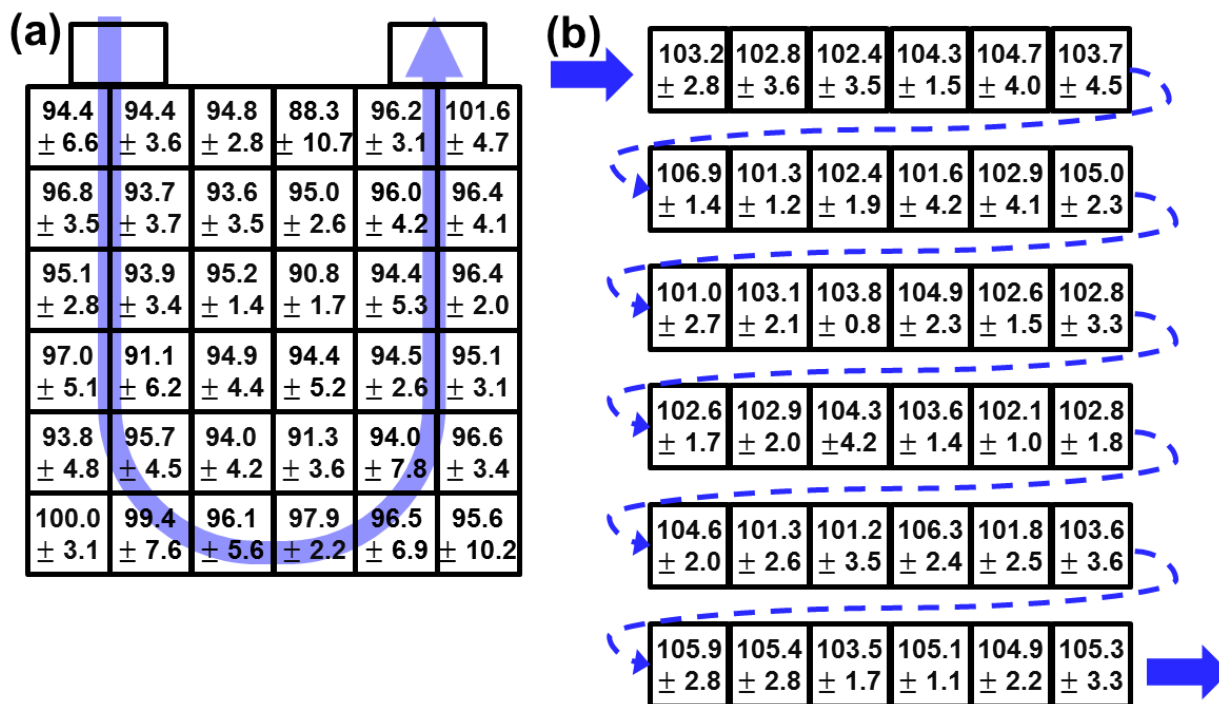


Figure 2.5 Euclidean distance and standard deviation values for each spot in the (a) 6 x 6 and (b) linear arrays used in the flow path analysis.

2.3.2 Substrate Comparison

2.3.2.1 Spot Quality

Spot quality was evaluated based on uniformity, size, and printing consistency. A qualitative ranking of the substrates, from highest to lowest, is PVDF ~ PP > PET > Glass > SG81 ~ Paper (**Figure 2.6**). Spots printed on PVDF were well formed, evenly colored and consistent among arrays in both color and size. The spots printed on PP were similar in quality but with a slightly more noticeable “coffee-ring effect”. We speculate this may be mitigated by using a different surfactant, surfactant concentration, or solvent. Most spots printed on PET exhibited similar uniformity and consistency; however, some were very small (e.g., spot 18) or showed a spider-web effect (e.g., spot 19). The color and size of spots printed on glass were inconsistent.

The paper substrates produced the poorest quality arrays. Spots on both SG81 and paper were relatively uniform in size and color, but were inhomogeneous throughout, largely due to the macroscale surface texture of the papers themselves combined with significant spreading due to capillary action. This was especially problematic for spots printed on printer paper and uncoated chromatography paper (not shown), where the spots were so large that they abutted or overlapped adjacent spots.

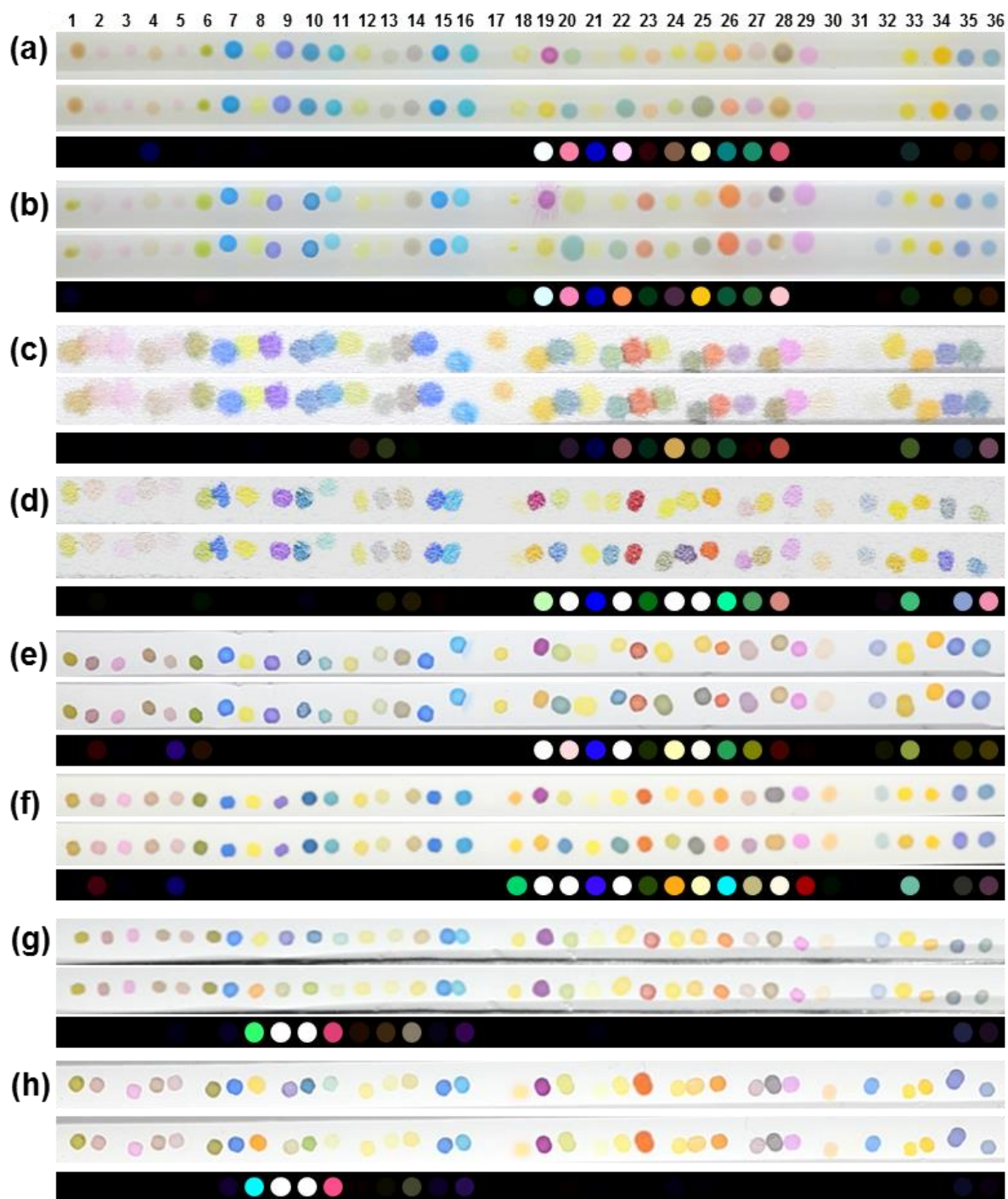


Figure 2.6 Raw images and difference maps for arrays printed on various substrates exposed to **(a–f)** NH_3 (50 ppm) and **(g and h)** SO_2 (100 ppm). **(a)** Glass slide, **(b)** polyethylene terephthalate, **(c)** printer paper, **(d)** SG81 chromatography paper, **(e)** polypropylene membrane, **(f)** polyvinylidene difluoride membrane, **(g)** polypropylene membrane, **(h)** polyvinylidene difluoride membrane. For each substrate **(a–h)**, the top image is the array before exposure, the middle image is after exposure, and the bottom is the difference map (red value minus red value, green minus green, blue minus blue). For display purposes, the color ranges of these difference maps are expanded from five to eight bits per color (*RGB* range of 2–33 expanded to 0–255).

2.3.2.2 Array Response

A comparison of arrays printed with ormosil immobilized dyes on each substrate is given in **Table 2.3** for response to NH_3 at 50 ppm (PEL) and SO_2 at 100 ppm (IDLH). The total *ED* with respect to time for the arrays upon exposure to NH_3 and SO_2 are given in **Figure 2.7**.

Table 2.3 Comparison of analyte response of arrays printed on various substrates.

	NH_3 (50 ppm)						SO_2 (100 ppm)	
	Glass	PET	Paper	SG81	PP	PVDF	PP	PVDF
Average Euclidean distance ^a	199.7	163.2	72	218.1	228.0	314.6	135.7	165.3
Relative standard deviation ^a (%)	8.0	4.8	11.4	4.4	1.1	1.5	1.2	9.9
Response time (s)	173	143	91	31	12	23	4	68
Noise ^b	0.655	0.614	0.898	0.920	0.591	0.555	0.546	0.646

^aSeptuplicate trials after 240s analyte exposure.

^bStandard deviation of the residuals from a linear regression of the control response for all non-saturated channels over all trials.

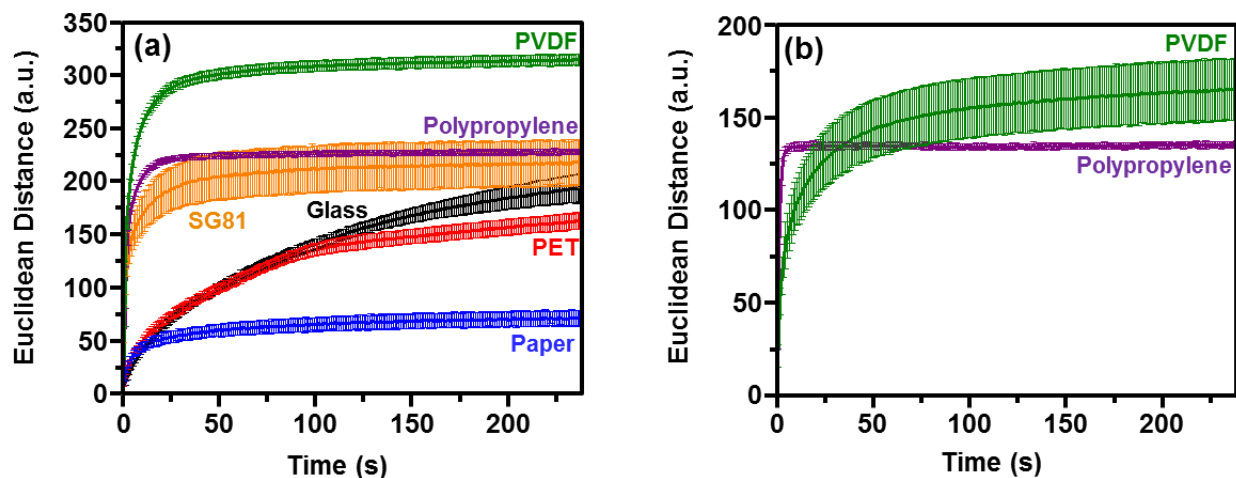


Figure 2.7 Euclidean distance versus time graphs for ormosil arrays printed on various substrates exposed to (a) NH_3 (50 ppm) and (b) SO_2 (100 ppm).

Upon exposure to NH_3 or SO_2 , arrays printed on PVDF showed a significantly higher total response than those printed on other substrates. There were spot dependent changes in signal observed that correlate to differences in initial spot color among substrates (**Figure 2.6**);

this may be reflective of variations in the acid/base properties and chemical functionality of each substrate. We suggest this could largely be overcome by optimizing the dye formulations for each substrate (e.g., through the addition of small amounts of acid or base before printing). The decrease in signal for the PET and glass slide arrays is dominated by the larger distance between the array and the reflective white background (i.e., the Teflon holder), which could be ameliorated by increasing the illumination.

Upon exposure to NH_3 , arrays printed on impermeable substrates (glass and PET) showed a slower response time relative to the porous substrates (Paper, SG81, PP and PVDF), which we attribute to slower diffusion of the analyte through the ormosil matrix caused by reduced hierarchical porosity. The RSD, a major limiting factor in the arrays' potential for discriminating among analytes, was significantly lower for arrays printed on porous polymer substrates: e.g., the NH_3 responsive spots printed on PP and PVDF were more consistent between printings of arrays than those printed on other substrates. Arrays printed on the paper substrates showed significantly higher noise due to inhomogeneity within the spots as discussed in **Section 2.3.2.1**.

When exposed to SO_2 , arrays printed on PP and PVDF membranes had very different response profiles (**Table 2.3** and **Figure 2.7b**). Arrays on PP were two to three times faster to respond than arrays on PVDF for both NH_3 and SO_2 . The faster reaction times for sensors on PP correlates with the SEM images of spots printed on PVDF and PP (**Figure 2.8**) that show increased porosity and surface area for the dye-coated PP versus PVDF. In addition, PVDF arrays had higher RSD (and thus poorer reproducibility) than PP arrays, which suggests the printing consistency of the SO_2 responsive spots was worse on PVDF.

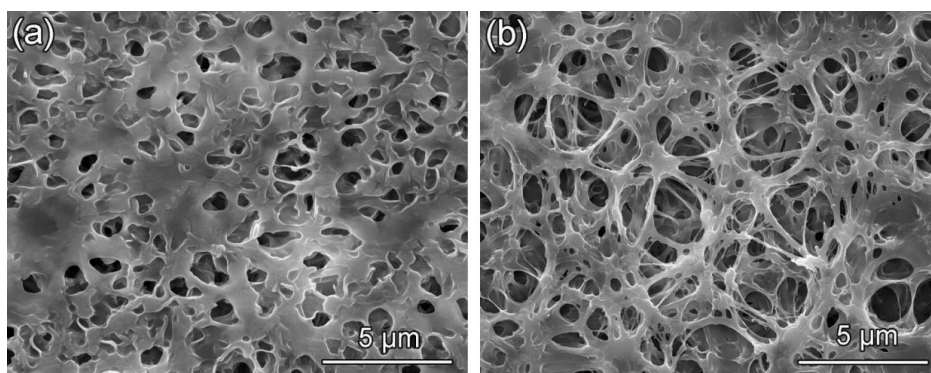


Figure 2.8 Scanning electron micrographs of ormosil spots printed on (a) polyvinylidene difluoride (PVDF) and (b) polypropylene (PP) membranes.

2.3.3 Formulation Comparison

Figure 2.9 shows a comparison of the relative responses of each plasticizer and ormosil spot printed on PP and PVDF membranes upon exposure to NH_3 or SO_2 . In general, the plasticizer formulations were favored on PP, whereas the ormosil formulations were favored on PVDF. There were exceptions, however, and the most responsive dye/formulation combination was dependent on both dye identity and substrate (**Table 2.4**). When printed on PP, the SO_2 sensitive spots showed a universal increase in response when immobilized in a plasticizer versus ormosil matrix. This trend was not observed with the spots printed on PVDF, and all but bromothymol blue + TBAH showed a higher response when immobilized in ormosils. The higher signal for the plasticizer immobilized dyes was likely due to improved spot uniformity and color intensity (**Figure 2.10**), apparent in the before and after images of the bromothymol blue + TBAH on both PP and PVDF. Spot response was not solely dependent on dye concentration, as many of the plasticizer spots were more sensitive despite a lower dye concentration (e.g., methyl red + TBAH). The Nile red and fluorescein dyes (NH_3 sensitive) showed a much higher response when immobilized in ormosils versus plasticizer, and the before images showed a discrepancy in the starting color of these dyes when immobilized in plasticizer versus ormosil. We speculate this may be due to non-optimal spot pH or differences in matrix polarity. Array-to-array reproducibility was similar between ormosil and plasticizer immobilized dyes (**Table 2.4**).

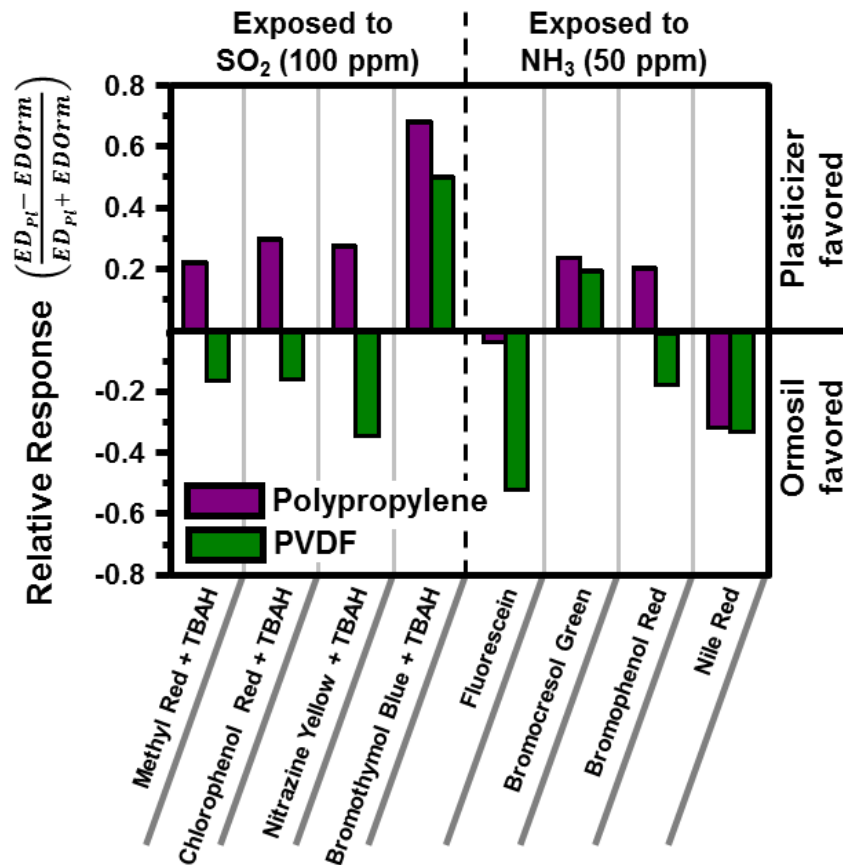


Figure 2.9 Comparison of plasticizer and ormosil immobilized colorants printed on polypropylene and polyvinylidene difluoride (PVDF) and exposed to SO₂ (100 ppm) or NH₃ (50 ppm).

Table 2.4 Average Euclidean distances and standard deviations for dyes immobilized in plasticizers or ormosils. The most responsive formulation/substrate combination for each dye is shown in boldface.

	Polypropylene		PVDF	
	Plasticizer	Ormosil	Plasticizer	Ormosil
Methyl red + TBAH	65.9 ± 1.6	42.0 ± 3.1	51.2 ± 2.1	70.5 ± 4.8
Chlorophenol red + TBAH	128.2 ± 4.1	69.2 ± 3.9	54.3 ± 1.7	73.7 ± 6.6
Nitrazine yellow + TBAH	163.2 ± 6.4	93.1 ± 2.3	56.3 ± 2.6	114.2 ± 4.8
Bromothymol blue + TBAH	185.4 ± 4.1	35.1 ± 2.9	133.8 ± 4.3	44.6 ± 8.7
Fluorescein	56.0 ± 1.4	60.5 ± 3.3	29.4 ± 1.6	93.6 ± 5.6
Bromocresol green	185.1 ± 3.6	114.2 ± 3.2	197.0 ± 8.1	132.7 ± 3.2
Bromophenol red	136.7 ± 3.5	89.6 ± 2.0	77.2 ± 2.8	108.4 ± 3.0
Nile red	1.6 ± 0.3	3.0 ± 0.8	10.7 ± 1.9	21.2 ± 1.7

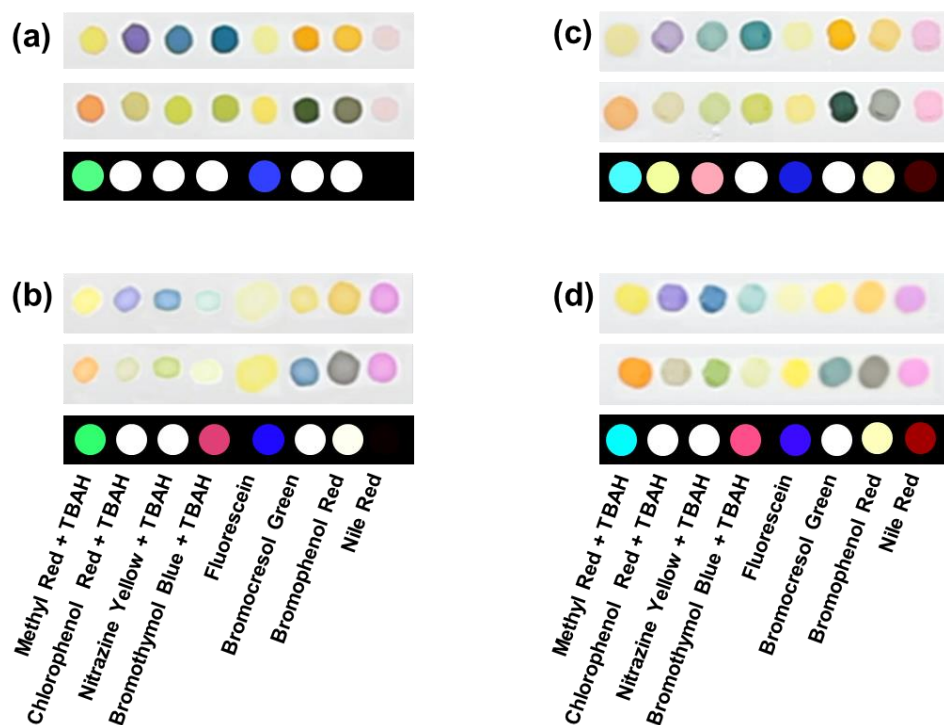


Figure 2.10 Raw images and difference maps for arrays of plasticizer (**a and c**) and ormosil (**b and d**) immobilized colorants printed on polypropylene (**a and b**) or polyvinylidene difluoride (**c and d**) membranes upon exposure to SO₂ (100 ppm) or NH₃ (50 ppm). Within the images for each formulation: (**top**) image of array before exposure, (**middle**) image of array after exposure, and (**bottom**) difference map. For display purposes, the color ranges of these difference maps are expanded from five to eight bits per color (RGB range of 2-33).

2.4 Conclusions

This work has demonstrated the importance and interdependence of geometry, substrate, and immobilization method on colorimetric sensor array response. Linearization of the array provides many benefits, including a more uniform response, a higher overall signal, a shorter response time, and better reproducibility. Additionally, a linear array has greater experimental versatility than a two-dimensional array: e.g., linear arrays are suitable for kinetic measurements and may be imaged with one-dimensional (line) scanners with much higher scan rates. Arrays printed in ormosil formulations on impermeable substrates have longer response times than those printed on permeable substrates, likely caused by a lack of hierarchical porosity and limited analyte diffusion through the sensor spot. The difference in response time of the less-porous PVDF arrays and the more-porous PP arrays provides further evidence of the importance of substrate porosity in sensor response time. Cellulose substrates have intermediate response times,

but also have higher noise due to their highly textured surface. Arrays printed on porous polymer membranes exhibited the fastest reaction times, the best reproducibility, and the lowest noise. The optimum immobilization matrix is highly dependent on dye identity, formulation, and substrate. In general, plasticizer formulations were preferred for PP while ormosil formulations were preferred for PVDF.

2.5 References

1. Askim, J. R.; Mahmoudi, M.; Suslick, K. S., Optical sensor arrays for chemical sensing: the optoelectronic nose. *Chemical Society Reviews* **2013**, *42* (22), 8649-8682.
2. Diehl, K. L.; Anslyn, E. V., Array sensing using optical methods for detection of chemical and biological hazards. *Chemical Society Reviews* **2013**, *42* (22), 8596-8611.
3. Guillermo, O.; Moreno-Bondi, M. C.; Garcia-Fresnadillo, D.; Marazuela, M. D., The interplay of indicator, support and analyte in optical sensor layers. In *Frontiers in Chemical Sensors*, Springer: 2005; pp 189-225.
4. Lim, S. H.; Feng, L.; Kemling, J. W.; Musto, C. J.; Suslick, K. S., An optoelectronic nose for the detection of toxic gases. *Nature chemistry* **2009**, *1* (7), 562-567.
5. Zhu, Z.; Garcia-Gancedo, L.; Flewitt, A. J.; Xie, H.; Moussy, F.; Milne, W. I., A critical review of glucose biosensors based on carbon nanomaterials: carbon nanotubes and graphene. *Sensors* **2012**, *12* (5), 5996-6022.
6. Jerónimo, P. C.; Araújo, A. N.; Montenegro, M. C. B., Optical sensors and biosensors based on sol-gel films. *Talanta* **2007**, *72* (1), 13-27.
7. Rottman, C.; Grader, G.; De Hazan, Y.; Melchior, S.; Avnir, D., Surfactant-induced modification of dopants reactivity in sol-gel matrixes. *Journal of the American Chemical Society* **1999**, *121* (37), 8533-8543.
8. Costa-Fernández, J.; Sanz-Medel, A., Air moisture sensing materials based on the room temperature phosphorescence quenching of immobilized mercurochrome. *Analytica chimica acta* **2000**, *407* (1), 61-69.
9. Suslick, K. S.; Bailey, D. P.; Ingison, C. K.; Janzen, M.; Kosal, M. E.; McNamara III, W. B.; Rakow, N. A.; Sen, A.; Weaver, J. J.; Wilson, J. B., Seeing smells: development of an optoelectronic nose. *Quimica Nova* **2007**, *30* (3), 677-681.
10. Suslick, K. S.; Rakow, N. A.; Sen, A., Colorimetric sensor arrays for molecular recognition. *Tetrahedron* **2004**, *60* (49), 11133-11138.

11. Rakow, N. A.; Suslick, K. S., A colorimetric sensor array for odour visualization. *Nature* **2000**, *406* (6797), 710-713.
12. Suslick, K. S., An optoelectronic nose:“seeing” smells by means of colorimetric sensor arrays. *MRS bulletin* **2004**, *29* (10), 720-725.
13. Salinas, Y.; Ros-Lis, J. V.; Vivancos, J.-L.; Martínez-Máñez, R.; Aucejo, S.; Herranz, N.; Lorente, I.; Garcia, E., A chromogenic sensor array for boiled marinated turkey freshness monitoring. *Sensors and Actuators B: Chemical* **2014**, *190*, 326-333.
14. Soga, T.; Jimbo, Y.; Suzuki, K.; Citterio, D., Inkjet-printed paper-based colorimetric sensor array for the discrimination of volatile primary amines. *Analytical chemistry* **2013**, *85* (19), 8973-8978.
15. Torsi, L.; Magliulo, M.; Manoli, K.; Palazzo, G., Organic field-effect transistor sensors: a tutorial review. *Chemical Society Reviews* **2013**, *42* (22), 8612-8628.
16. Grinthal, A.; Aizenberg, J., Adaptive all the way down: building responsive materials from hierarchies of chemomechanical feedback. *Chemical Society Reviews* **2013**, *42* (17), 7072-7085.
17. Tamayo, J.; Kosaka, P. M.; Ruz, J. J.; San Paulo, Á.; Calleja, M., Biosensors based on nanomechanical systems. *Chemical Society Reviews* **2013**, *42* (3), 1287-1311.
18. Janzen, M. C.; Ponder, J. B.; Bailey, D. P.; Ingison, C. K.; Suslick, K. S., Colorimetric sensor arrays for volatile organic compounds. *Analytical chemistry* **2006**, *78* (11), 3591-3600.
19. Kemling, J. W.; Qavi, A. J.; Bailey, R. C.; Suslick, K. S., Nanostructured substrates for optical sensing. *The journal of physical chemistry letters* **2011**, *2* (22), 2934-2944.
20. MacCraith, B.; McDonagh, C.; O'Keeffe, G.; McEvoy, A.; Butler, T.; Sheridan, F., Sol-gel coatings for optical chemical sensors and biosensors. *Sensors and Actuators B: Chemical* **1995**, *29* (1), 51-57.
21. Steinberg, I. M.; Lobnik, A.; Wolfbeis, O. S., Characterisation of an optical sensor membrane based on the metal ion indicator Pyrocatechol Violet. *Sensors and Actuators B: Chemical* **2003**, *90* (1), 230-235.
22. Lukowiak, A.; Streck, W., Sensing abilities of materials prepared by sol-gel technology. *Journal of sol-gel science and technology* **2009**, *50* (2), 201-215.
23. Podbielska, H.; Ulatowska-Jarża, A.; Müller, G.; Eichler, H. J., Sol-Gels for Optical Sensors. In *Optical Chemical Sensors*, Springer: 2006; pp 353-385.

24. Kemling, J. W.; Suslick, K. S., Nanoscale porosity in pigments for chemical sensing. *Nanoscale* **2011**, *3* (5), 1971-1973.
25. Lim, S. H.; Kemling, J. W.; Feng, L.; Suslick, K. S., A colorimetric sensor array of porous pigments. *Analyst* **2009**, *134* (12), 2453-2457.
26. Feng, L.; Musto, C. J.; Kemling, J. W.; Lim, S. H.; Suslick, K. S., A colorimetric sensor array for identification of toxic gases below permissible exposure limits. *Chem. Commun.* **2010**, *46* (12), 2037-2039.
27. Levitsky, I.; Krivoshlykov, S. G.; Grate, J. W., Rational design of a Nile Red/polymer composite film for fluorescence sensing of organophosphonate vapors using hydrogen bond acidic polymers. *Analytical chemistry* **2001**, *73* (14), 3441-3448.
28. Johnson, R. D.; Bachas, L. G., Ionophore-based ion-selective potentiometric and optical sensors. *Analytical and bioanalytical chemistry* **2003**, *376* (3), 328-341.
29. Feng, L.; Musto, C. J.; Kemling, J. W.; Lim, S. H.; Zhong, W.; Suslick, K. S., Colorimetric sensor array for determination and identification of toxic industrial chemicals. *Analytical chemistry* **2010**, *82* (22), 9433-9440.
30. Suslick, B. A.; Feng, L.; Suslick, K. S., Discrimination of complex mixtures by a colorimetric sensor array: coffee aromas. *Analytical chemistry* **2010**, *82* (5), 2067-2073.
31. Zhang, C.; Bailey, D. P.; Suslick, K. S., Colorimetric sensor arrays for the analysis of beers: a feasibility study. *Journal of agricultural and food chemistry* **2006**, *54* (14), 4925-4931.
32. Zhang, C.; Suslick, K. S., Colorimetric sensor array for soft drink analysis. *Journal of agricultural and food chemistry* **2007**, *55* (2), 237-242.
33. Carey, J. R.; Suslick, K. S.; Hulkower, K. I.; Imlay, J. A.; Imlay, K. R.; Ingison, C. K.; Ponder, J. B.; Sen, A.; Wittrig, A. E., Rapid identification of bacteria with a disposable colorimetric sensing array. *Journal of the American Chemical Society* **2011**, *133* (19), 7571-7576.

Chapter 3:

RGB versus Spectrophotometric Systems for Detection of Colorimetric Sensor Arrays

3.1 Introduction

Colorimetric sensor arrays, the properties of which were explored in **Chapter 2**, are a powerful tool made up of a series of optical sensors that can be used to detect the chemical environment. The term “optical sensor” is used to signify the signal transduction method used to measure sensor response. In contrast to electrical sensors that measure resistance or capacitance¹⁻³ or thermometric sensors that rely on the measurement of local heat change,⁴ optical sensors use visible or ultraviolet light to interrogate sensors for analysis.

In general, optical sensors can be broken up into 3 components: the light source, the sensor material used to interact with analytes, and a light detector (**Figure 3.1**). Several types of interactions and transitions can occur when light (covering different regions of the electromagnetic spectrum) interacts with a sensing material, such as scattering, diffraction, absorbance, reflectance, photoluminescence, and chemiluminescence and, depending on the detection method, multiple properties can be measured (e.g., intensity of light, lifetime, polarization, etc.).^{5, 6} Colorimetric sensor arrays, in particular, rely on colorimetry which is the quantitative measurement of reflectance or absorbance spectra.

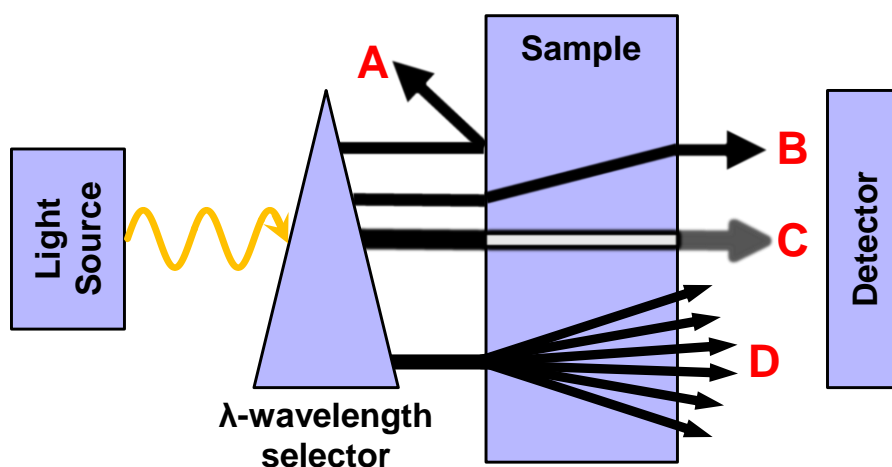


Figure 3.1 General arrangement of spectroscopic measurements: (A) light reflection; (B) light refraction; (C) light absorbance (D) fluorescent emission. Reproduced with permission of The Royal Society of Chemistry.⁷

One of the first physical methods used in analytical chemistry was based on the color quality (i.e., hue, depth, intensity) of solutions or, more recently, solid state optical sensor arrays.⁸ Colorimetry can be used to identify a species based on hue or identify the concentration of that species based on the color's intensity. There are a number of detection methods used in colorimetry, from the most simple three color (i.e., RGB) imaging used in digital imaging devices such as scanners and cameras to the more complex full spectrophotometry (i.e., hundreds of color channels with nanometer resolution). While colorimetry can be applied to various types of optical sensors, the following discussion will pertain to RGB-based imaging and spectrophotometry as they are relevant to the detection of colorimetric sensor arrays.

The rapid spread of highly capable, inexpensive consumer electronics has ignited a spark in the science community to exploit this technology to bring automated chemical analysis and analytical diagnostics to the general public. Thus one of the marked advantages of RGB imaging is that it is simple, fast, and affordable. In cases where measurements must be taken on a large number of samples, as is the case with the numerous sensor spots in a colorimetric sensor array, all the data needed at a given timepoint is contained in a single image. However, there are a number of considerations that must be made in the attempt to turn RGB imaging devices (e.g., cell-phone camera, digital camera, flatbed scanner) into a reliable method for recovering spectral information as there are a number of characteristics inherent in the device itself that can be problematic.⁹

To understand these drawbacks, it is necessary to comprehend the way an image is formed when using this technology. Object information, when captured by a digital imaging device, is calculated in terms of a color signal, which is a product of the object's spectral reflectance and the illuminant. The manner in which spectral reflectance is handled to yield the red, green and blue values obtained from each image is device-dependent and is contingent on a number of factors. If a linear response is assumed, the response of the k^{th} ($k=1,2,3$ for three-color channels) sensor at a pixel can be given as:¹⁰

$$v_k = \int_{\lambda_L}^{\lambda_H} f_k(\lambda) d(\lambda) r(\lambda) l_s(\lambda) d\lambda + n_k$$

Where $f_k(\lambda)$ is the spectral transmittance of the k th color filter, $d(\lambda)$ is the spectral sensitivity of the detector in the measurement, $r(\lambda)$ is the spectral reflectance of the object being scanned, $l_s(\lambda)$ is the spectral radiance of the illuminant, and n_k is time-dependent noise. The spectral window for each color channel can be chosen using color filters on the detector surface, a dispersing element (e.g., gratings, prisms) or narrowly tuned light sources. Flatbed scanners, the RGB-system used in the study, typically rely on color filters (**Figure 3.2**). A study by Shen and Xin¹¹ presented an estimate of the spectral responsivity of a flatbed scanner (Epson GT-10000+) using adaptive estimation (**Figure 3.2**) where the full width half maximum (FWHM) of each color channel is approximately 50 nm. As one can imagine, the width and sensitivity of these color channels are subject to change from manufacturer to manufacturer depending on the filters-detector combination used, so when one desires to calibrate the response of an optical sensor using these devices, the obtained output is only valid using the same device for imaging.

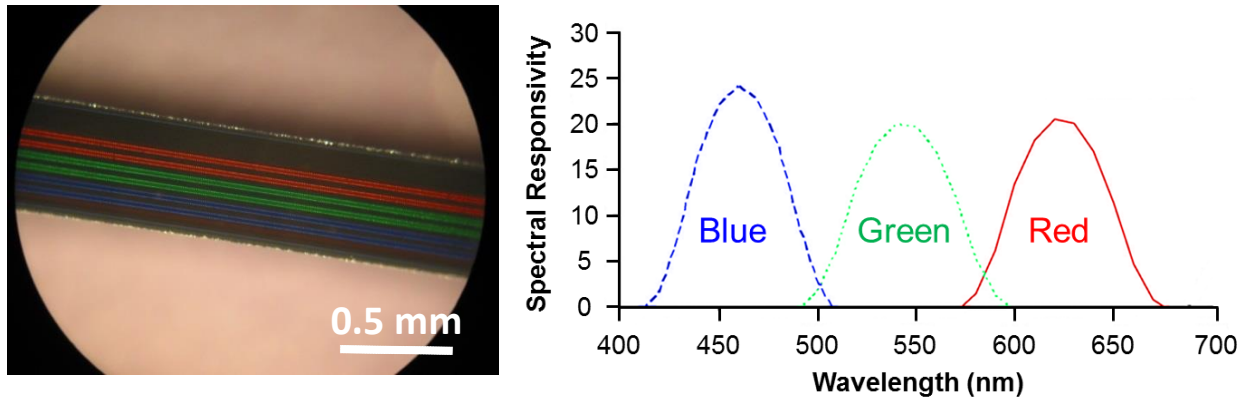


Figure 3.2 (left) Microscope image of RGB-filtered CCD detector in flatbed scanner and (right) Recovered spectral responsivity of Epson GT-10000+ using adaptive estimation.¹¹

As mentioned above, in addition to dependency on device components, spectral reflectance is also illuminant-dependent. While flatbed scanners have a light source built in to account for this fact, other imaging devices (e.g., mobile phone cameras, digital cameras) are subject to changes in ambient lighting (unless additional steps are taken to control this). Thus the spectral sampling of cumulative energy from a broad range of wavelengths in select portions of the visible spectrum coupled with changes in illumination can give rise to a phenomenon called metamerism, a problem in applications requiring color discrimination.¹² Two materials are termed a metameric pair when the perceived color of these objects match without matching their

spectral power distribution. For this reason, RGB-based devices are generally considered metameric imaging devices; they are similar to the human visual system, which uses three types of cone receptors to process spectral data over the visible wavelength range of 380-780 nm in order to produce a three-channel color image.¹³

Another drawback to RGB-based devices is that most do not give a digital output in the form of raw pixel response but have built-in post-processing steps (e.g., white balance, color interpolation, color correction, gamma correction, color space conversion, saturation enhancement, compression, etc.) that undoubtedly have an effect on reflectance values.^{14, 15} These additional steps stem from the fact that RGB cameras were not built with the idea of recovering spectral information, but rather of obtaining an image that is visually pleasant for the observer.

Therefore, when using RGB-imaging capable of accurate and precise colorimetry, it is necessary to create an imaging platform that ensures control over the above variables. This requires uniform lighting (e.g., elimination of stray light, consistent light source, post-processing using an internal reference to correct for lighting inconsistencies), accurate positioning of the sample within the frame of the image, and accounting for the device-dependent methods of detection and output (either by using post-processing steps or ensuring the device used to create the library is the same device used for detection). There has been considerable innovation in this area and various applications can be found in the literature.¹⁶⁻²⁰

Spectral-based systems, on the other hand, have a long history of use in the field of colorimetry, and therefore are well-understood and have numerous setups readily available both commercially (e.g., portable spectrophotometers from HunterLab, Konica Minolta, x-rite, Hach, etc.) and developed in the academic community²¹⁻²⁴ for reliable colorimetric measurements. Additionally, this spectral-based measurement method offers high spectral dimensionality (i.e., a continuous spectrum for sample), allows access to the UV portion of the spectrum, and gives information on the electronic structure of the dye. However, there are drawbacks: for instance, even the most affordable spectral-imaging devices are far more expensive than RGB-imaging devices, they require higher processing power, further adjustments may need to be made to the measurement setup for a given application, and data collection tends to be slow especially in evaluating a large number of samples at once (for a single channel spectrometer).

While each of these methods has been employed for the detection of colorimetric sensors, comprehensive analyses of the pros and cons (quantitative and qualitative) for each method has not, to our knowledge, been explored. This study in particular will focus on two metrics important for the accurate detection and differentiation of target analytes using colorimetric sensor arrays. As a measure of each method's potential for discriminating among analytes, we report the variance of multiple relevant parameters between trials. Additionally, limit of detection (LOD) is reported as a measure of signal to noise and detection ability.

3.2 Materials and Methods

3.2.1 Materials

All reagents were of analytical grade and used without any further purification. Certified, premixed gas tanks were obtained from Matheson Tri-Gas through S.J. Smith. Arrays were printed on a polyvinylidene difluoride (PVDF) membrane (VWR Scientific, Batavia, IL; thickness: 165 μm , pore size: 0.45 μm).

3.2.2 Formulation Preparation

Four pH indicator dyes (**Figure 3.3**) immobilized in an ormosil matrix were chosen as the benchmark sensors in this study. Ormosil solutions were prepared according to previous methods.²⁵ Briefly, ormosil formulations were prepared by acid-catalyzed hydrolysis of solutions containing commercially-available silane precursors and low concentrations of surfactant dissolved in low volatility solvents. The surfactant acts to reduce capillary stress and improve print quality and the low volatility solvents act as porogens on the nanometer scale.

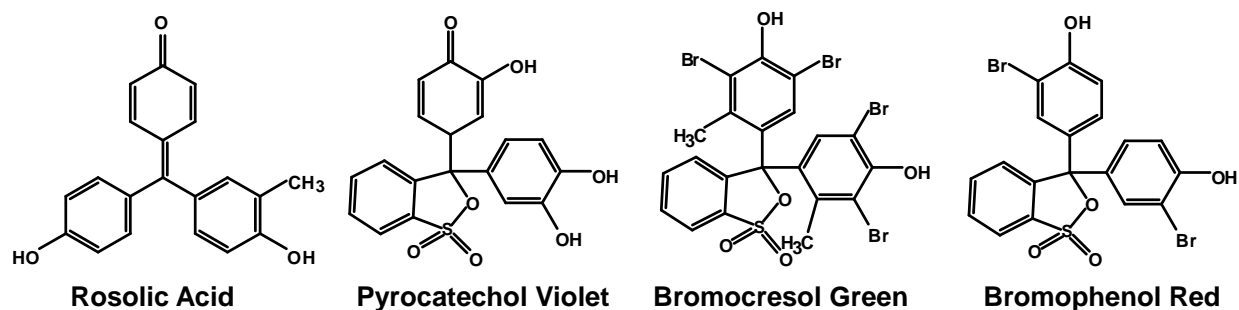


Figure 3.3 Molecular structure of four pH indicator dyes used in this study.

3.2.3 Array Printing

Formulations with chemoresponsive dyes were loaded into a Teflon ink well with a 3×12 pattern of $\sim 50 \mu\text{L}$ holes. An ArrayIt NanoPrint LM60 Microarray Printer (ArrayIt Corporation, Sunnyvale, CA) holding five 0.787 mm diameter floating pins was used to robotically print arrays in one pass by dipping into the ink well and transferring to the substrate. The diameter of the sensor spot after printing was roughly 1 mm to ensure the spot area filled the entire sampling area of the reflectance probe. Before use, arrays were stored in a nitrogen-filled glove bag for three days.

3.3 Experimental Procedure

Gas mixtures were prepared according to previous methods. Briefly, MKS mass flow controllers were used to achieve gas streams with the desired concentration (0, 10, 50, 150, 300, 600 ppm NH_3), flow (500 sccm) and relative humidity (50% RH) by mixing the appropriate amount of stock gas with wet (100% RH) and dry (0% RH) nitrogen gas. A MKS multigas analyzer (model 2030) was used in-line to verify gas concentrations. A diagram of the setup is shown in **Chapter 2 (Figure 2.1)**.

Sensor spots printed on strips of PVDF membrane were placed in the bottom channel of a custom designed flow cell machined from aluminum (**Figure 3.4**) with channel dimensions of $4 \times 0.5 \times 65$ mm. To hold the sensor spots in place, a small amount of silicon grease was placed at either end of the PVDF strips. An O-ring was placed in a groove around the channel and compressed by a quartz slide using screws at either end of the holder to create a leak-free seal.

Arrays were exposed to a control stream (50% RH N₂) for 3 min followed by 2 minutes (time required for sensor spots to reach equilibrium uptake regime) of a calibrated 50% RH analyte stream with 0, 10, 50, 150, 300, or 600 ppm ammonia. For spectral measurements, separate trials were run for each sensor spot (due to the use of a single-channel spectrophotometer) whereas all four sensor spots were exposed together for each trial with the RGB-based system (i.e., all four spots captured in a single image).

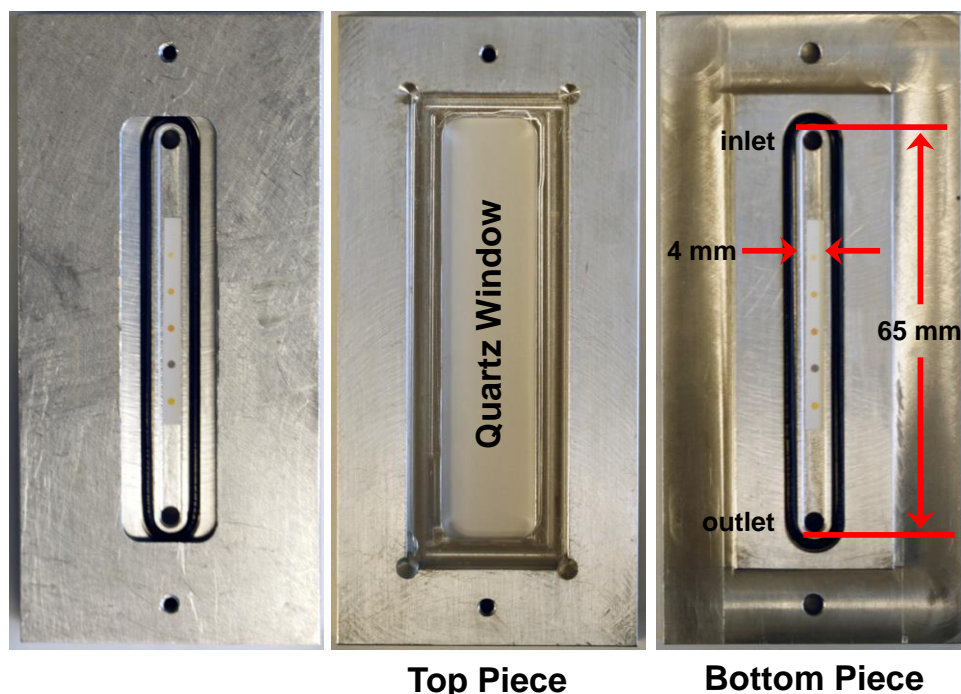


Figure 3.4 Photographs of (left) fully assembled aluminum array holder; (middle) top piece to array holder with quartz window and (right) bottom piece to array holder with array placed in the bottom of the channel (dimensions: $4 \times 0.5 \times 65$ mm), o-ring in a groove around the channel, and gas inlet and outlet. The pieces are put together using two screws at the top and the bottom of the holder.

An Epson Perfection V600 photo scanner (model RGB-based system) captured 1200 dpi images of the entire 4 spot array every 30 seconds during control and analyte exposure. A Prime-X™ back-thinned CCD array spectrometer (2.5 nm resolution), Deuterium (30 W)-Tungsten (5 W) light source, and fiber optic reflectance probe (R600-8-UVVIS-SR) with fibers in a 7 (400 μ m illuminates) around 1 (600 μ m read fiber) configuration was used to obtain spectral reflectance measurements every 30 seconds during control and analyte exposure for each spot. It was found that the read diameter for this probe at the height used for these experiments (~ 5 mm from surface of the array) is around 1 mm. A custom system to obtain *in-situ* spectral

measurements of sensor spots during exposure was fabricated by the University of Illinois School of Chemical Sciences Machine Shop. This system, shown in **Figure 3.5**, holds the reflectance probe at a fixed position above the array surface (i.e., height: 5 mm, angle: 80° to eliminate spectral reflectance off of quartz cover slide) to minimize within-trial and between-trial inconsistencies in reflectance measurement. The array holder was placed on an x-y translational stage adapted to hold the array in place during measurement and enable precise movement of sensor spots into the optimal sampling area (highest reflectance signal). This setup was placed in a custom-made black box to isolate the system from ambient lighting.

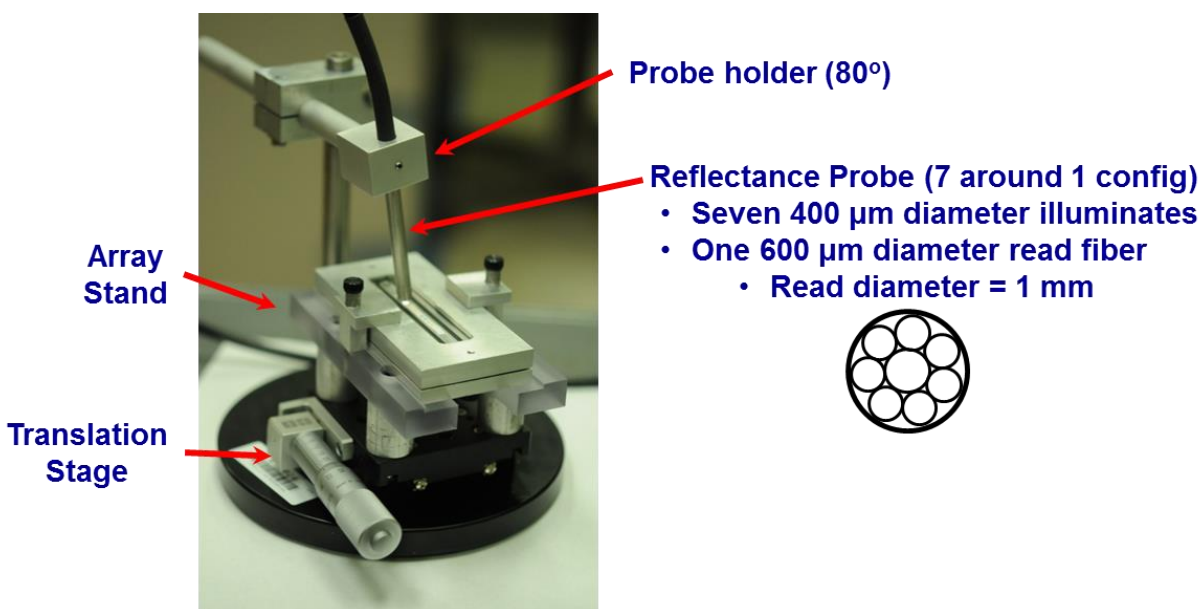


Figure 3.5 Image of custom setup to measure UV-Vis reflectance spectrum of colorimetric sensor spots during exposure to analyte. Setup consists of an array stand to hold array holder in place during measurement, x-y translation stage for precise movement of sensor spots into probe sampling area, probe holder tilted at an 80° angle to minimize spectral reflectance off of quartz slide and fiber optic reflectance probe with seven illumination fibers and one read fiber in a 7 around 1 configuration (shown in bottom right portion of figure).

3.4 Data Processing and Analysis

To prepare each spectrum for analysis, the areas of the spectrum distorted by hydrogen emission lines (characteristic of the deuterium light source) were removed (i.e., four points from 485.35-487.76 nm and six points from 654.08-657.89 nm) and then each section around these points were smoothed separately using a Savitzky-Golay 20-point smoothing filter (20 points

chosen due to literature suggestion that the optimum width of a smoothing array be 0.7 times the FWHM of narrowest Gaussian line of spectra).

From there, data pre-treatment for RGB and spectral data was kept consistent for both techniques. First reflectance values (R) were converted to pseudo-absorbance (A') using the Kubelka-Munk approximation $A' (K - M \text{ units}) = (1 - R)^2 / 2R$ where R corresponds to RGB values (RGB data) or reflectance at each wavelength (spectral data). Then, each spectrum within a given trial was normalized to the tallest peak in the 0 min exposure spectrum.

3.5 Results and Discussion

Upon interaction with ammonia, each sensor spot undergoes a characteristic color change due to changes in the electronic structure of the dye (i.e., deprotonation of substituent groups, opening of thiolactone ring in sulfonephthalein dyes).²⁶ This change can be observed visually or spectrally (**Figure 3.6**). Spectrally, as the pH of the environment changes around these sensor spots, the entire absorbance spectrum of the spot undergoes a transformation (e.g., disappearance of one peak and appearance of others in another portion of the spectrum). The number of unique peaks present in each spectrum depends on the number of pH-sensitive substituents (e.g., -OH, -SO₃H) of the dye. Labelled by the grey arrows in **Figure 3.6**, three out of the four dyes (rosolic acid, bromocresol green, bromophenol red) transition between two species as pH is increased, whereas pyrocatechol violet transitions between three

(Species A $\xrightarrow{\text{Transition 1}}$ Species B $\xrightarrow{\text{Transition 2}}$ Species C).²⁷

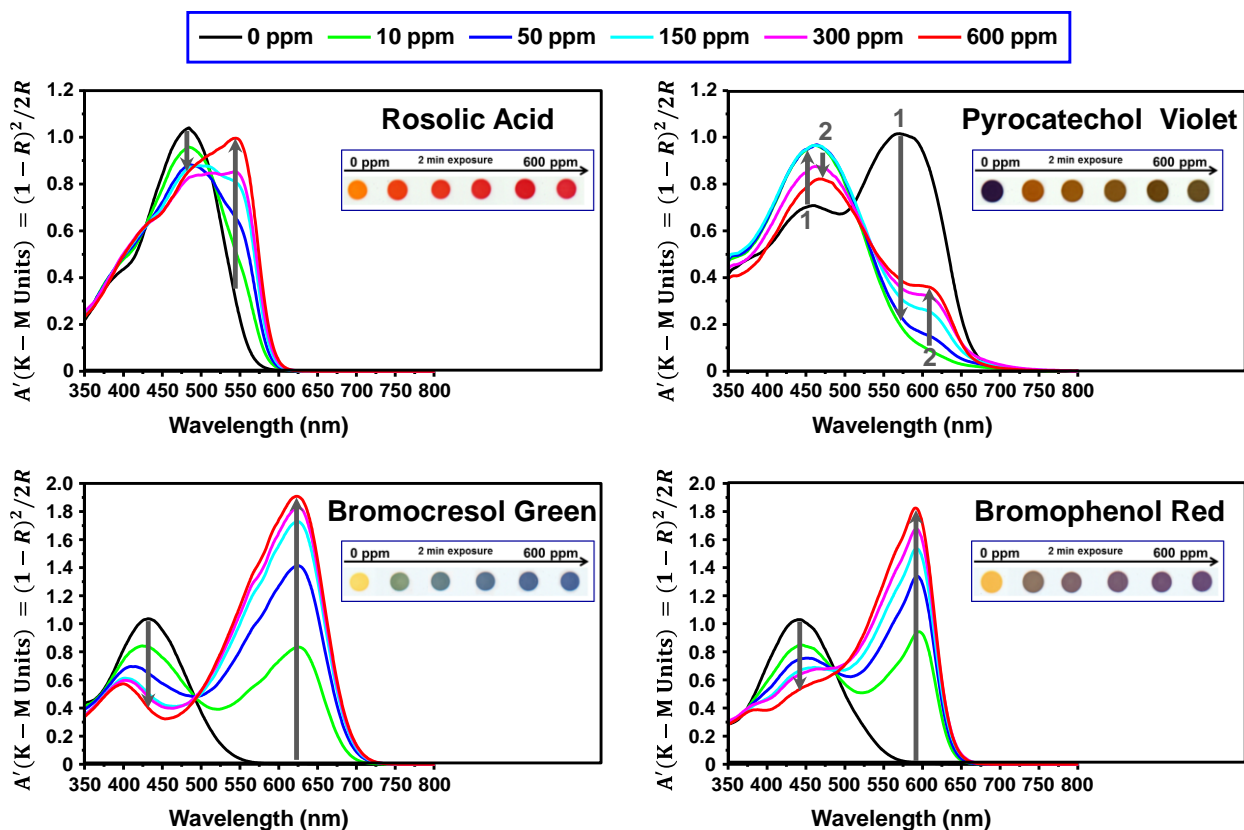


Figure 3.6 Pseudo-absorbance spectrum in Kubelka-Munk units of the four dyes used in this study (rosolic Acid, pyrocatechol violet, bromocresol green, bromophenol red) exposed to ammonia (10-600 ppm) for 2 min. Grey arrows indicate direction of change in peaks (where change in peaks indicates the transition of the dye from one species to another) with increasing pH of the environment. Pyrocatechol violet transitions between three species (Species A $\xrightarrow{\text{Transition 1}}$ Species B $\xrightarrow{\text{Transition 2}}$ Species C) as pH increases while the other indicators transition between two. Photographs of visual change in spot color with increased ammonia concentration for the four indicators are shown in the graph area.

3.5.1 Variance

For comparison to the ΔRGB values obtained from the flatbed scanner, a difference spectrum ($R_t - R_{0 \text{ min}}$ vs. wavelength) was generated for spectral data. The difference spectrum for each spot was divided into the peaks which represent areas of pH-dependent changes (**Figure 3.7**). These changes can also be monitored with the ΔRGB values from images taken using the flatbed scanner (**Figure 3.7**). From each of the spectral peaks, parameters to distinguish between analytes (i.e. peak height, peak position, FWHM, area) were used for a variance comparison to

the RGB values (**Figure 3.8**). **Table 3.1** gives variance data for the tallest peak in both spectral and RGB data.

If we compare variation in ΔRGB values and relevant parameters for the spectral data, we see comparable reproducibility between both methods. While reproducibility is an indicator of separation ability, further experiments are necessary to determine whether an improvement in separation ability will be achieved in moving from RGB to spectral data acquisition.

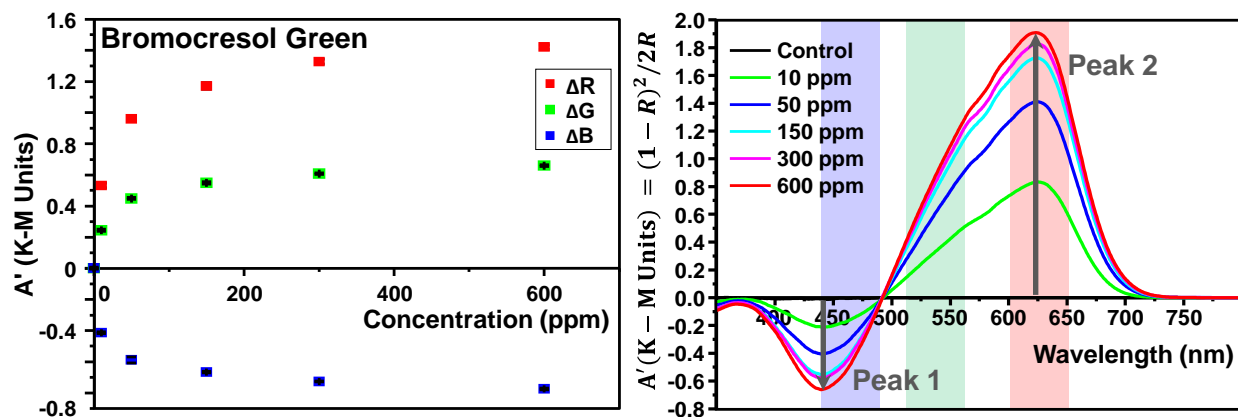


Figure 3.7 Response characteristics for bromocresol green printed on polyvinylidene difluoride upon exposure to NH_3 (0-600 ppm) for 2 min. (**left**) ΔRGB taken with flatbed scanner and (**right**) average difference spectra ($R_t - R_0 \text{ mins}$ vs. wavelength) in Kubelka-Munk units taken with reflectance probe. Red, green and blue bars on graph of difference spectra indicate the area of the spectrum where RGB values are calculated using the flatbed scanner. Grey arrows indicate direction of change in peaks with increasing pH of the environment. All trials were done in triplicate.

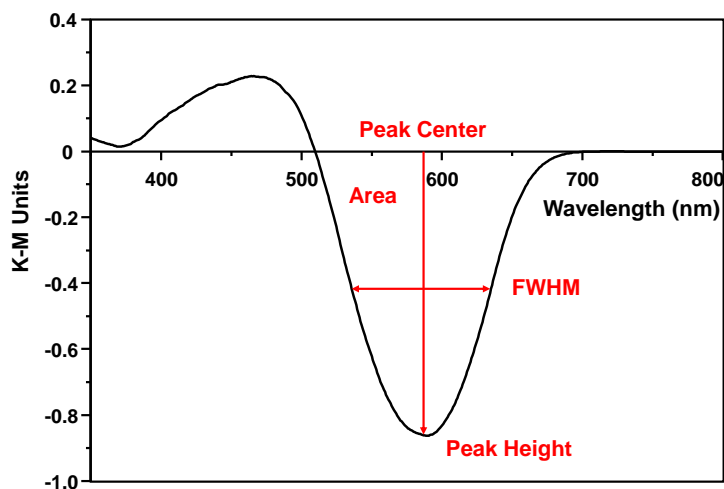


Figure 3.8 Peak parameters (i.e. peak height, peak position, FWHM, area) from the difference spectra that can be used to measure spectral changes in sensor spots.

Table 3.1 Averaged variance data for largest peak in spectral and RGB data.

	Spectrophotometric				RGB
	Peak Center	FWHM	Height	Area	$\Delta R, G, \text{ or } B$
	Average Standard Dev. (nm)	Average RSD (%)			Average RSD (%)
Bromocresol Green	1.29	0.9	5.3	5.4	1.7 (ΔR)
Bromophenol Red	0.49	1.4	2.2	2.8	1.3 (ΔG)
Rosolic Acid	0.09	0.8	1.3	1.7	3.9 (ΔB)
Pyrocatechol Violet	0.37	2.3	2.3	2.3	5.3 (ΔB)
Average	0.56	1.4	2.8	3.1	3.1

3.5.2 Limit of Detection (LOD)

Since variance decreases at lower concentrations and variance is roughly proportional to concentration, limit of detection (LOD) can be extrapolated based on variance at higher concentrations by plotting $LOD = (3 * N * [A])/S_t$ versus concentration (ppm) where $[A]$ is analyte concentration in ppm and $S_t = S_{2\ min} - S_{0\ min}$ for each peak or RGB channel. Peak height and ΔR , ΔG , and ΔB values during analyte exposure were used as the signal (S) and noise (N) was taken as the standard deviation in these parameters (at wavelength equivalent to signal) for control measurement over all trials. A second order polynomial fit is used to extrapolate where $LOD = [A]$ (**Figure 3.9**). From this, the channel or peak (in every case the largest peak or RGB channel with the largest change) that gives the lowest LOD is taken as the LOD for that spot (**Figure 3.10**). The spectral method provides an LOD approximately half that of the RGB method. This outcome points to one of the major benefits of using the spectrophotometry over the RGB method: the ability to adjust analysis parameters to maximize the signal from each indicator-analyte interaction (i.e., using signal from only the most responsive area in spectrum).

Bromocresol Green

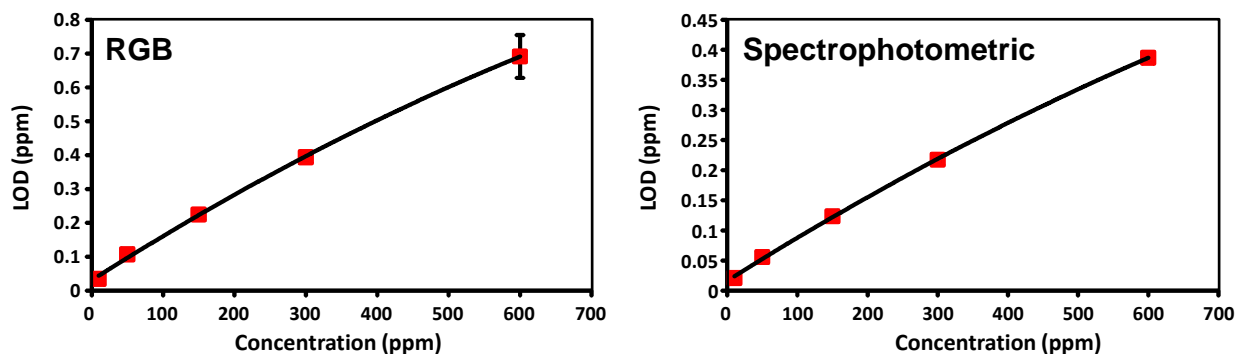


Figure 3.9 Plot of limit of detection ($LOD = (3 * N * [A]) / S_t$) versus concentration (ppm) where $[A]$ is analyte concentration in ppm and $S_t = S_{2\ min} - S_{0\ min}$ for response of bromocresol green sensor spot to ammonia exposure (10-600 ppm). (left) Most responsive channel using RGB system and (right) largest peak using spectrophotometry. These plots can then be used to extrapolate limit of detection for the response of each sensor spot to ammonia.

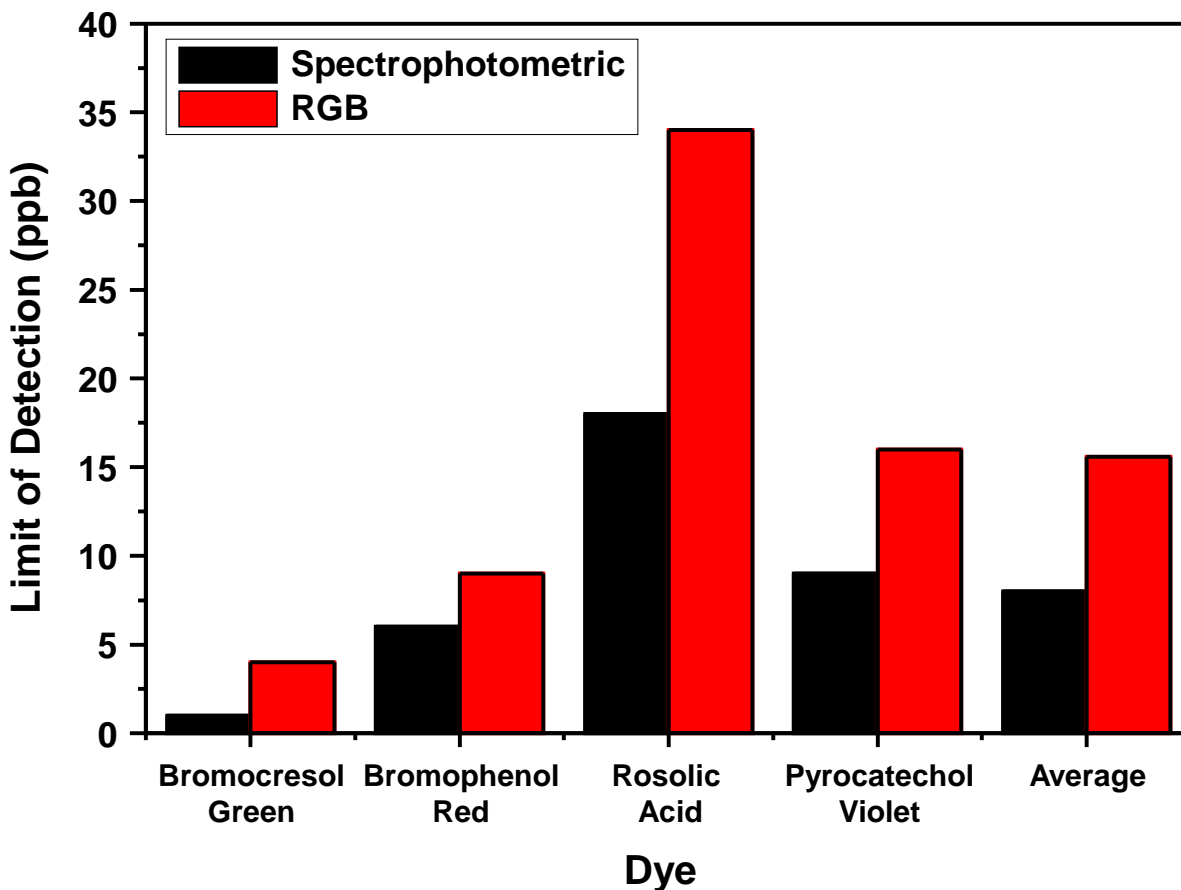


Figure 3.10 Limit of detection vs. dye (ie., bromocresol green, bromophenol red, rosolic acid, and pyrocatechol violet) for each detection method (ie., spectrophotometric vs. RGB-imaging).

3.6 Conclusions and Outlook

A system for *in-situ* reflectance measurement of changes in colorimetric sensors in response to ammonia has been developed. A method to compare performance of an RGB-imaging system to a spectral-based system has been presented. Variance, an indication of separation ability between analytes, was similar between both RGB-imaging and spectral-based systems. Limit of detection was cut in half when the spectrophotometry-based method was employed, suggesting that having the full spectrum of the indicator allows for the adjustment of analysis parameters to maximize the signal from each indicator-analyte interaction (i.e., using signal from only the most responsive area in spectrum).

Further characterization of the sources of error in both systems (i.e., sample positioning, sample preparation, instrument noise) could offer some insight as to whether further improvements could be made. Rothman, Crouch, and Ingle give a detailed outline for the investigation of factors affecting precision in molecular absorption spectrophotometry that could be utilized to investigate both systems.^{28, 29}

3.7 References

1. Janata, J., *Principles of chemical sensors*. Springer Science & Business Media: 2010.
2. Stetter, J. R.; Li, J., Amperometric Gas Sensors A Review. *Chemical Reviews* **2008**, *108* (2), 352-366.
3. Ahmed, M. U.; Hossain, M. M.; Tamiya, E., Electrochemical Biosensors for Medical and Food Applications. *Electroanalysis* **2008**, *20* (6), 616-626.
4. Barsony, I.; Dücső, C.; Fürjes, P., Thermometric gas sensing. In *Solid State Gas Sensing*, Springer: 2009; pp 1-24.
5. Gründler, P.; Janata, J., Chemical sensors: an introduction for scientists and engineers. *Physics Today* **2008**, *61* (3), 56.
6. Jerónimo, P. C. A.; Araújo, A. N.; Conceição B.S.M. Montenegro, M., Optical sensors and biosensors based on sol-gel films. *Talanta* **2007**, *72* (1), 13-27.
7. Askim, J. R.; Mahmoudi, M.; Suslick, K. S., Optical sensor arrays for chemical sensing: the optoelectronic nose. *Chemical Society Reviews* **2013**, *42* (22), 8649-8682.

8. Nassau, K., The physics and chemistry of color: the fifteen causes of color. *The Physics and Chemistry of Color: The Fifteen Causes of Color, 2nd Edition, by Kurt Nassau, pp. 496. ISBN 0-471-39106-9. Wiley-VCH, July 2001. 2001, 1.*
9. Scheeline, A., Cell Phone Spectrometry: Science in Your Pocket? *TrAC Trends in Analytical Chemistry* **2016**.
10. Sharma, G.; Trussell, H. J., Digital color imaging. *Image Processing, IEEE Transactions on* **1997**, 6 (7), 901-932.
11. Shen, H.-L.; Xin, J. H., Spectral characterization of a color scanner by adaptive estimation. *JOSA A* **2004**, 21 (7), 1125-1130.
12. Ohta, N.; Robertson, A., *Colorimetry: fundamentals and applications*. John Wiley & Sons: 2006.
13. Fairchild, M. D.; Rosen, M. R.; Johnson, G. M., Spectral and metameric color imaging. *RIT-MCSL Technical Report* **2001**.
14. Zhou, J.; Glotzbach, J. In *Image pipeline tuning for digital cameras*, Consumer Electronics, 2007. ISCE 2007. IEEE International Symposium on, IEEE: 2007; pp 1-4.
15. Huang, B.-C.; Fuh, C.-S. In *Image pipeline algorithms for standard mobile imaging architecture sensors*, 18th IPPR Conference on Computer Vision, Graphics and Image Processing (CVGIP 2005), 2005.
16. Hong, J. I.; Chang, B.-Y., Development of the smartphone-based colorimetry for multi-analyte sensing arrays. *Lab on a Chip* **2014**, 14 (10), 1725-1732.
17. Guan, L.; Tian, J.; Cao, R.; Li, M.; Cai, Z.; Shen, W., Barcode-like paper sensor for smartphone diagnostics: An application of blood typing. *Analytical chemistry* **2014**, 86 (22), 11362-11367.
18. Jia, M.-Y.; Wu, Q.-S.; Li, H.; Zhang, Y.; Guan, Y.-F.; Feng, L., The calibration of cellphone camera-based colorimetric sensor array and its application in the determination of glucose in urine. *Biosensors and Bioelectronics* **2015**, 74, 1029-1037.
19. Meng, X.; Schultz, C. W.; Cui, C.; Li, X.; Yu, H.-Z., On-site chip-based colorimetric quantitation of organophosphorus pesticides using an office scanner. *Sensors and Actuators B: Chemical* **2015**, 215, 577-583.
20. Debus, B.; Kirsanov, D.; Yaroshenko, I.; Sidorova, A.; Piven, A.; Legin, A., Two low-cost digital camera-based platforms for quantitative creatinine analysis in urine. *Analytica chimica acta* **2015**, 895, 71-79.

21. Yuan, K.; Wu, Y.; Wang, C.; Jin, S., Spectrophotometric colorimeter based on LED light source and method for realizing the same. US Patent 9,243,953: 2016.
22. Chen, X.; Zhou, Y.; Peng, X.; Yoon, J., Fluorescent and colorimetric probes for detection of thiols. *Chemical Society Reviews* **2010**, *39* (6), 2120-2135.
23. Suzuki, Y.; Nakano, N.; Suzuki, K., Portable sick house syndrome gas monitoring system based on novel colorimetric reagents for the highly selective and sensitive detection of formaldehyde. *Environmental science & technology* **2003**, *37* (24), 5695-5700.
24. Germain, M. E.; Knapp, M. J., Optical explosives detection: from color changes to fluorescence turn-on. *Chemical Society Reviews* **2009**, *38* (9), 2543-2555.
25. Feng, L.; Musto, C. J.; Kemling, J. W.; Lim, S. H.; Suslick, K. S., A colorimetric sensor array for identification of toxic gases below permissible exposure limits. *Chemical Communications* **2010**, *46* (12), 2037-2039.
26. Sadaoka, Y.; Sakai, Y.; Yamada, M., Optical properties of sulfonephthalein dyes entrapped within polymer matrices for quantification of ammonia vapour and humidity in air. *Journal of Materials Chemistry* **1993**, *3* (8), 877-881.
27. Cheng, K. L.; Ueno, K.; Imamura, T., *CRC handbook of organic analytical reagents*. Crc Press: 1992.
28. Ingle Jr, J.; Crouch, S., Evaluation of precision of quantitative molecular absorption spectrometric measurements. *Analytical chemistry* **1972**, *44* (8), 1375-1386.
29. Rothman, L.; Crouch, S.; Ingle Jr, J., Theoretical and experimental investigation of factors affecting precision in molecular absorption spectrophotometry. *Analytical chemistry* **1975**, *47* (8), 1226-1233.

Chapter 4:

Colorimetric Sensor Arrays: Development and Application to Art Conservation

4.1 Introduction

This chapter presents a collaborative effort between the University of Illinois, the Getty Conservation Institute, and the Walt Disney Animation Research Library (ARL) to extend, with new sensor array chemistry and detection techniques, an optoelectronic nose technology developed by the Suslick group that has proven to be an exceptionally sensitive, portable and versatile detector for nose technology. **Chapter 1** introduced the state of the art currently for monitoring museum pollutants along with the damaging effects these pollutants can have on cultural heritage pieces. **Chapter 2** introduced colorimetric sensor arrays and the impact of various secondary factors (i.e., immobilization method, sensor geometry and substrate) on sensor performance. **Chapter 3** examined two methods (i.e., RGB imaging and spectrophotometry) for measuring changes in reflectance of sensor spots during exposure to analytes and the viability of RGB-imaging as a method for signal transduction in comparison to the more traditional spectrophotometric methods used in colorimetry was proven. With this knowledge we hope to develop a version of this technology suitable for monitoring museum pollutants and to demonstrate its usefulness in the field of preventive conservation (e.g., to monitor microenvironments surrounding valuable artwork, as a screening method for materials used to house these cultural heritage pieces).

The goal of this project is to show, as a proof of concept, that this technology is capable of providing valuable insight (both qualitative and quantitative) of museum air quality for the protection of cultural heritage objects. **Section 4.3** will present the steps taken to develop sensor spots that are not only selective for main museum pollutants (**Table 1.1**) but can detect these pollutants in the concentration regimes (i.e., at or below the few ppb regime; only ~1% of the permissible exposure limits for humans) in an effort to minimize damage to sensitive collection materials. **Section 4.4** will explore the response characteristics of these sensors in both passive and active environments; important in identifying the best way to use this technology as a tool for conservation professionals (e.g., passive sampling devices to be placed in microenvironments throughout the museum, active sampling devices to sample select microenvironments that show

signs of distress, screening device for construction materials, non-destructive method to gain insight on potentially harmful volatiles coming off artwork materials themselves). **Section 4.4.4.3** will introduce a new method for colorimetric array detection that relies on an imaging platform based on an iPhone camera as a means to detect changes in the array upon exposure to pollutants. **Section 4.5** will present findings from the application of this technology to measure air quality surrounding 8 pieces from Walt Disney’s animation archives during their journey from the Walt Disney ARL to exhibitions in Beijing and then in Shanghai until their return four months later. The powerful potential of this technology to provide a portable, quantitative and cost effective method for monitoring low levels of pollutants in a large number of locations and microenvironments will also be discussed.

4.2 Equilibrium Real Time Imaging vs. Cumulative (Dosimetric) Sensor Arrays

At the core of our past colorimetric sensor array technology is an array of cross-responsive sensors based on strong dye-analyte interactions (i.e., Brönsted and Lewis acid–base, hydrogen bonding, dipolar, and π – π interactions).¹⁻³ These arrays have proven highly effective and provide up to 20 or more independent dimensions for 90% discrimination of a wide variety of analytes and mixtures with sensitivities in the ppb regime (e.g., toxic industrial chemicals,^{1, 4} volatile organic compounds,⁵ explosives,² bacterial metabolites,⁶ beers,⁷ soft drinks⁸).

These sensors are essentially “chemical fuses”: they are highly reversible for most analytes (especially at moderate concentrations) but after exposure to very high concentrations of volatile chemicals (which would take too long to flush away) or to very aggressive analytes (which react irreversibly with the colorants) the array undergoes well-defined irreversible color changes. Thus the interactions between gaseous analytes and colorants in the array represent an equilibrium interaction and for this reason, sensors are imaged during exposure in real-time so that once response enters the equilibrium uptake region (see **Figure 1.4**), analysis of the response provides quantitative information of pollutant concentration. The disadvantage of a chemical fuse is that there is no improvement in sensitivity with increased dosage (i.e., exposure time) and, as mentioned, arrays must be imaged in real-time.

While past design characteristics have worked well for the applications they were designed for, some alterations needed to be made to the current colorimetric sensor array

technology to meet the extraordinary sensitivities demanded for artwork monitoring and the unique sampling conditions required for long-term exposure of the array in the museum environment.

There are two possible modes of action with a colorimetric sensor array. The first, similar to methods the group has used in the past, involves real-time analysis of a sensor array placed in a reader/analyzer which actively samples the environment with a micro gas pump and then communicates wirelessly with a laptop or command center. The Suslick group has recently developed a hand-held reader as part of a separate project funded by the U.S. NSF and U.S. Department of Defense to rapidly collect low-noise colorimetric data for chemical sensing (described in more detail in the literature⁹ and summarized in **Section 4.4.4.1**). This technology shows great promise but development is still in its infancy and the reader was developed for short-term measurements that can later be uploaded to a laptop. In order for this technology to work for long-term measurements where data is transferred wirelessly, significant alterations would need to be made. There are also concerns, similar to those found with other active monitoring devices mentioned previously in **Chapter 1**, with using this device to sample a large number of locations in closed environments such as display cases. For example, the cost of the handheld reader (as it stands now) limits the number of locations that can be sampled at one time, the size of the reader while small enough to be portable (12.5 x 9.5 x 4.0 cm) is still large enough that it may be difficult to find an area within a display case that is aesthetically pleasing, and active sampling of a closed system will inevitably disrupt the ambient environment. It comes to mind that periodic sampling of a display case using a tube through an opening in the case could be a viable option however, changes to the ambient environment as a result of opening a case is cause for concern and it has also been pointed out by our professional museum counterparts that opening a display case is a big ordeal that is only done when absolutely necessary (e.g., an emergent problem with the objects on display, switching out collections). While there are certainly solutions to the above problems that can be explored and still potential to use the handheld reader to improve sampling time when screening materials for harmful pollutants, the focus of this work is on an alternative approach that could offer a low-cost and versatile tool to be used as a pre-screening technology and a method to monitor a large number of microenvironments within the museum.

This alternative approach involves the development of a colorimetric sensor array that acts as cumulative (dosimetric) passive sampling device. This small device, the thickness of a piece of paper and as small as a credit card can be placed discretely in a display case to be removed periodically for immediate imaging. The benefit of using cumulative (dosimetric) sensors (as discussed in **Section 1.4.2**) is that color change is linear as a function of dose and concentration measurements are representative of a time-weighted average (**Figure 4.1**). This device draws on colorimetric concepts already in use with current direct-reading passive sampling devices (as discussed in **Section 1.4.1**) but with our array technology dozens of these (analyte-specific) passive sampling devices can be incorporated into a single test thus reducing the cost of buying multiple tests.

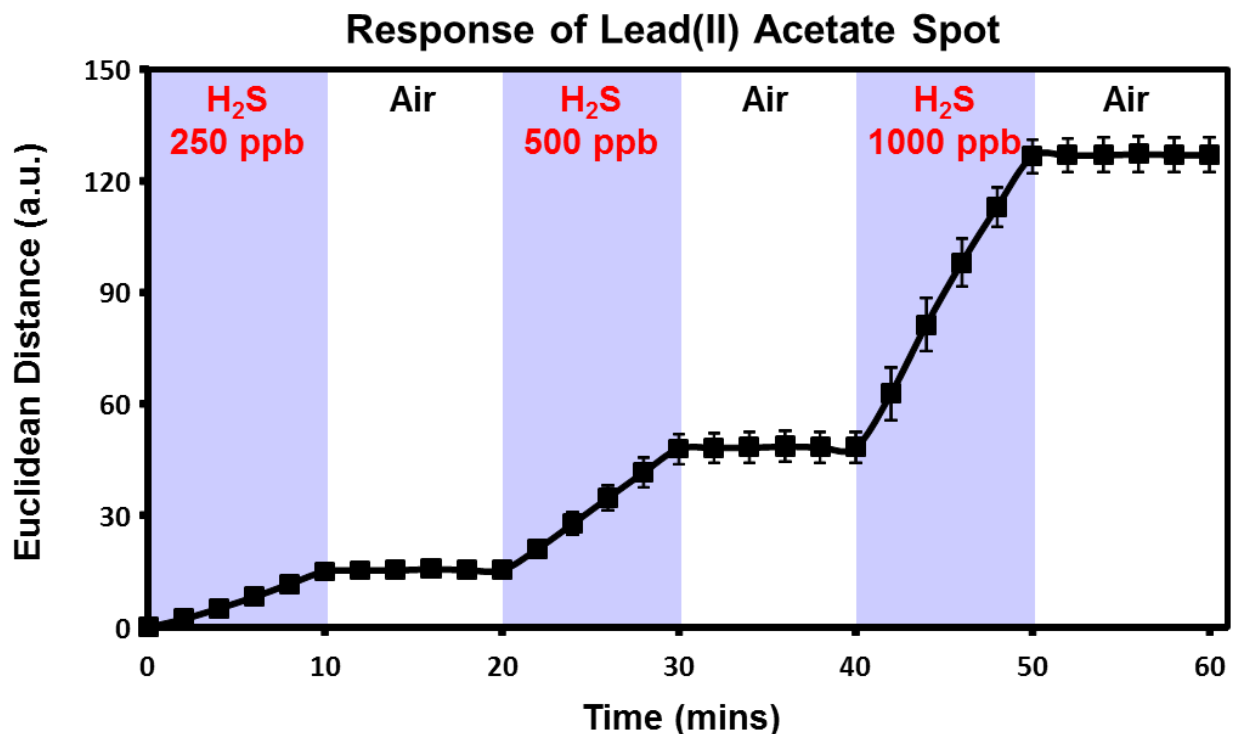


Figure 4.1 Response profile from cycling experiments with H₂S and 50% relative humidity filtered air. Color change is measured from a lead(II) acetate sensor spot that undergoes a metal sulfide precipitation reaction to produce lead(II) sulfide. The slope of response is proportional to sulfide concentration; consistent with sensing using a cumulative (dosimetric) sensor.

4.3 Development of 1st Generation Cumulative (Dosimetric) Sensor Array

In the past, our group specifically tuned the sensors in our array to interact with analytes in a reversible manner where dye-analyte reactions at room temperature would have enthalpies of interaction (**Figure 4.2**) that are less than ~120 kJ/mol (given the strongly negative entropies of binding gas molecules). Therefore, in order to develop spots that act as cumulative irreversible sensors, we had to turn to reactions with chromophores whose enthalpies are greater than ~150 kJ/mol (e.g., metal sulfide precipitations, irreversible oxidations of dyes or bleaching, redox reactions with large ΔE°). An additional design requirement for these reactions is, in an effort to de-convolute the response to the total environment into responses from individual analytes or classes of analytes, each chromophore is chosen to react specifically with a class of analytes (i.e., oxidants, sulfides, aldehydes, acids); a departure from the cross-reactive sensor spots of the past.

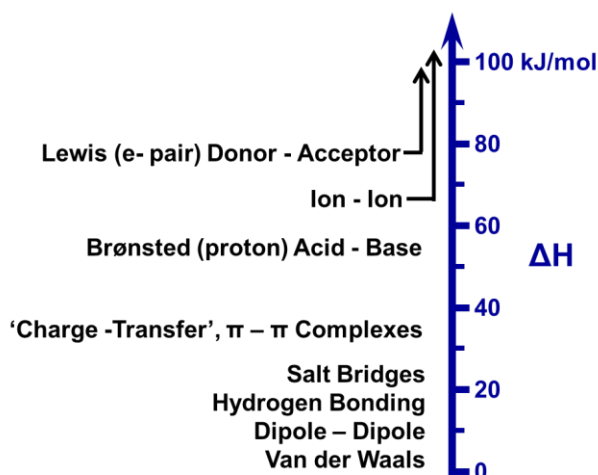
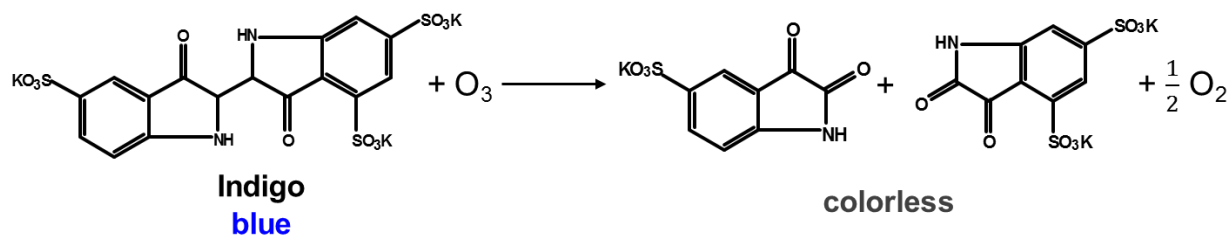


Figure 4.2 The range of intermolecular interactions on a semi-quantitative energy scale. Such interactions are a continuum from the very weakest van der Waals and dispersion forces to the strongest covalent or ionic bonds. Reproduced with permission of The Royal Society of Chemistry.³

4.3.1 Oxidants (Ozone, NO_2)

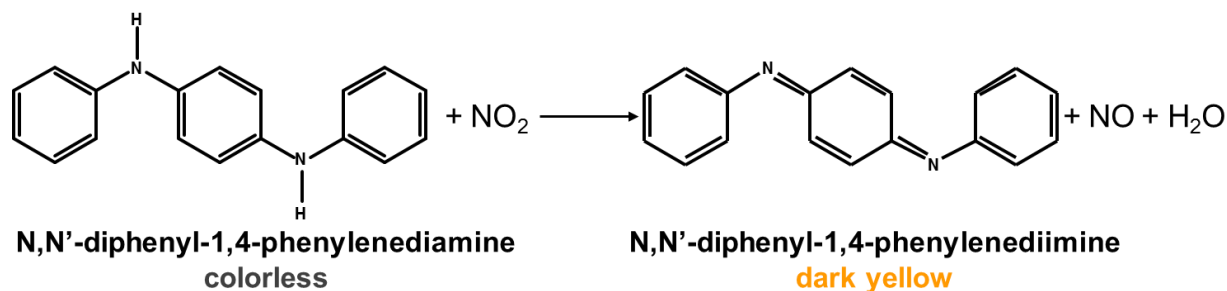
We explored two possible reaction pathways suitable for monitoring oxidants. The first, shown in **Scheme 4.1**, is the oxidative decomposition of organic dyes (i.e., bleaching) and is the most prevalent colorimetric method for detection of oxidants, particularly ozone. As many of the

indicators used in our array are highly colored organic dyes, we felt that this interaction was already being targeted and chose to focus on development of sensor spots that utilize the second reaction pathway.



Scheme 4.1 Example of oxidative decomposition (i.e., bleaching) of the organic dye indigo.

The second reaction pathway, shown in **Scheme 4.2**, utilizes redox reactions that typically start out colorless then change into a colored product. While a single redox indicator is not suitable in this application, as this class of indicators tends to have a relatively narrow detection range and are easily contaminated by other potential oxidative interferents, rational design of an array using a series of reactive indicators with different reaction mechanisms can overcome this problem.



Scheme 4.2 Example of redox reaction between nitrogen dioxide (NO_2) and N,N'-diphenyl-1,4-phenylenediamine.

All of the indicators used in this study are either benzidine or phenylenediamine derivatives (**Figure 4.3**) and their mechanism of reactivity in liquid¹⁰⁻¹³ and solid¹⁴⁻¹⁶ reaction media has been well documented. In short, due to the manner in which these indicators react with oxidants and the products and intermediates that result (e.g., semiquinone radicals), the composition of the reaction media (e.g., pH, immobilization method, concentration of its

components) can have a profound impact on the activity of the resulting sensor spot (e.g., reversibility, color change, response time, selectivity for one oxidant over the other). For this reason, a combinatorial study of indicator-reaction media combinations at various pH's was performed to determine the optimal set of sensor spots with irreversible behavior that could discriminate among oxidants of interest (i.e., ozone and NO₂).

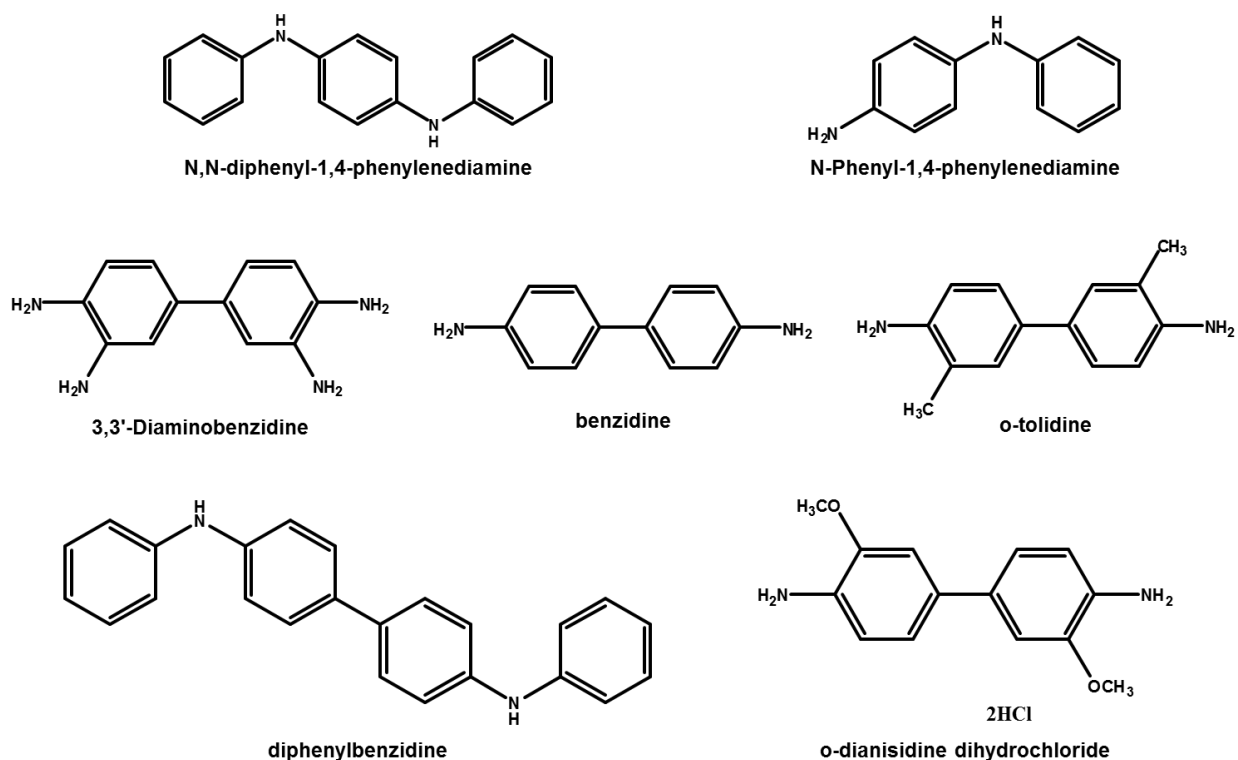
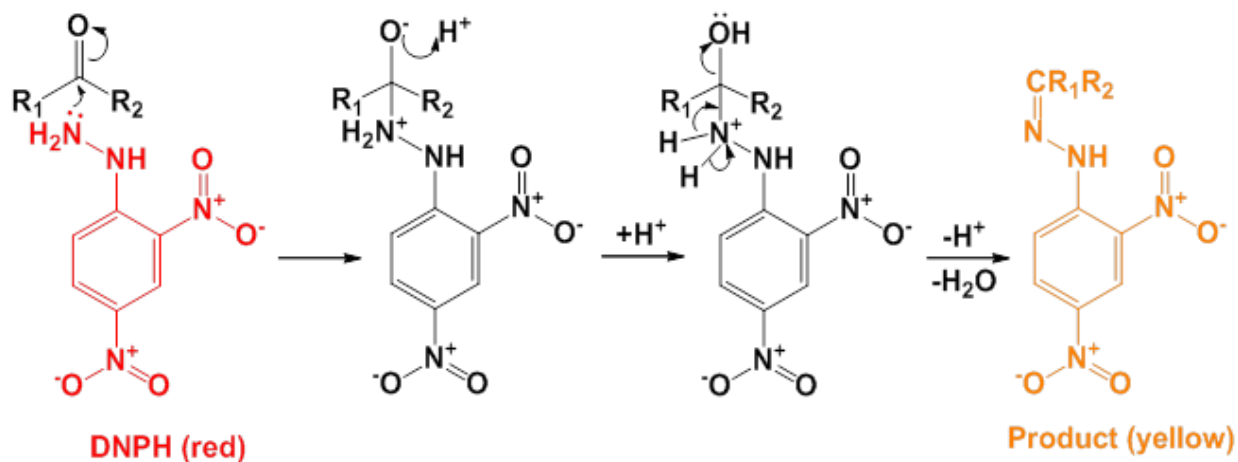


Figure 4.3 Structures of redox indicators used in this study.

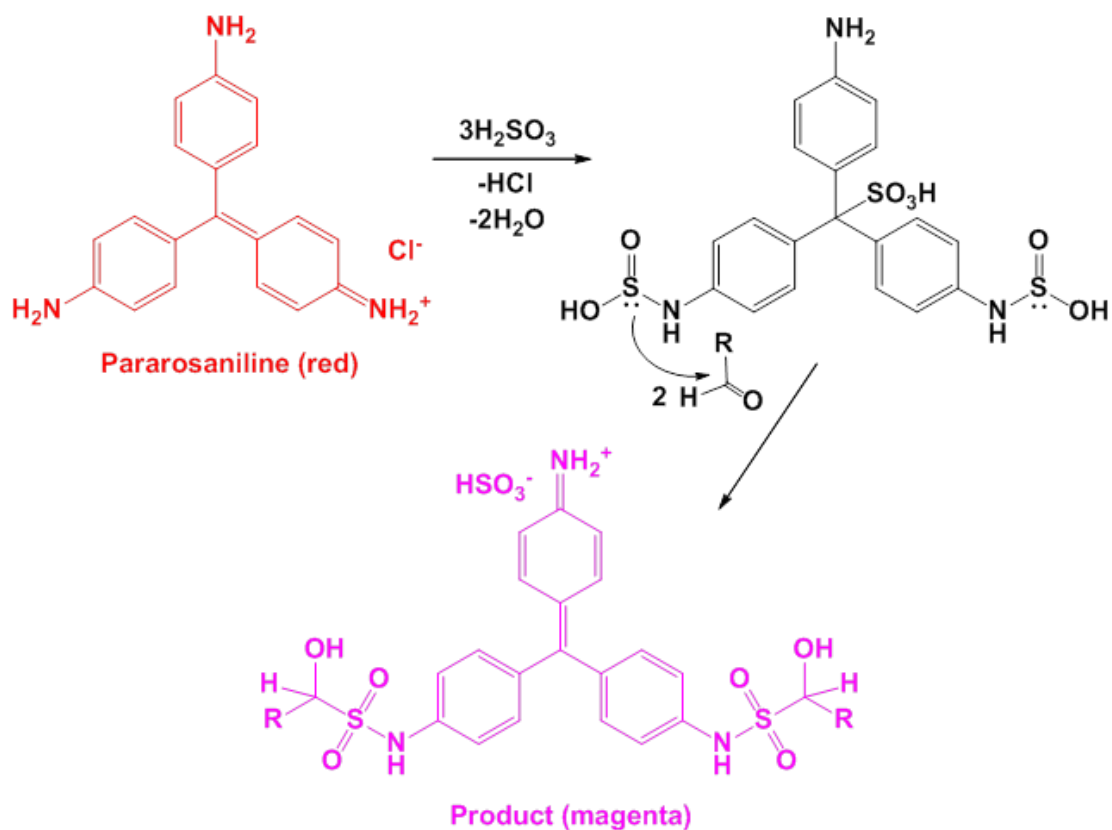
4.3.2 Aldehydes (Formaldehyde, Acetaldehyde)

There are two reaction pathways that we have used to monitor aldehydes (that are also sensitive to some ketones). The first, an analog to Brady's Test (**Scheme 3**),¹⁷ uses 2,4-dinitrophenylhydrazine (DNPH) immobilized in an acidified environment. In the presence of an aldehyde, this spot changes from light yellow to a darker yellow color. The second, an analog to Schiff's test (**Scheme 4.4**),¹⁸ uses a combination of pararosaniline and DNPH in an acidified matrix. While this is a departure from traditional preparation methods for Schiff's reagent (i.e., sulfonation of the central carbon atom by sulfurous acid or its conjugate base bisulfite), we found

that out of several pH indicators tested, only triphenylmethane dyes (e.g. methyl violet, crystal violet, pararosaniline, etc.) showed any reaction and the color of these dyes changed significantly upon addition of DNPH (i.e., going from red to purple upon exposure to formaldehyde). There is evidence suggesting that this mixture forms the DNPH analog of Schiff's reagent.¹⁹



Scheme 4.3 Reaction mechanism for Brady's test.



Scheme 4.4 Reaction mechanism for traditional Schiff's test.

4.3.3 Sulfide (H₂S)

Sensor spots for sulfide detection were taken from previous iterations of colorimetric sensor arrays developed by the group.⁴ The first, a metal sulfide precipitation reaction where lead(II) acetate (colorless) is converted to a solid precipitate of lead(II) sulfide (brown) in the presence of H₂S.²⁰ The second is a two-step reaction where mercuric chloride is first converted to mercuric sulfide in the presence of hydrogen sulfide yielding two moles of acid with each iteration.²¹ This resulting change in acidity can be monitored by incorporating pH indicators into the sensor spot. In this instance two spots, one with bromocresol green (pH range: 3.8 - 5.4) and the other with bromophenol blue (pH range: 3.0 - 4.6), are included in the dye formulation and undergo a color change from blue to yellow with decreasing pH. To ensure both pH indicators start in their basic form, additional base (1 M TBAH in water) is added to the formulation.

4.3.4 Acids (Formic Acid, Acetic Acid, SO₂)

Organic acids were perhaps the most problematic analytes to monitor as the most popular colorimetric methods rely on reversible pH indicators (e.g., A-D test strips use bromocresol green impregnated paper).²²⁻²³ In order to make the sensor spot cumulative (i.e., dosimetric) we screened a series of pH indicators in a *highly basic matrix* that had a working range deep in the basic regime with the hope that upon interaction with an acid, the color change would be irreversible. There were two indicators that met this requirement: Alizarin (yellow to red, pH 5.8-7.2; red to purple, pH 11.0-13.0) and indigo carmine (blue to yellow, pH 12-14). After these spots were incorporated into the array, we discovered that these spots have a relatively limited shelf life; the sensitivity of these spots to calibrated acid environments becomes highly variable as the sensor spots age. This is likely due to changes in the pH of these spots as the *t*-butylammonium hydroxide (TBAH) in the formulation is neutralized by CO₂ in the air. We have explored other options for acid detection to be incorporated in future arrays, including a spot analogous to the Oddy test which uses immobilized metal nanoparticles (i.e., copper) to detect acidic species and have had some success however these spots are still in development and were not included in the first generation sensor array.

4.3.5 First Generation Array for Monitoring Museum Pollutants

Using the reaction principles described above, we were able to compile sensor spots into a first generation array for detection of multiple museum pollutants, the array incorporates into one cohesive system a series of chemically responsive dyes that respond specifically to the main museum pollutants (**Figure 4.4**). This array gives us a starting point to explore the utility of colorimetric sensor array technology for preventive conservation but will undoubtedly need to undergo further development to improve the capabilities of future sensor arrays.

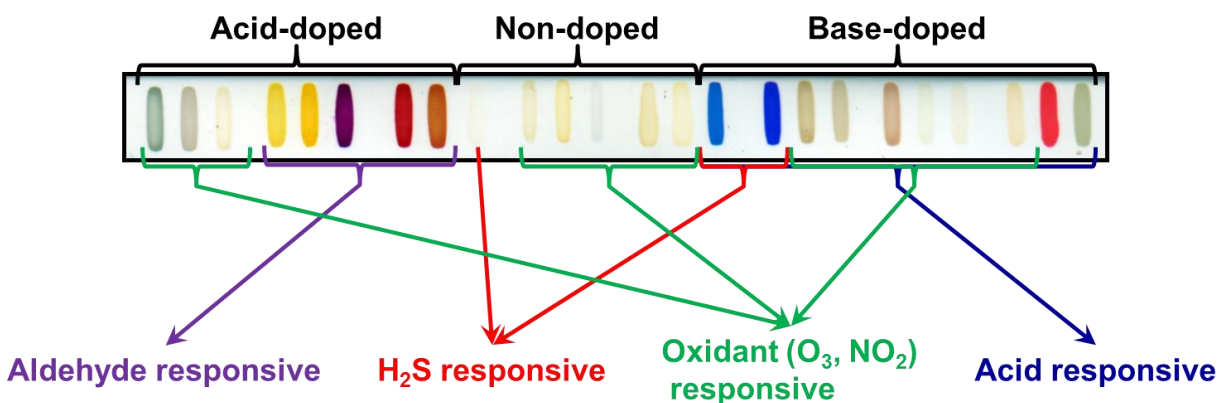


Figure 4.4 Image of 1st generation sensor array consisting of cumulative (dosimetric) sensor spots and the analyte classes they target.

4.4 Experimental

4.4.1 Formulation Preparation and Array Printing

All reagents were analytical-reagent grade, purchased from Sigma-Aldrich and used without further purification. Each sensor spot was immobilized in a plasticizer or polymer matrix optimized for best chemical compatibility and sensor performance (**Table 4.1**). If appropriate, 1 M solutions of *t*-butylammonium hydroxide (TBAH) or *p*-toluenesulfonic acid (TsOH) in water were added immediately before printing. Formulations with chemoresponsive dyes, plasticizer/polymer and a high volatility solvent were then loaded into a Teflon ink well. An ArrayIt NanoPrint LM60 Microarray Printer (ArrayIt Corporation, Sunnyvale, CA) holding

custom-designed rectangular pins (**Figure 4.5**) was used to robotically print arrays in a linear geometry by dipping into the ink well and transferring to the substrate. All arrays were printed on polypropylene membrane (Sterlitech Corporation; thickness: 130–170 μm , pore size: 0.22 μm) attached to custom injection-molded cartridges or a sensing platform (described in detail in **Section 4.4.2**) using a solvent welding method (dichloromethane). Acid treated spots were printed first and dried in a vacuum oven at room temperature (RT) for 24 hours then all other spots were printed and dried in a vacuum oven (RT) for an additional 4 hours. Arrays were then stored in nitrogen filled bags until use. **Figure 4.6** gives a detailed schematic of the printing process.

Table 4.1 Detailed outline of formulations for printing of 1st generation array for artwork monitoring.

Spots	Indicator	mg/mL	Additive	Concentration Additive (M)	Amount ($\mu\text{L}/\text{mL}$)				
1	N,N-diphenyl-1,4-phenylenediamine	5	TsOH	1	50	TEG (10 vol%)			
2	N-phenyl-1,4-phenylenediamine	5							Vol (mL)
3	3,3-Diaminobenzidine	4						TEG	1
4	DNPH	10						ME	9
5		10			Total	10			
6	Pararosaniline	1	H ₂ SO ₄	0.5	25				
7	DNPH + Pararosaniline	10+1						PEG - 400 (10 vol%)	
8						100			
9	Pb(OAc) ₂	15				PEG-400	1		
10	3,3-Diaminobenzidine	4				ME	9		
11	benzidine	4				Total	10		
12	diphenylbenzidine	5							
13	o-dianisidine dihydrochloride	4				TX25			
14	o-tolidine	4							Vol (mL)
15	HgCl ₂ + Bromocresol Green	5 + 4	TBAH			50	Triton X-100	2.5	
16	HgCl ₂ + Bromophenol Blue	5 + 4					1	70	ME
17	N,N-diphenyl-1,4-phenylenediamine	5							Total
18	N-phenyl-1,4-phenylenediamine	5							
19	3,3-Diaminobenzidine	4							
20	diphenylbenzidine	5							
21	o-dianisidine dihydrochloride	4							
22	o-tolidine	4							
23	Thiazol yellow g	5							
24	Indigo Carmine	5							

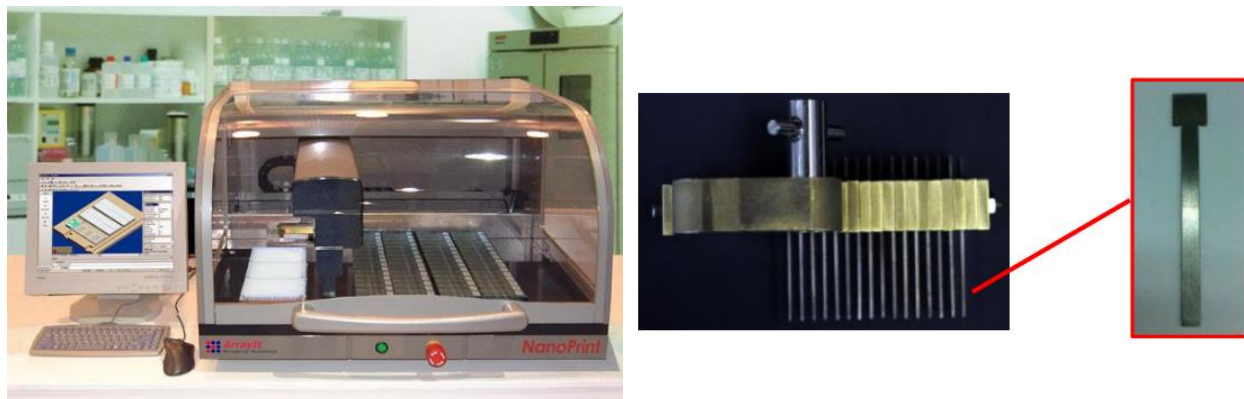


Figure 4.5 (left) Array-it Nano Printer used to print array cartridges and (right) rectangular pin-holder and pins for printing.

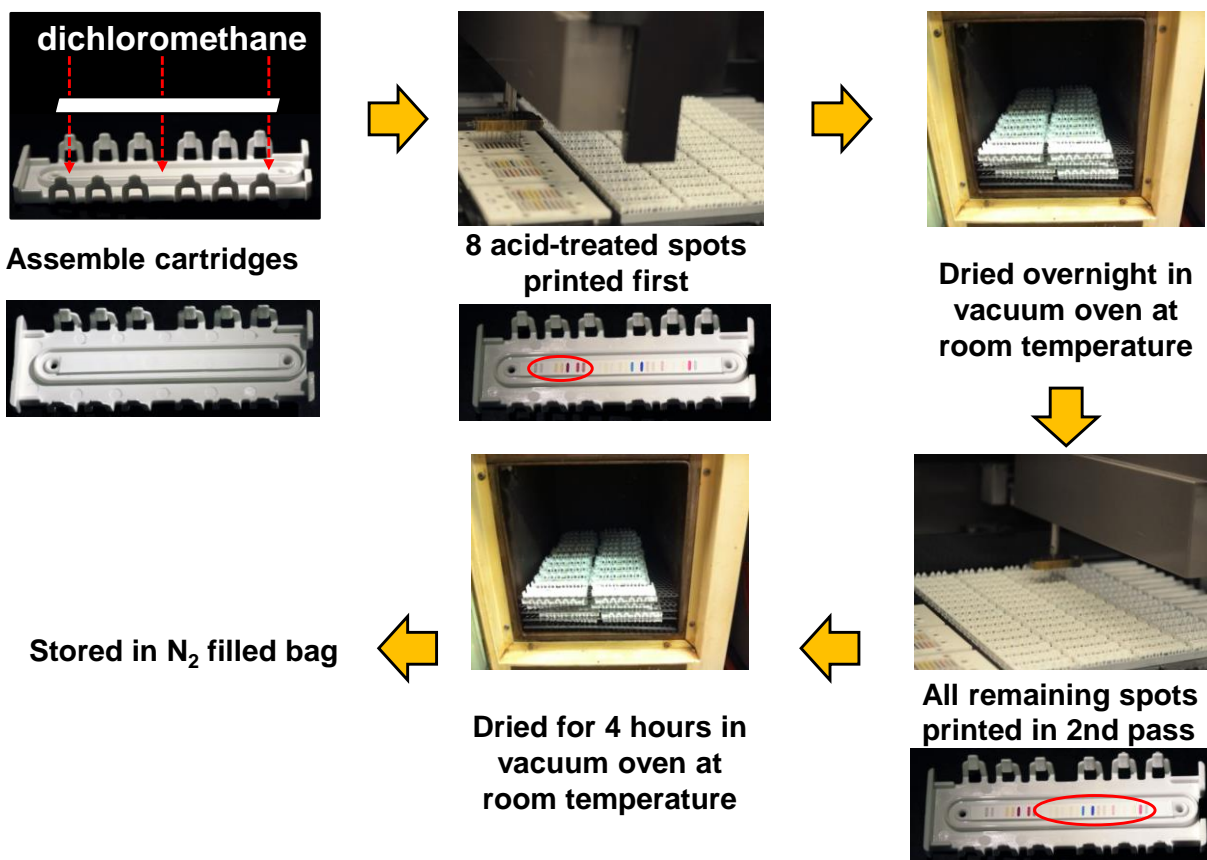


Figure 4.6 Detailed schematic of cartridge preparation, printing and drying protocol for sensor arrays.

4.4.2 Array Cartridges and Sensing Platform

Injection-molded cartridges (**Figure 4.7a**) customized for compatibility with the handheld reader were utilized for all active-sampling (imaged using handheld reader and flatbed scanner) and passive-sampling (imaged using a flatbed scanner). These cartridges, made out of polycarbonate, have an o-ring placed in a groove around the flow path (volume: <math><180\ \mu\text{L}</math>, dimensions: 77 x 4.5 x 0.5 mm) and a glass slide cover that snaps into place. For all passive-sampling experiments the o-ring and glass slide were removed to allow for easy diffusion of the analyte to sensor spots.

For iPhone imaging (passive sampling), a customized sensing platform was fabricated (**Figure 4.7b**). The sensing platform consists of sensor spots printed on a white polypropylene membrane with a gray reference strip mounted 1 cm below sensor spots. The polypropylene and gray reference strip was then attached to an impact resistant polycarbonate film the size of a glass slide (McMaster Carr; thickness: 0.040") and printed on acid free paper (HP Premium Choice). Printed on the acid free paper is an identifying number unique to each array, the date the array was printed and a trapezoid which has been sized to aid in image alignment. Each component of the sensing platform has been attached using a solvent (dichloromethane) welding method.

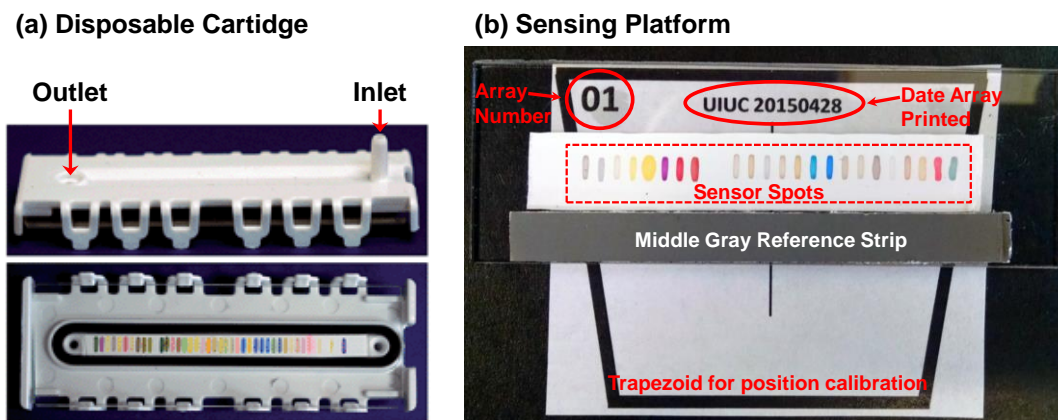


Figure 4.7 (a) Sensor array mounted on a polycarbonate cartridge with an o-ring placed in a groove and glass slide cover in place, which provides an ideal flow path for analytes and flow volume <math><180\ \mu\text{L}</math> (77 x 4.5 0.5 mm). Stem on the back of the cartridge is placed on the side of the handheld where ambient air flows in where the outlet is attached to a diaphragm micropump.⁹ (b) Sensing platform compatible with iPhone camera imaging. Cell phone camera (not shown) would be positioned at the base of the trapezoid so that the field of view is the trapezoid area.

4.4.3 Data Processing and Analysis Techniques relevant to Colorimetric Sensor Analysis

From the digital images, obtained using the various imaging devices described in **Section 4.4.4**, a difference map (**Figure 4.8**) is easily generated by digital subtraction, pixel by pixel, of the image of the array before and after exposure: red value after exposure minus red value before, green minus green, blue minus blue. Averaging of the centers of the spots avoids artifacts from non-uniformity of the dye spots, especially at their edges. The other advantage of using the differences in RGB colors is that it tends to cancel out discrepancies in printing because the color differences are only a weak function of variation of the dye concentration or spot intensity from array to array.⁵ The resulting data is inherently digital (simply a vector of 3N dimensions where N = total number of spots) and all quantitative and statistical analysis is done directly from the digital difference vectors. The color difference maps are useful primarily for convenient visualization of color changes of the dyes in the array; note that the color values are absolute values of the differences and that expansion of the color space is useful for visualization.

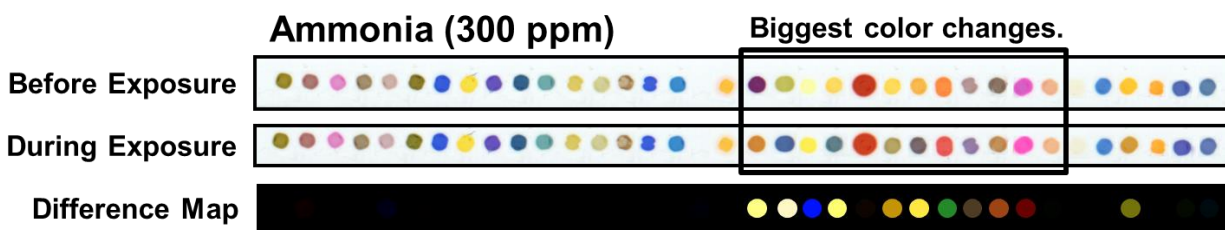


Figure 4.8 Image of 36-dye colorimetric sensor array (**top**) before exposure and (**middle**) during exposure to ammonia at 300 ppm or IDLH concentration (immediately dangerous to life or health concentration). (**bottom**) Subtraction of the two images yields a difference vector in 108 dimensions (i.e., 36 changes in red, green and blue color values); this vector is usefully visualized using a difference map, which shows the absolute values of the color changes. For purposes of display, the color range of difference maps are usually expanded.

The ΔRGB values at a given timepoint can be combined into a Euclidean distance, defined by the equation $ED_t = (\Delta R_1^2 + \Delta G_1^2 + \Delta B_1^2 + \Delta R_2^2 + \dots + \Delta B_n^2)_t^{1/2}$, where n is the number of spots under consideration and t is the time. To generate a response profile for a given analyte, the average Euclidean distance (\overline{ED} for $n = 24$ spots) at a given timepoint is plotted with respect to time. From this response profile, we are able to determine the reaction kinetics, whether a sensor gives a linear response until saturation implies it is dosimetric or if it eventually levels off

before saturation (reaches equilibrium with the external environment) indicates an equilibrium reaction. If a sensor indeed gives a dosimetric response, the slope of this response profile and signal at a given timepoint in the presence various analyte concentrations can be used to determine dosimetric sensitivity and limit of detection (discussed in greater detail in **Section 4.4.8**). Reproducibility of sensor response can also be elucidated from these profiles by examining the results from different trials at the same analyte concentration.

Arrays based on chemical properties intrinsically have a much higher dimensionality. Having a high dimensionality has the advantage of much greater ability, at least in principle, of being able to differentiate among analytes with much greater discriminatory power. The greater dimensionality, however, must also involve a more sophisticated approach to statistics.²⁴ Statistical methods for multidimensional data all share the common goals of displaying multidimensional data effectively, evaluating data sets, and predicting the identity of unidentified samples based on a known library. There are a variety of statistical methods available to deal with high dimensional data,²⁵⁻²⁶ however the main technique used in this study is hierarchical cluster analysis (HCA). Cluster analysis essentially tells one what resembles what, e.g., how close the vectors representing data are to one another in a high dimensional space. These clusters are determined from the Euclidean distance between experimental data and, in its simplest form, nearest-neighbor points are paired into a single cluster which is then paired with other nearest-neighbor points or clusters until all points and clusters are connected to each other, shown schematically in **Figure 4.9**. The clustering criterion used in this study is Ward's minimum variance method, which minimizes the total within cluster variance. The resultant dendrogram shows connectivity and some measure of the distance between each of the pairs. In the context of chemical analyses, these two important pieces of data answer two questions: connectivity explains relationship similarity, i.e. 'what species/samples are similar to each other?' and distance explains magnitude, i.e. 'how similar are they?'. There are three primary limitations to the HCA technique: (1) HCA is not easily capable of predictive analysis, (2) dendrograms created using HCA must be re-created with each addition of a new analyte, so comparing dendrograms (even with a very similar data set) is typically only useful for rough qualitative purposes, i.e. 'what does this new sample look most like?', and (3) confusion may arise in the interpretation of noisy data.

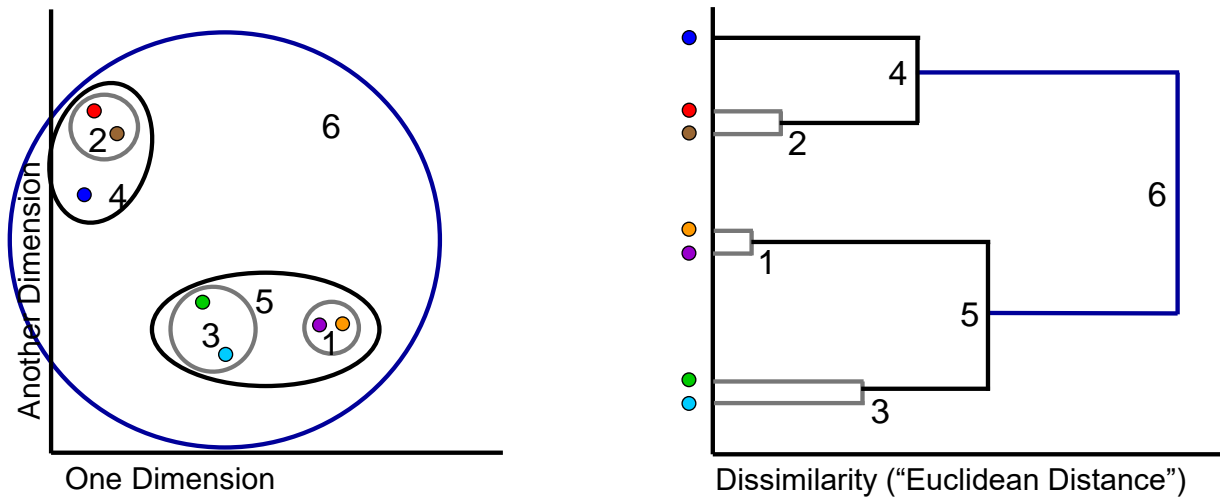


Figure 4.9 (left) Schematic representation of a hierarchical cluster analysis (HCA) of multidimensional data, shown in only two dimensions, that forms a **(right)** dendrogram based on clustering of those experimental measurements.³

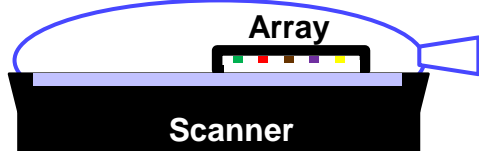
4.4.4 Passive and Active Sampling: Methods and Image Analysis

There are three different modes of exposure and imaging used in this study: (1) passive sampling and real-time imaging (using a flatbed scanner), (2) passive sampling and periodic imaging (using an iPhone 4S camera) and (3) active sampling and real-time imaging (using a flatbed scanner and a handheld reader). **Figure 4.10** summarizes these three modes and imaging methods.

Passive Monitoring

1. Passive Exposure + Real Time Monitoring

22 L Ziploc Bag
Filled with known concentration of analyte.



2. Passive Exposure + Periodic Monitoring

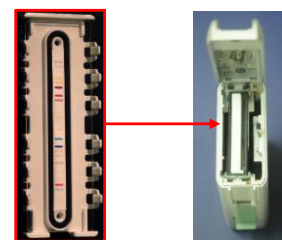


Active Monitoring

Handheld Reader



Top Inlet



Array

CCIS Imager

Figure 4.10 (left) Methods for exposure in a passive environment (system at the top) using real-time imaging with a flatbed scanner or periodic imaging using an iPhone 4S imaging platform and compatible sensing platform. **(right)** Method for active exposure using handheld reader developed by the Suslick group.⁹ The reader is 12.5 cm tall by 9.5 cm wide by 4.0 cm thick. The cartridge is loaded into the reader at the top and a diaphragm pump pulls ambient air into the reader through the top inlet. The other active sampling method using a flatbed scanner is not shown but is described in detail in **Chapter 3**.

All reagents were of analytical grade and used without any further purification. Gas analyte streams were generated with the use of certified, premixed gas tanks obtained from Matheson Tri-Gas through S.J. Smith (SO_2 , NO_2 , H_2S), ozone was prepared using a photometric ozone calibrator (Advanced Pollution Instrumentation, Inc. Model 401) connected to a compressed air tank as the oxygen source, liquid analytes (formic acid, acetic acid, acetaldehyde) were generated by bubbling through the liquid reagent, and solid analytes (formaldehyde) were generated by flushing filtered air through a Teflon tube containing paraformaldehyde fine powder. MKS digital mass flow controllers were used to achieve the desired concentrations and relative humidity in a manner similar to that shown in **Figure 2.1** and flow out of these controllers was confirmed using a bubble flowmeter. Importantly, gas stream concentrations and relative humidity were confirmed by in-line analysis using an FTIR multi-gas analyzer (MKS Instruments model 2030).

4.4.4.1 Active Sampling and Real-Time Imaging (Flatbed Scanner and Handheld Imager)

Active sampling using a flatbed scanner was performed using the same methods described in **Chapter 3**. The RGB values for the pixels corresponding to the center two-thirds of each spot were averaged to avoid spot edge artifacts using a customized software package, SpotFinder (iSense).

Operating procedures and performance of the handheld scanner (**Figure 4.10**) is described in detail in a previous publication from Askim and Suslick.⁹ In short, a diaphragm micropump is used to sample analyte gas and a color contact image sensor (CIS) collects colorimetric data. The handheld device sampled gas from polyethylene bags either containing 50% RH filtered air or analyte at a premixed concentration in 50% RH filtered air (**Figure 4.11**). Explanation of analyte bag preparation is described in detail in **Section 4.4.4.2**. The handheld device has built in spot finder software that normalizes RGB values using a calibration created from a one-time measurement of a 0% reflectance standard (i.e., the sensor array with all LEDs turned off) and a 100% reflectance standard (i.e., a white blank array).

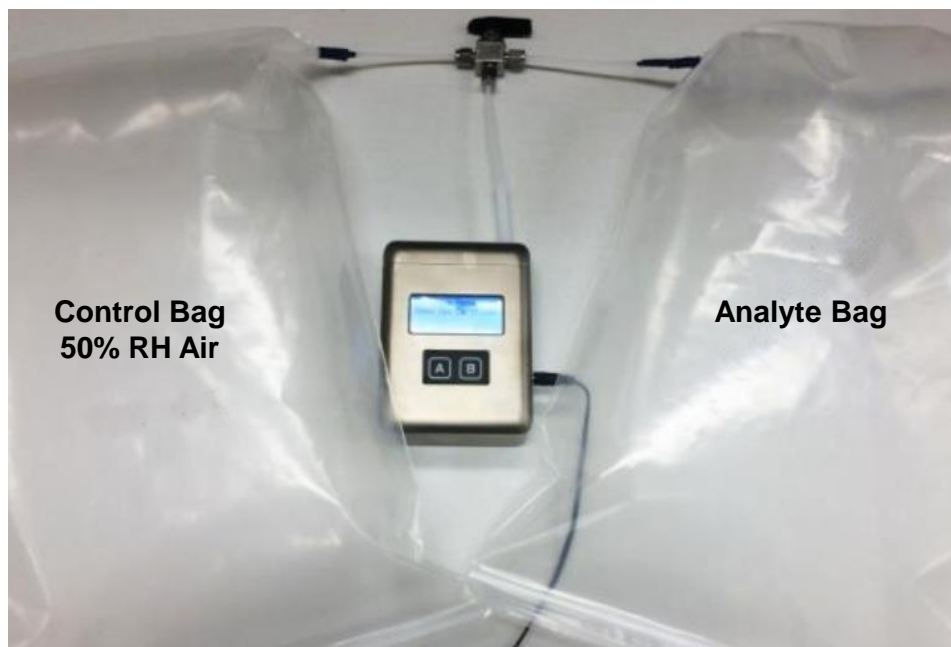


Figure 4.11 Handheld device setup to sample gas from polyethylene Ziploc bags either (**left**) containing 50% RH filtered air or (**right**) a premixed concentration of analyte in 50% RH air.

4.4.4.2 Passive Sampling and Real-time Imaging

Figure 4.10 depicts details of the setup used for these experiments. Arrays (printed on the injection-molded cartridge without o-ring or glass slide) were imaged face down on the scanner surface through a clear Ziploc bag (total volume: 22 L). The ridges on either side of the cartridge, used to hold on to the glass slide, held the array above the scanner surface to allow for diffusion of the analyte to sensor spots. Attached to the Ziploc bag is a rubber septum and a 3-way valve. Once the array was placed in the bag, the bag was closed and excess air removed. The bag was then filled with a fixed volume (7.8 L) of 50% relative humidity filtered air. After 3 minutes a “before-exposure” image of the array was taken. Analyte gas (with a known concentration confirmed using FTIR multi-gas analyzer) was then drawn out of another bag using a syringe through a rubber septum attachment and injected into the experimental bag containing the array to create an environment with the desired concentration of analyte. Immediately after analyte addition, images of arrays were taken at set time increments during exposure. The RGB values for the pixels corresponding to the center two-thirds of each spot were averaged to avoid spot edge artifacts using a customized software package; SpotFinder (iSense).

There are some limitations to this passive sampling method that must be discussed. First, since a point source (syringe) is used to inject a concentrated stream of analyte into the bag there is a concentration and analyte dependent lag time, illustrated in **Figure 4.12**. This lag time is seen as a slow increase in response (or no response at all) before giving a linear (dosimetric) response. For this reason, the euclidean distance (ED) at the time points used to calculate the dosimetric sensitivity and the calibration curve have been corrected to account for this.

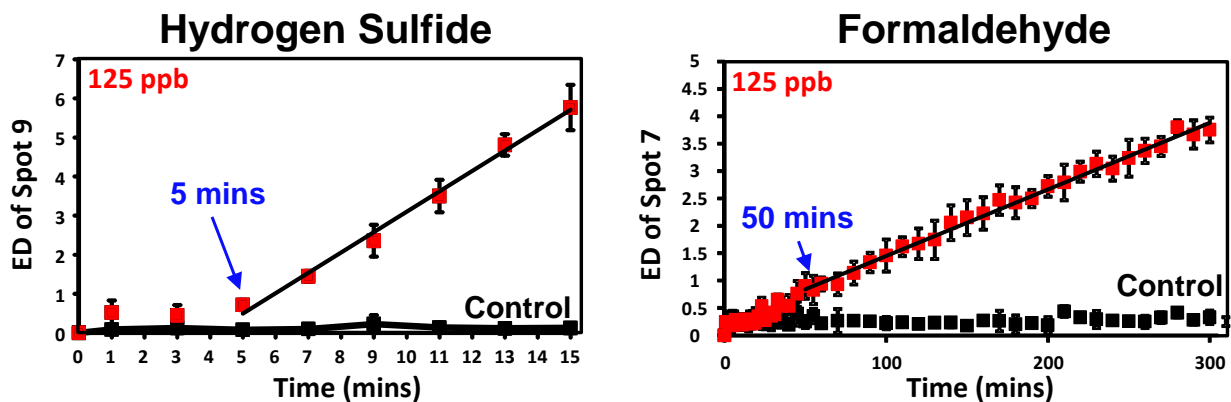


Figure 4.12 Response profile for 125 ppb (**left**) hydrogen sulfide and (**right**) formaldehyde exposure in a passive environment as monitored by a flatbed scanner. Indicated in blue, is the time at which the analyte has reached a steady state and dosimetric changes in response occur.

Second, depending on the analytes affinity for the surface of the plastic Ziploc bag, diffusion through the bag and stability of the analyte over time, there is a finite time that trials can be run without significant loss of analyte. **Figure 4.13** gives an example of change in bag concentration vs. time of a 1 ppm formaldehyde environment prepared as described above. Concentration measurements were taken using the FTIR multi-gas analyzer and pump connection that pulled air from the bag into the gas analyzer. Given the data presented in **Figure 4.13**, sampling times should not extend beyond 1-2 hours.

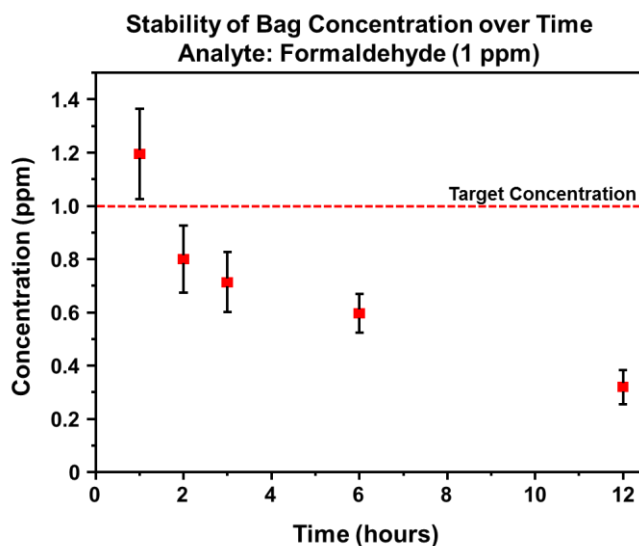


Figure 4.13 Concentration changes over time (measurements taken using an MKS FT-IR Multigas Analyzer) on a bag prepared with 1 ppm formaldehyde. After 6 hours, the concentration within the bag is roughly 50% of the starting concentration.

4.4.4.3 Passive Sampling and Periodic Imaging

This sampling and imaging method was used in a comparison study of noise and signal from a flatbed scanner vs. iPhone 4S camera imaging platform (**Section 4.4.6**), a case study of volatiles coming off passepartout materials used to encase artwork during the Disney exhibition (**Section 4.5.1.1**) and for all air quality analyses performed during the Disney exhibition (**Section 4.6**). The sensing platform described in **Section 4.4.2** (compatible with iPhone camera imaging) was used for all of these experiments.

For analyte calibration experiments, arrays were imaged before and after exposure to a passive analyte environment created using the same methods described in **Section 4.4.4.2** for passive sampling and real-time imaging. The only difference is that the sensing platform was placed face-up in the bag to allow for easier diffusion of analyte to the sensor spots. The experimental methods used for passepartout material analysis and Disney exhibition experiments will be described in the later sections that discuss the results from these studies.

The imaging platform used for these analyses consisted of an iPhone 4S nestled in a custom mount that was machined to hold the iPhone at a fixed 30° angle and fixed height above the array surface (**Figure 4.14**). This mount, when used in conjunction with the trapezoid attached to the sensing platform allows images of each array to be taken from the same position. To obtain an image, the phone-mount setup was moved towards the sensing platform until the sides of the trapezoid aligned with the sides of the phone screen and the bottom of the trapezoid aligned with where the top of the mount meets the screen (**Figure 4.15**). This ensured that iPhone camera imaging settings were kept consistent from image to image (i.e., flash: on; mode: square; HDR: off; and filter: none). Triplicate images were taken each time and later averaged to eliminate noise.

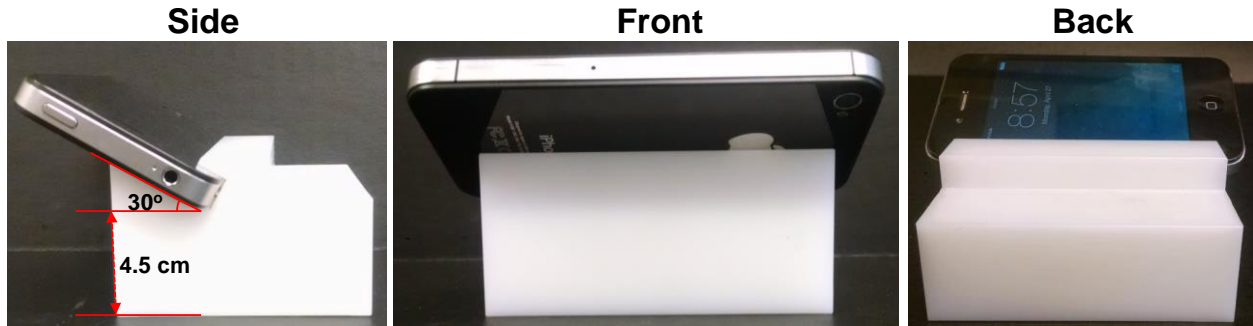


Figure 4.14 Photographs of mount with iPhone 4S nestled into a groove that holds the cellphone at a set angle (30°) and height (4.5 cm) for consistent imaging position.



Figure 4.15 Screen shot taken using iPhone camera of sensing platform, properly aligned for consistent imaging position.

No special effort was taken to isolate the system from ambient lighting. In order to reduce the effect of changes in ambient lighting, each image was taken with the flash turned on. Without strict control over ambient lighting, even with the use of the camera flash, inevitable changes in position of the array in the imaging field and changes in ambient lighting result in lighting differences from image to image and even across the array surface within the same image (**Figure 4.16**). As can be seen in the gradient map shown on the bottom-right of **Figure 4.16**, due to the use of flash the lightest area (with the most intense lighting) in each image is concentrated in the center of the image and decreases concentrically outward. This not only means that the light intensity reaching the spots printed in the center of the array can deviate 20% from the spots on the end but also that the light reaching the gray reference strip directly

below a given spot is undoubtedly different from the light reaching the spot itself. For this reason, we have chosen to eliminate the gray reference strip and rely solely on the white (polypropylene) reference as our means for light correction.

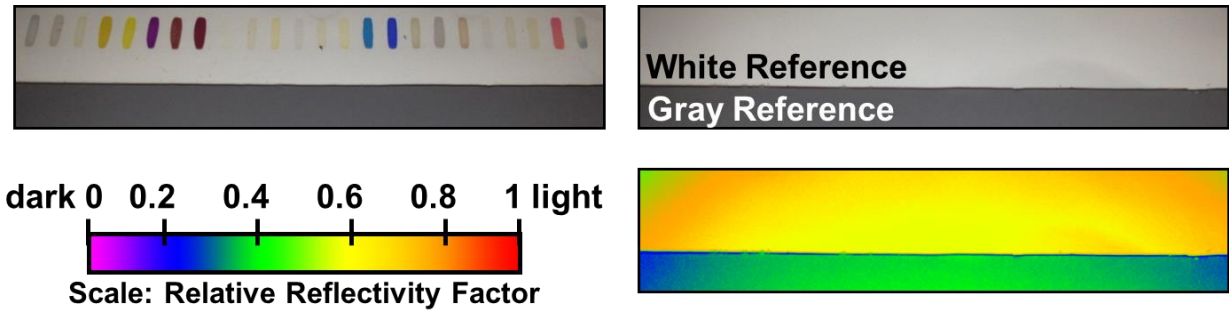
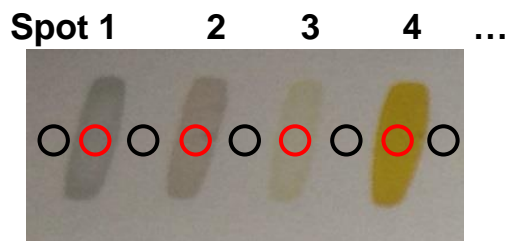


Figure 4.16 (top-left) Image of sensor spots on sensing platform. (top-right) Image of sensing platform without sensor spots. (bottom-right) Gradient map of blank sensing surface (reference scale of relative reflectivity factor in bottom-left) showing pattern of light intensity can deviate 20% from the spots on the end of the array to the spots in the middle.

Conveniently, our sensor spots are printed on top of the white surface that can be used as a reference to normalize the lighting across the array surface. Using the customized software package, SpotFinder (iSense), we are able to use an area on either side of each sensor spot to obtain white reference RGB values that are then averaged and used to normalize the lighting illuminating each spot (**Figure 4.17**). Therefore, each spot across the array for each image at each time point has a measured R, G and B value (*i.e.*, R_{meas}) and then a coinciding R, G, B value (*i.e.*, R_{white}) averaged from either side of the spot for the white reference. Using the equation, $R_{corr} = (R_{meas}/R_{white}) * 255$, a corrected value (*i.e.*, R_{corr}) was calculated.



- : Area where RGB values for each spot taken from (R_{spot}).
- : Area where RGB values for white reference taken from (\bar{R}_{white}).

Figure 4.17 Illustration of areas where white reference and spot RGB values are taken from.

To assess the improvement in reproducibility using uncorrected RGB values versus RGB values corrected using the above method, the same array (unexposed) was imaged in triplicate under the different ambient lighting conditions described in **Table 4.2**.

Table 4.2 Description of ambient lighting conditions used in noise analysis study. In all cases, built in cell phone flash was used for additional illumination.

Light Source	Intensity
fluorescent	room illumination
halogen (max: 5000K at setting 10)	Setting 1 (S1)
	Setting 3 (S3)
	Setting 5 (S5)
	Setting 7 (S7)
	Setting 9 (S9)

In looking at the HCA in **Figure 4.18** we see that the degree of dissimilarity is cut in half when using the correction method.

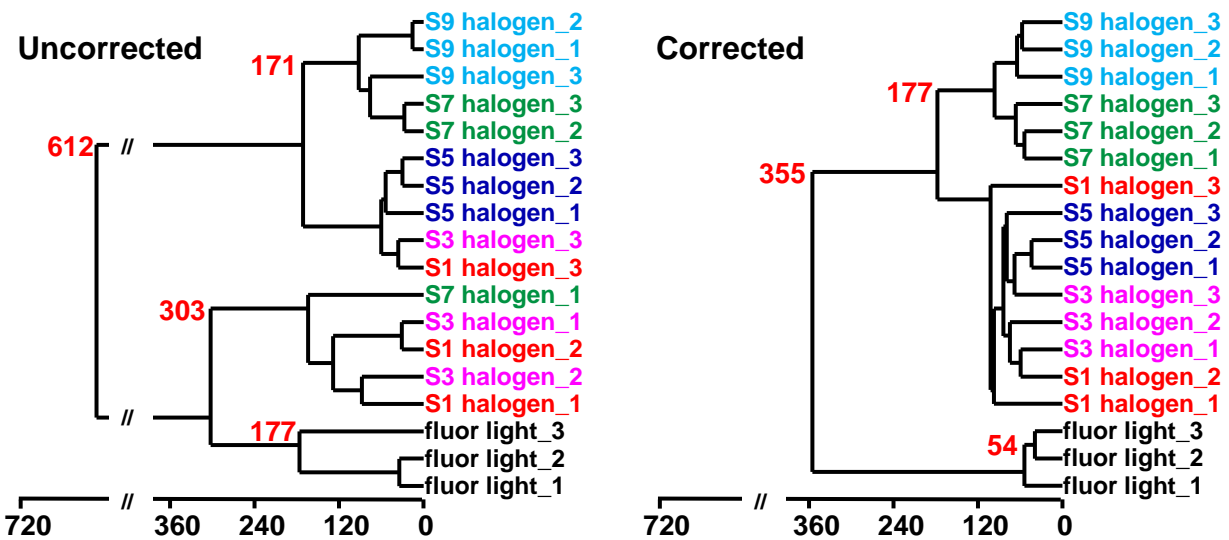


Figure 4.18 HCA of (left) uncorrected and (right) corrected values of unchanging array under different lighting conditions. The degree of dissimilarity is cut in half when using the post-processing correction method.

4.4.5 Array Response in Active versus Passive Sampling Environments

Active sampling uses a pump to direct a stream of air right over the sensor spots while passive sampling relies on the principles of mass transport for the diffusion of air to the sensor spots. One might hypothesize that reproducibility and response time would be drastically improved using the active sampling method over the passive. To test this theory, arrays were exposed to hydrogen sulfide (62.5, 125, 250, and 500 ppb) in 50% RH filtered air for two minutes and imaged using the handheld reader (Active Sampling) and flatbed scanner (Passive Sampling). Difference maps in **Figure 4.19** show the response of the array at 2 minutes in both of these environments. **Figure 4.20** plots signal/noise versus concentration, where signal is the Euclidean distance of the most responsive sensor spot (lead(II) acetate) and noise is the standard deviation among the control data. It is clear from this data that array response is significantly faster; S/N on average 4 times that of passive environment at 2 minutes exposure and the standard deviation (i.e., consistency of sensor response from trial to trial) is ~ 7.5 times higher in a passive environment.

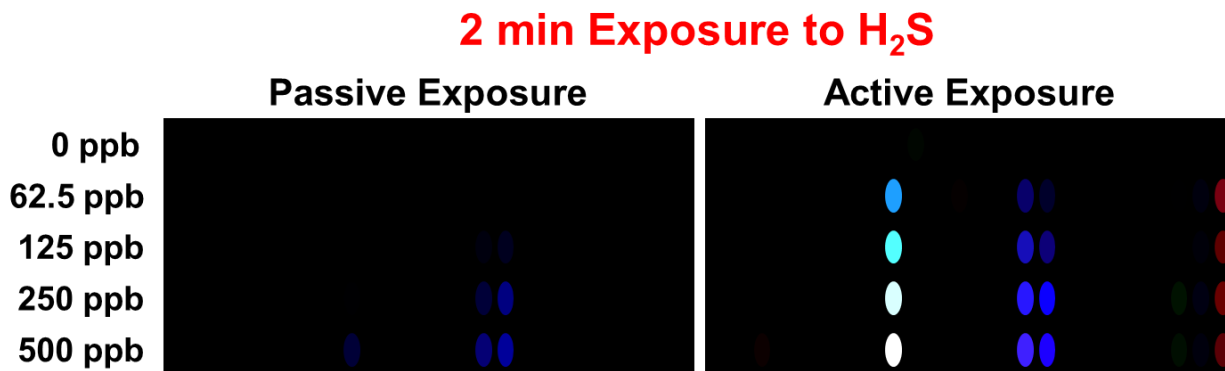


Figure 4.19 Difference maps (average over 3 trials) of arrays exposed to Hydrogen Sulfide after 2 minutes in **(left)** a passive environment and imaged using a flatbed scanner and **(right)** an active environment imaged using a handheld reader. Color is expanded from 2 to 17 and trials were done in triplicate.

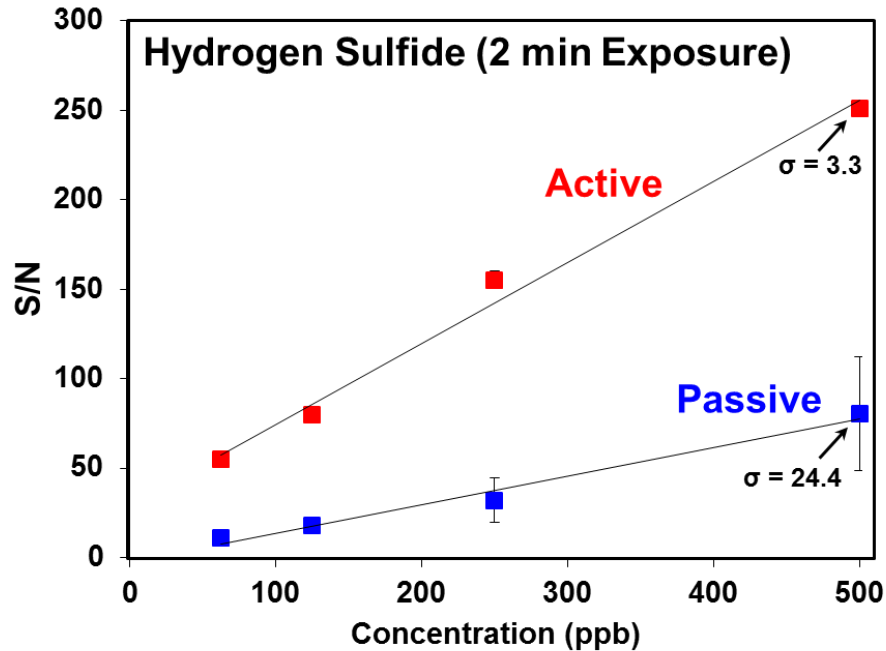


Figure 4.20 Signal to noise ratios from the most responsive spot exposed to hydrogen sulfide for two minutes in an active and passive environment as a function concentration. The average value with error bars is set to 2σ from triplicate trials.

4.4.6 Performance of iPhone imager versus Flatbed Scanner in Passive Environment

When imaging arrays with a flatbed scanner, the system is isolated from ambient lighting whereas iPhone imaging is not. In spite of the use of flash and post-processing steps to normalize the impact of changes in ambient lighting on the resulting RGB values from images taken using the iPhone imager, these steps do not eliminate the effects of ambient lighting completely. In a study similar to the one in **Section 4.4.5**, arrays were exposed to hydrogen sulfide (62.5, 125, 250, and 500 ppb) in 50% RH filtered air for 15 minutes in the passive environment described in **Section 4.4.4.2**. The difference maps in **Figure 4.21** show that while the response is similar, the S/N vs. concentration plot (**Figure 4.22**) shows S/N is 5.5 times higher when the flatbed scanner setup is used, largely due to the amount of noise using the iPhone imaging method (7 times higher than the flatbed scanner).

15 min Passive Exposure to H₂S

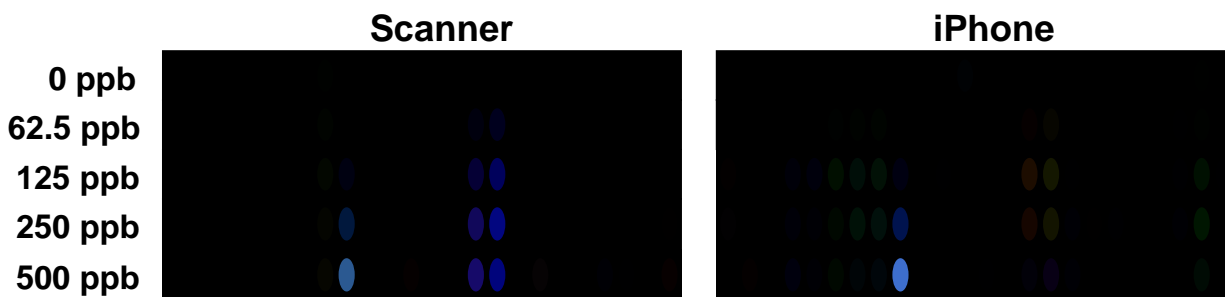


Figure 4.21 Difference maps of arrays exposed to Hydrogen Sulfide after 15 minutes in a passive environment and imaged using **(left)** flatbed scanner and **(right)** an iPhone camera. Color is expanded from 2 to 65 and trials were done in triplicate.

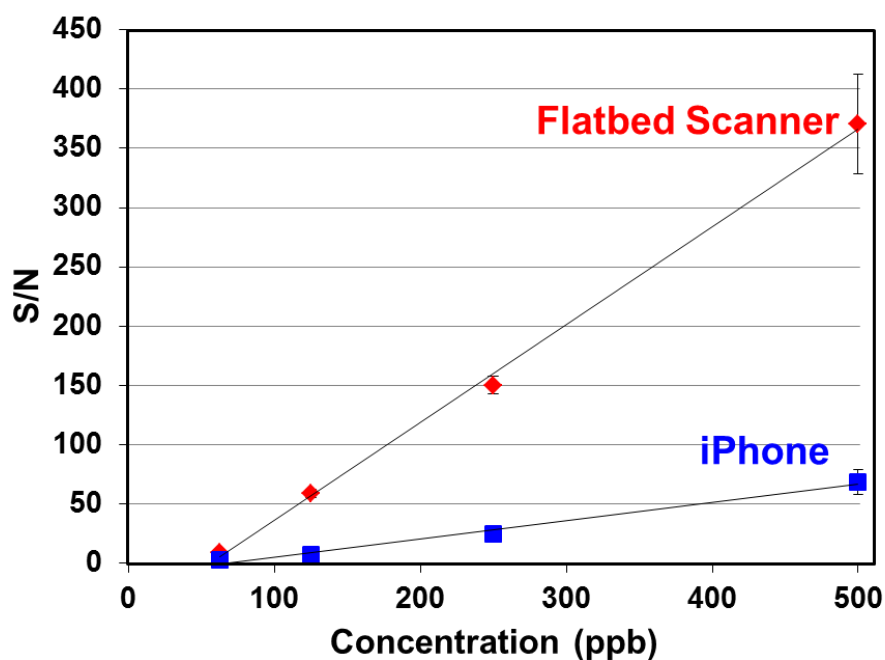


Figure 4.22 Signal to noise ratios from the most responsive spot exposed to Hydrogen Sulfide for fifteen minutes in a passive environment as a function of concentration and imaged using the handheld scanner and iPhone imager. The average value with error bars is set to 2σ from triplicate trials.

4.4.7 Discriminating Power of Colorimetric Sensor array: Active Environment

Images in this study were obtained using the flatbed scanner setup described in **Section 4.4.4.1**. To get an idea of discrimination ability of our array for the main museum pollutants, each array was exposed to a 50% RH analyte stream in filtered air (concentration: 7 ppm for all

analytes except ozone) for 2 minutes. As can be seen from the difference maps (**Figure 4.23**) and HCA (**Figure 4.24**), the response pattern for each of the analytes is unique and we are capable of discriminating between all analytes tested with the exception of acetic acid and SO₂ which are both acidic analytes that target the same sensor spots in this array. This fact is not surprising as we've chosen spots to specifically target each analyte class.

However, if we take this a step further and look at the HCA from array exposure to two similar analytes (ozone and NO₂) we see that NO₂ and ozone cluster separately from each other; with some confusion at higher concentrations (5 and 7 ppm) within each analyte (**Figure 4.25**). There is some confusion at higher concentrations (5 and 7 ppm) likely due to the quick response of these sensor spots in an active environment. As seen in **Figure 4.26**, by reducing the flow rate we are capable of separating between these higher concentrations.

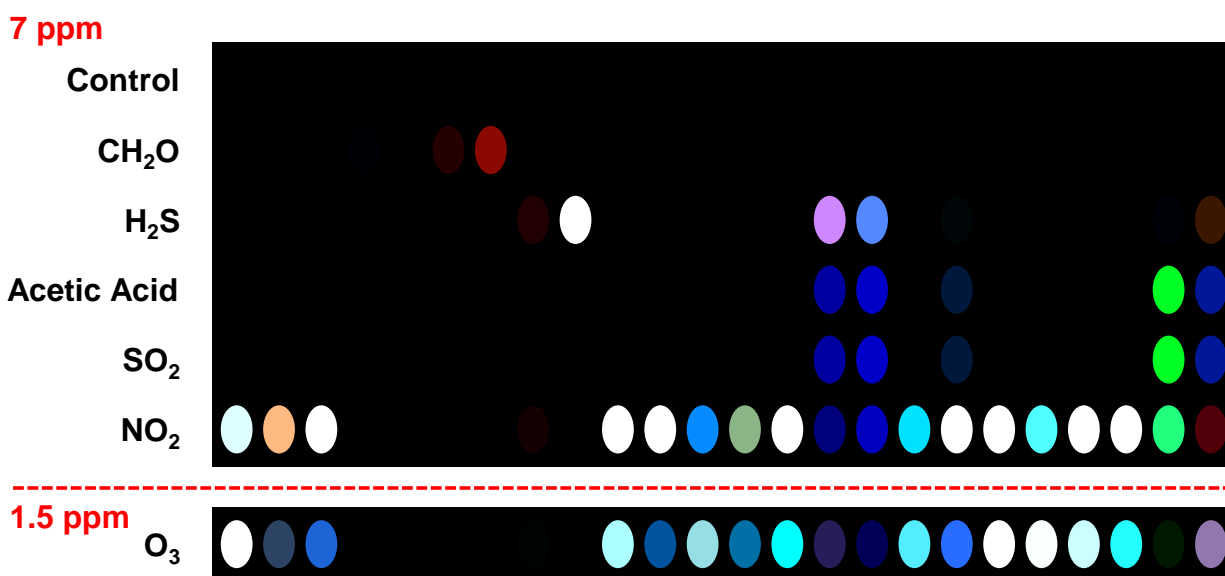


Figure 4.23 Difference maps of arrays exposed to main museum pollutants after 2 minutes in an active environment and imaged using a flatbed scanner. Color is expanded from 4 to 35 and trials were done in triplicate.

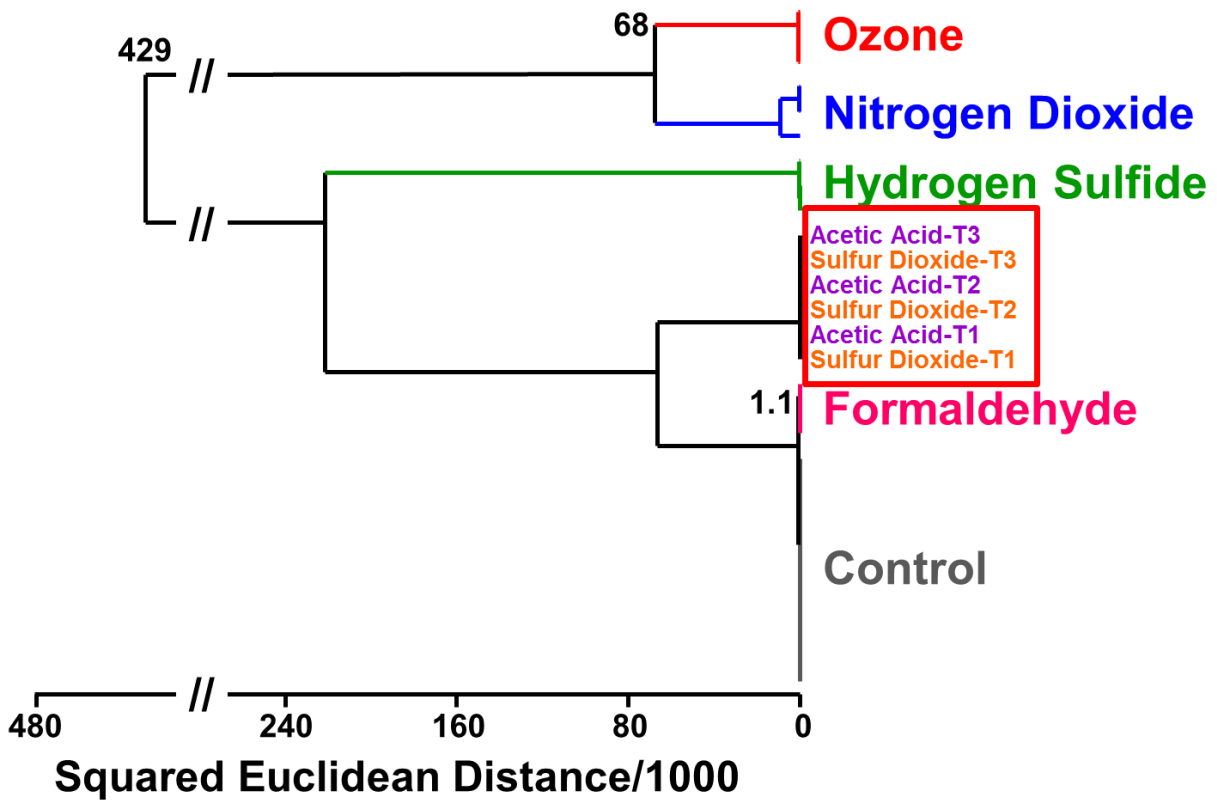


Figure 4.24 HCA dendrogram for main museum pollutants at 7 ppm (all but ozone which was done at 1 ppm). All experiments were run in triplicate and values used were taken after 2 minutes exposure. The red box shows an error in classification between two similar analytes (acetic acid and SO₂).

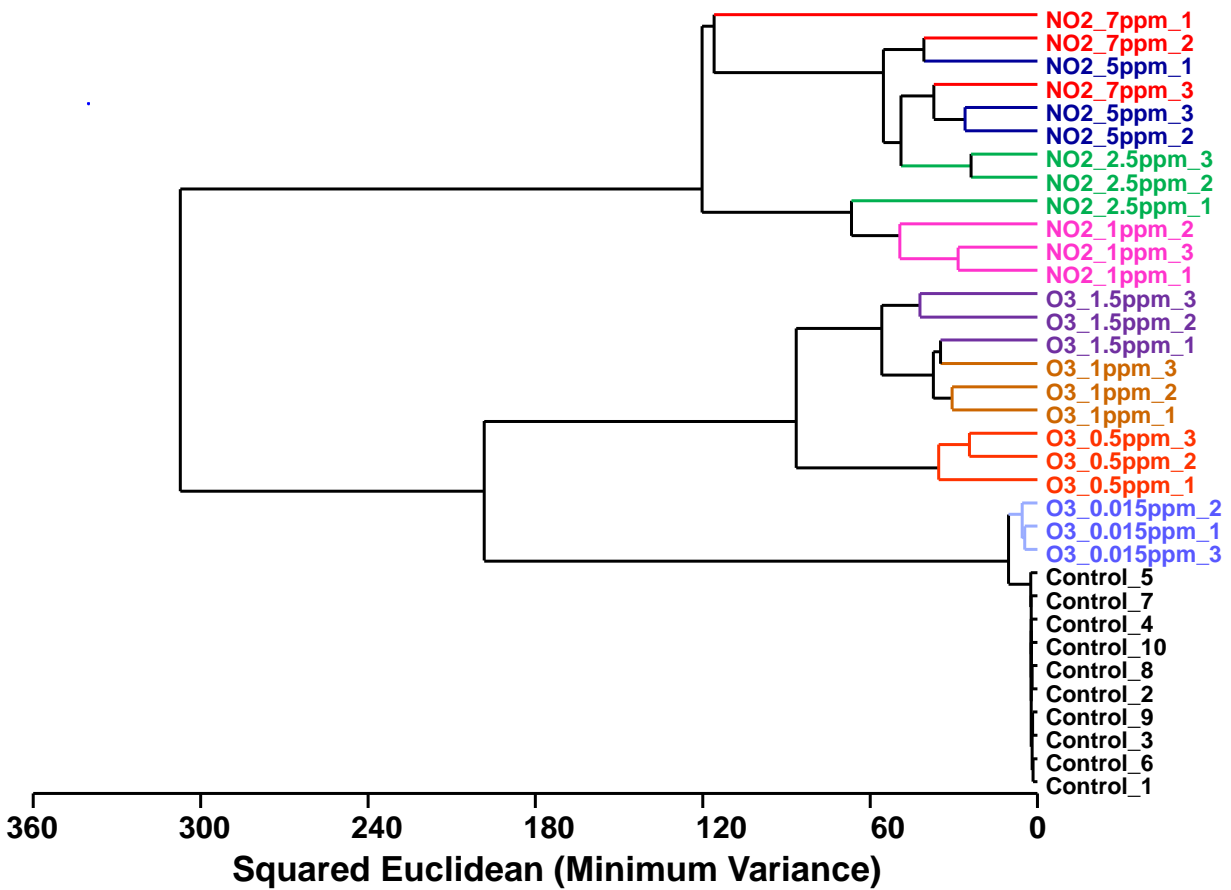


Figure 4.25 HCA dendrogram for two oxidative pollutants (NO₂ and Ozone) at various concentrations. All experiments were run in triplicate and values used were taken after 2 minutes exposure. Misclassifications are evident within each analyte type, particularly in the high concentration regime, likely do to quick response of the oxidant-sensitive sensor spots in an active environment.

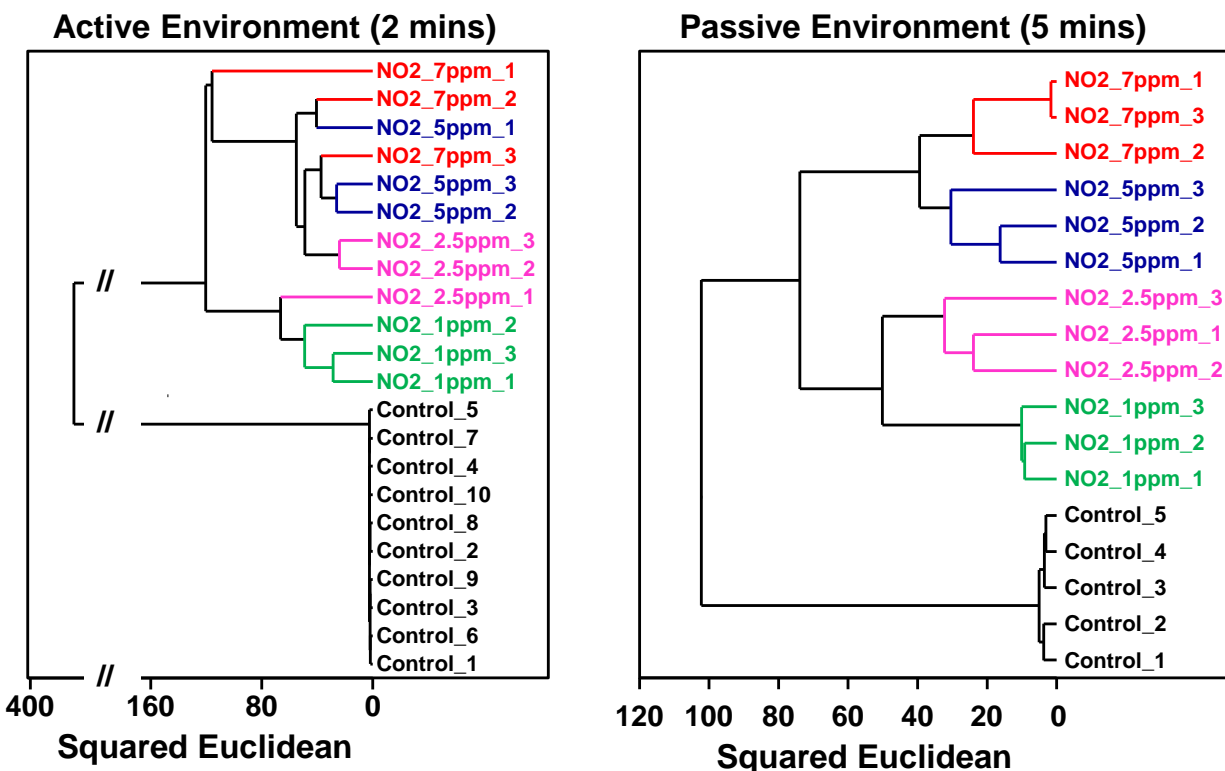


Figure 4.26 HCA dendrogram for array response upon exposure to NO₂ in a (left) active environment and (right) passive environment. All experiments were run in triplicate and values used were taken after 2 minutes exposure for active exposure and 5 minutes for passive exposure. The misclassifications seen with active sampling are completely eliminated with passive sampling.

4.4.8 Determination of Dosimetric Sensitivity and Time-Weighted Average

With cumulative sensors the definition of sensitivity is a function of concentration and exposure time (e.g., expressed in units of ppb*days); gives an idea of the lowest concentration of a given analyte our colorimetric sensor array is capable of measuring in a days sampling time. This metric is determined experimentally. In a passive environment and imaged with a flatbed scanner, arrays were exposed to the target analyte at 0, 62.5, 125, 250, 500, and 1000 ppb in 50% RH filtered air for up to 2 hours. Difference maps representing the unique response of the array to hydrogen sulfide and formaldehyde are shown in **Figure 4.27**. Response profiles for the most responsive spots to hydrogen sulfide and formaldehyde at these concentrations are shown in **Figure 4.28**.

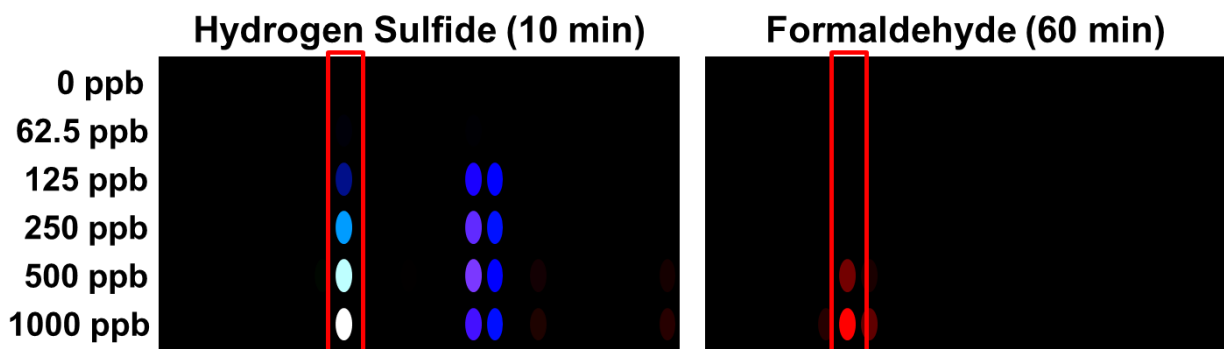


Figure 4.27 Difference maps of arrays exposed to (left) hydrogen sulfide for 10 minutes and (right) formaldehyde for 60 minutes. The longer sampling time for formaldehyde is due to the length of time it takes for the passive environment to reach a steady state at lower concentrations (Figure 4.12). The red boxes indicate the most responsive spots for each analyte that also give a dosimetric response. Color is expanded from 2 to 9 and trials were done in triplicate.

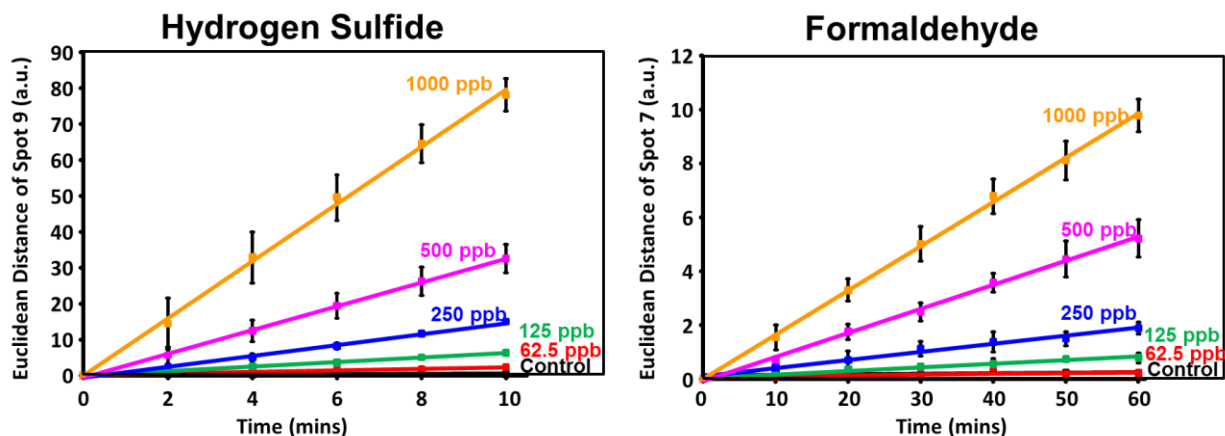


Figure 4.28 Response profiles representing changes in the most responsive spot for (left) hydrogen sulfide and (right) formaldehyde at various concentrations. In each case, a linear dosimetric response is observed. Trials were done in triplicate.

From the data collected in these experiments, the limit of detection can be determined. Limit of detection (LOD) was determined by plotting $LOD = (3 * N * [A]) / S_t$ versus concentration (ppm) where $[A]$ is analyte concentration in ppm and $S_t = S_{2 min} - S_{0 min}$ for ED of most responsive spot. A second order polynomial fit is used to extrapolate where $LOD = [A]$. Dosimetric sensitivity is then determined using the equation below:

$$Dosimetric\ Sensitivity\ (ppb * days) = LOD * \frac{Time\ Exposed\ (mins)}{1440\ mins\ (1\ day)}$$

Processing of the data from these experiments can be taken a step further to produce a calibration curve plotting ED/time (a.u./min) for the most responsive spots versus concentration (ppb) (**Figure 4.29**). The equation from a linear fit of this data is then used to determine a time-weighted average concentration in future real-world experiments (i.e., $\frac{ED}{t_{min}} = m * C_{ppb}$ where m is the slope of the line (ED*min/ppb) and C_{ppb} is the time weighted average concentration).

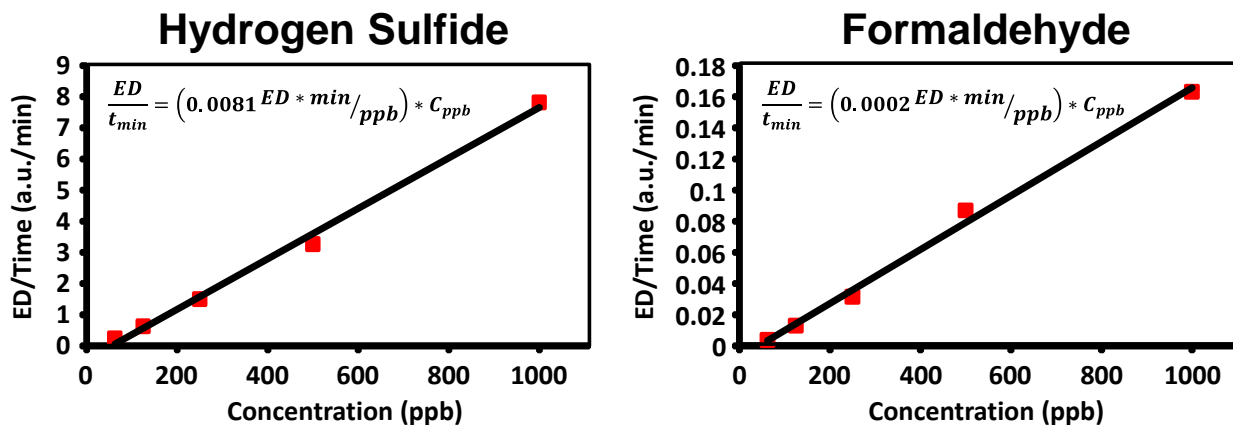


Figure 4.29 Calibration curves plotting ED/time versus concentration for (left) hydrogen sulfide and (right) formaldehyde. The equation on the chart, taken from a linear fit of these points, can then be used to determine the time weighted average concentration based on the response of spots in real world experiments.

Tables 4.3 and 4.4 give the dosimetric sensitivities achieved with our array both in a passive and active environment (scanner imaging method), respectively. In each case, sensor array sensitivities are vastly better than standard Draeger tubes and far less expensive

Table 4.3 Dosimetric sensitivity achieved with the sensor array in a passive environment and compared to long-term passive sampling draeger tubes. Column in red shows the degree of sensitivity increase when using the sensor array over the Draeger tube.

Analyte	Sensor Array	Draeger Tube	Improvement
Hydrogen Sulfide	0.05 ppb*days	0.80 ppb*days	100X
Formaldehyde	0.8 ppb*days	0.4 ppb*days	6X
Nitrogen Dioxide	0.005 ppb*days	0.02 ppb*days	5X
Ozone	0.002 ppb*days	0.1 ppb*days	50X

Table 4.4 Dosimetric sensitivity achieved with the sensor array in an active environment and compared to short term active sampling draeger tubes. Column in red shows the degree of sensitivity increase when using the sensor array over the Draeger tube.

Analyte	Sensor Array	Draeger Tube	Improvement
Hydrogen Sulfide	0.007 ppb*days	0.7 ppb*days	100X
Formaldehyde	0.07 ppb*days	0.4 ppb*days	6X
Nitrogen Dioxide	0.005 ppb*days	0.02 ppb*days	5X
Ozone	0.002 ppb*days	0.1 ppb*days	50X

4.5 Field Testing of 1st Generation Colorimetric Sensor Array

The work below covers a field testing application of our sensor arrays in an ongoing collaboration with Kristen McCormick and her colleagues at the Walt Disney Animation Research Library along with Herant Khanjian and Michael Schilling at the Getty Conservation Institute. Our colorimetric sensor arrays were placed at select locations (i.e., inside and outside of sealed and framed artworks, in sampling boxes placed in galleries, crates storing artwork as they travel from location to location) and used to monitor air quality surrounding artwork as it travelled to Beijing and Shanghai, China as part of an exhibition called “Drawn From Life: The Art of Disney Animation Studios”. More than 300 art objects were displayed at the National

Museum of China in Beijing and then the exhibit was moved to Shanghai before returning to the Walt Disney Animation Research Library in Los Angeles. The sensor arrays were imaged remotely with the digital camera built into an iPhone 4s (**Figure 4.14**) at key points throughout the exhibition (e.g., when mounted to artwork, upon arrival to exhibition sites, upon departure from exhibition sites).

4.5.1 Environments Monitored

4.5.1.1 Passepartout

The method of passepartout mounting, generally used for works on paper, produces a microclimate for the artwork inside a mat package. This packaging is used in an attempt to protect artwork from ambient pollutants present in atmosphere surrounding works of art. Two of our colorimetric sensor arrays were mounted to the back of the artwork: one inside the transparent polyester back wrapping panel and one outside of the backing (**Figure 4.30**).

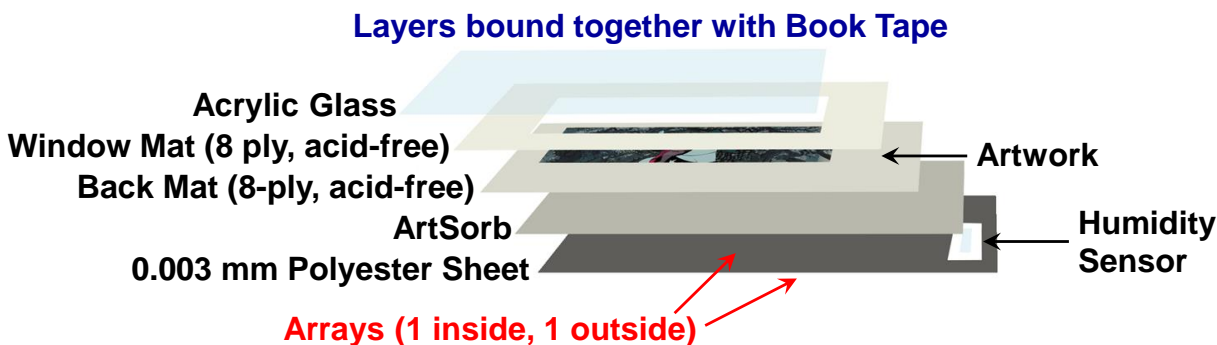


Figure 4.30 Contents of passepartout packaging and positioning of the arrays on the back panel.

It was quickly realized during controls conducted at the University of Illinois that one of the materials used in the construction of the passepartout was off-gassing a sulfide contaminant. To determine which passepartout material(s) were responsible for the sulfide emission, the cellphone setup and sensing platform was used to image arrays exposed to the passepartout materials in a passive environment. Array exposure to the materials was done by first imaging the array, then placing the array in a small polyethylene bag (4 mil) with the material of interest, heat sealing the bag under nitrogen and then imaging again 8 days later. The response of the

array to the various materials is shown in the **Figure 4.31**. In addition to the passepartout materials we also tested the material used to make the card used as a gray reference in the first generation sensing platform.

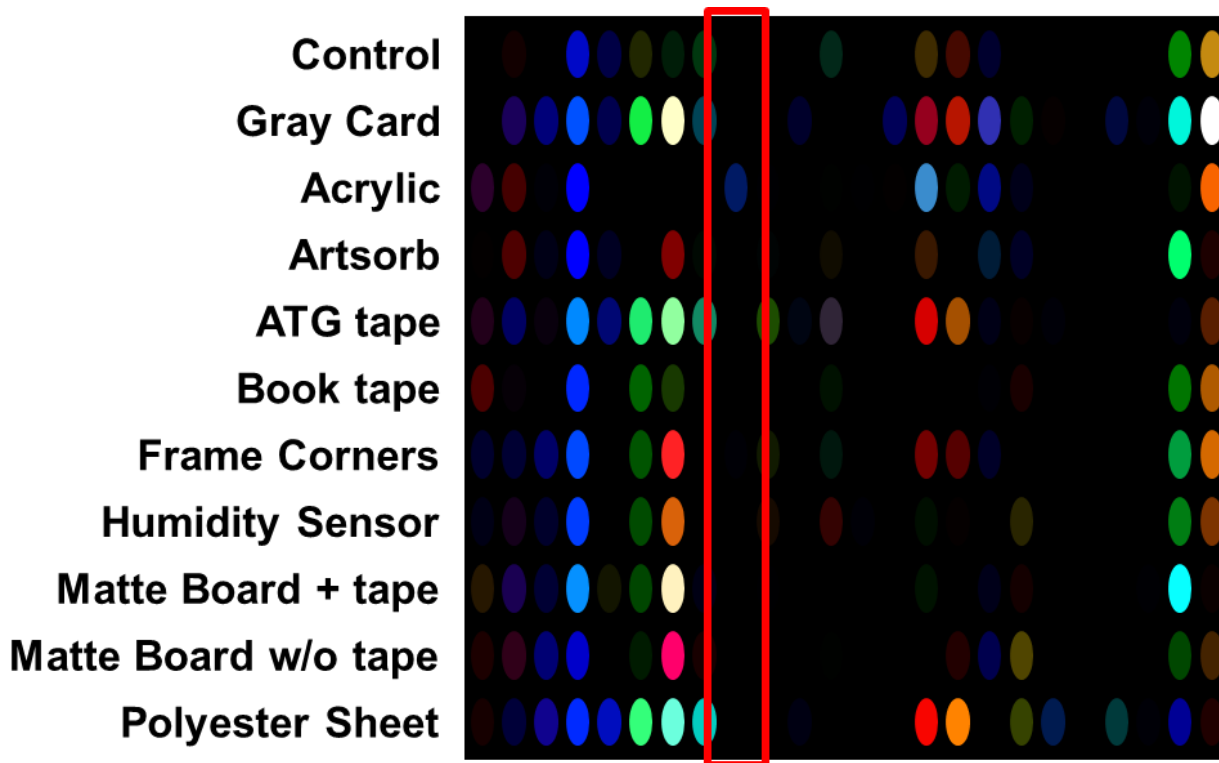


Figure 4.31 Difference maps showing array response to different materials in passepartout packaging after 8 days of exposure. Red box shows the position of the sulfide-sensitive lead(II) acetate spot. Only the Acrylic glass (Acrylite OP3 plex) causes the sulfide-sensitive spot to change color. Difference maps were expanded from 2 to 9 and trials were done in triplicate.

Using the equations obtained from the calibration plots described in **Section 4.4.8**, the time-weighted average concentration of sulfides off-gassing from each material over the 8 day exposure period was determined (**Figure 4.32**). From **Figure 4.32** it is clear that the acrylic glass (Acrylite OP3 plex) is the source of the sulfides (roughly 200 ± 80 ppb*days).

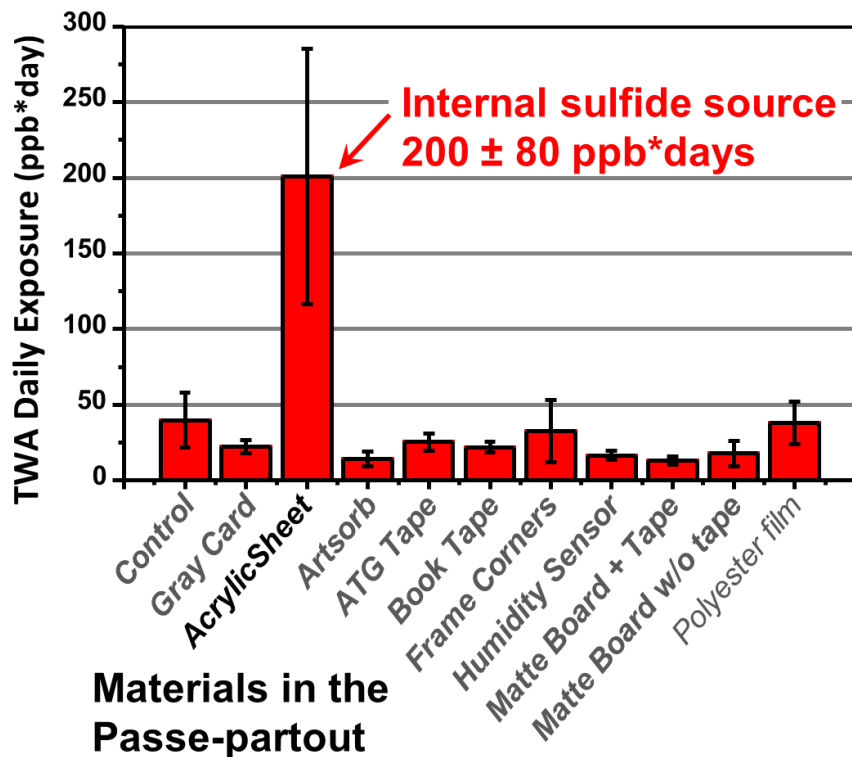


Figure 4.32 Time-weighted average concentration of sulfide calculated from array response to materials in the passepartout packaging; dosage (ppb*days) normalized to eight day exposure period. The acrylic sheet is the only material that shows significant off-gassing of sulfides (200 ± 80 ppb*days).

4.5.1.2 Artwork

Table 4.5 gives an outline of the pieces monitored with our arrays including their piece identifier number, a description of the composition of each piece of art and the crate number it was travelling in.

Table 4.5 Outline of pieces with arrays attached for monitoring including a description of composition and crate number each piece travelled in.

Piece Identifier	Movie Title	Description	Crate #
Exhibition #DFL.01.038	Boat Builders	reproduction (2015) cel: cellulose acetate and paints (cel layer); print on paper (background painting)	3
Exhibition #DFL.01.060	Jungle Book	original (1967) animation drawing: pen on paper	3
Exhibition #DFL.04.247	Snow White and the Seven Dwarfs	original (1937) animation drawing: graphite and colored pencil on paper	13
Exhibition #DFL.04.252	Lady and the Tramp	reproduction (2015) cel: cellulose acetate and paints (cel layer); print on paper (background painting)	13
Exhibition #DFL.01.313	Steamboat Willie	reproduction (2015) cel: cellulose acetate and paints (cel layer); print on paper (background painting)	1
Exhibition #DFL.04.266	Lady and the Tramp	original (1955) animation drawing: conte crayon on paper	12
Exhibition #DFL.04.253	Lady and the Tramp	original (1955) cel: charcoal on cellulose acetate (cel layer); background board (background layer)	12
Exhibition #DFL.04.244	Snow White and the Seven Dwarfs	reproduction (2013) cel: cellulose acetate and paints (cel layer); print on paper (background painting)	13

4.5.1.3 Crates

Our arrays were also mounted to the inside of crates (made from AC grade Plywood and heat treated, kiln dried #2 grade pine with Tyvek liner) used to transport the artwork from place to place. The crates chosen for monitoring were those used to ship the art pieces that were also monitored using our attached arrays. Difference maps, representative of array exposure during the 19-21 day trip from LA to Beijing, for the arrays mounted to the crates and to the outside of artwork passepartout travelling within each crate are shown in **Figure 4.33**. To deconvolute changes in the array due to spot aging from changes that occur due to pollutant exposure, a difference of differences was taken ($\Delta RGB_{Travelling\ Arrays} - \Delta RGB_{UIUC\ Control\ in\ Air}$) by subtracting out array response at the same timepoint as the travelling arrays in a controlled 50% RH filtered air environment obtained during experiments conducted at the University of Illinois. For these “UIUC Control in Air” experiments, three arrays were placed in a Ziploc bag filled with 7.8 L 50% RH filtered air. These arrays were printed in the same batch and aged the same amount of time as the travelling arrays. The control arrays were imaged about once a week where the air inside the bag would then be refilled with a fresh filtered air environment.

To get an idea of pollutant exposure the response of the sulfide, aldehyde and oxidant sensitive spots (**Figure 4.34**) was then converted to concentration values (ppb*days) using methods described in **Section 4.4.8**. Sulfide exposure of arrays mounted to the artwork is consistently higher than those mounted to the crates. This is likely due to the fact that these arrays are in closest proximity to the source of sulfide emission (the acrylic glass used in the passepartout). In contrast, aldehyde exposure is (with the exception of one instance) consistently higher with the crate arrays. This is potentially due to the fact that wood is a known source of formaldehyde emission and the close proximity of the crate arrays to the crate material could be the reason aldehyde exposure is measured at a higher concentration. Oxidant exposure appears to be similar between the crate arrays and the artwork arrays which we can hypothesize is due to the fact that the oxidant source comes from outside the crates. These findings are further summarized in **Figure 4.35**.

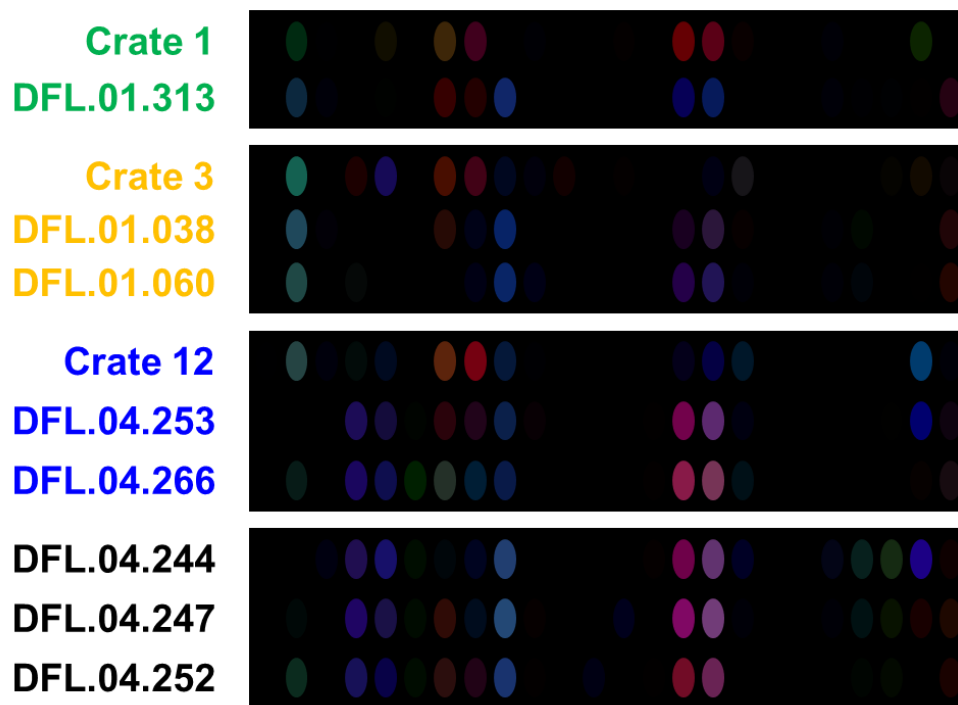


Figure 4.33 Difference maps representing response of arrays mounted on crates and on the outside of the passepartout during their travels from LA to Beijing (over a 19-21 day period). Difference maps were expanded from 2 to 65. Response of each spot is shown as a difference of differences ($\Delta RGB_{Travelling Arrays} - \Delta RGB_{UIUC Control in Air}$).

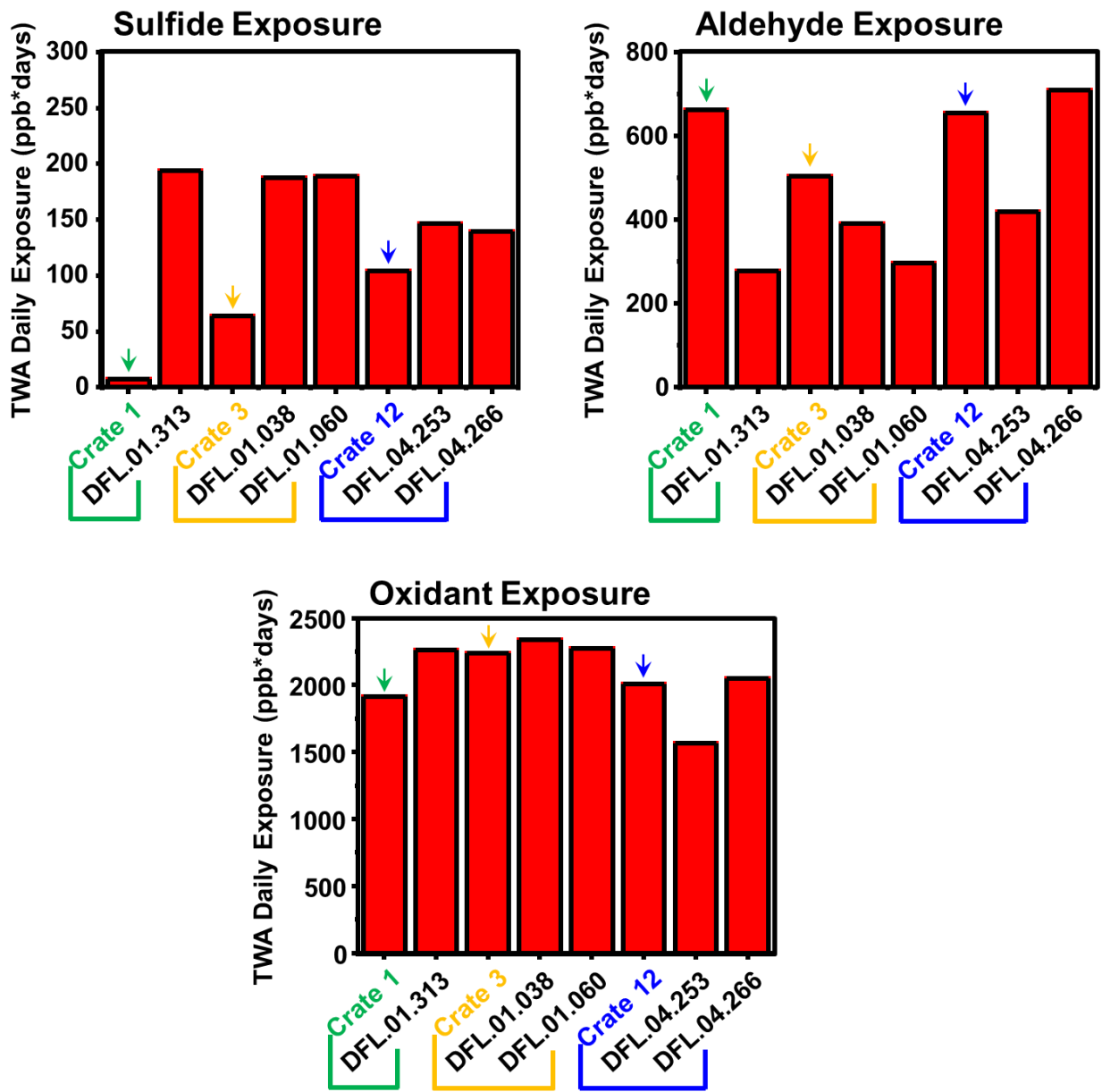


Figure 4.34 (top-left) Sulfide exposure, (top-right) aldehyde-exposure and (bottom) oxidant exposure in ppb*days of arrays mounted to crates (AC grade plywood, heat treated, kiln dried #2 grad pine with Tyvek liner) and arrays mounted to the outside of artwork passepartouts during the 19-21 day trip from LA to Beijing. Dosage (ppb*days) normalized to 19-21 day exposure period from the time sensors were mounted to arrival in Beijing.

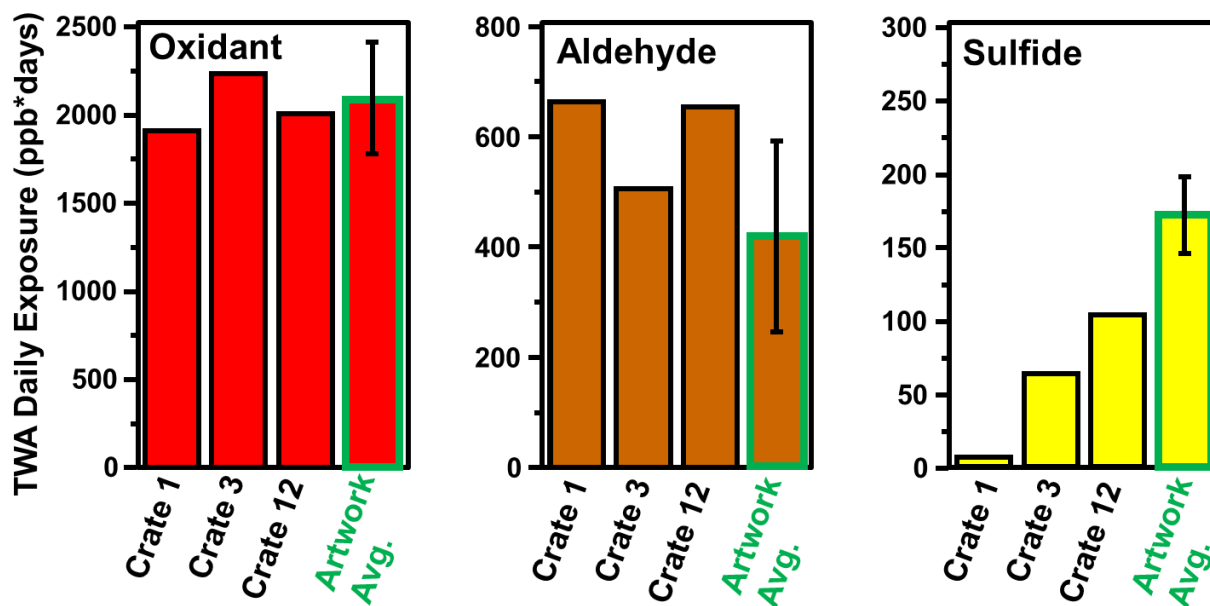


Figure 4.35 (left) Oxidant, (middle) aldehyde and (right) sulfide exposure of individual arrays mounted to crates (AC grade plywood, heat treated, kiln dried #2 grad pine with Tyvek liner) and average response of arrays mounted to the outside of passepartouts within the monitored crates. Dosage (ppb*days) normalized to 19-21 day exposure period from the time sensors were mounted to arrival in Beijing.

4.5.1.4 Gallery Boxes

Custom made gallery boxes were fabricated for array monitoring of select environments in two locations in the exhibition gallery. These boxes were specifically designed to promote air flow to the array surface while minimizing light exposure (**Figure 4.36**).

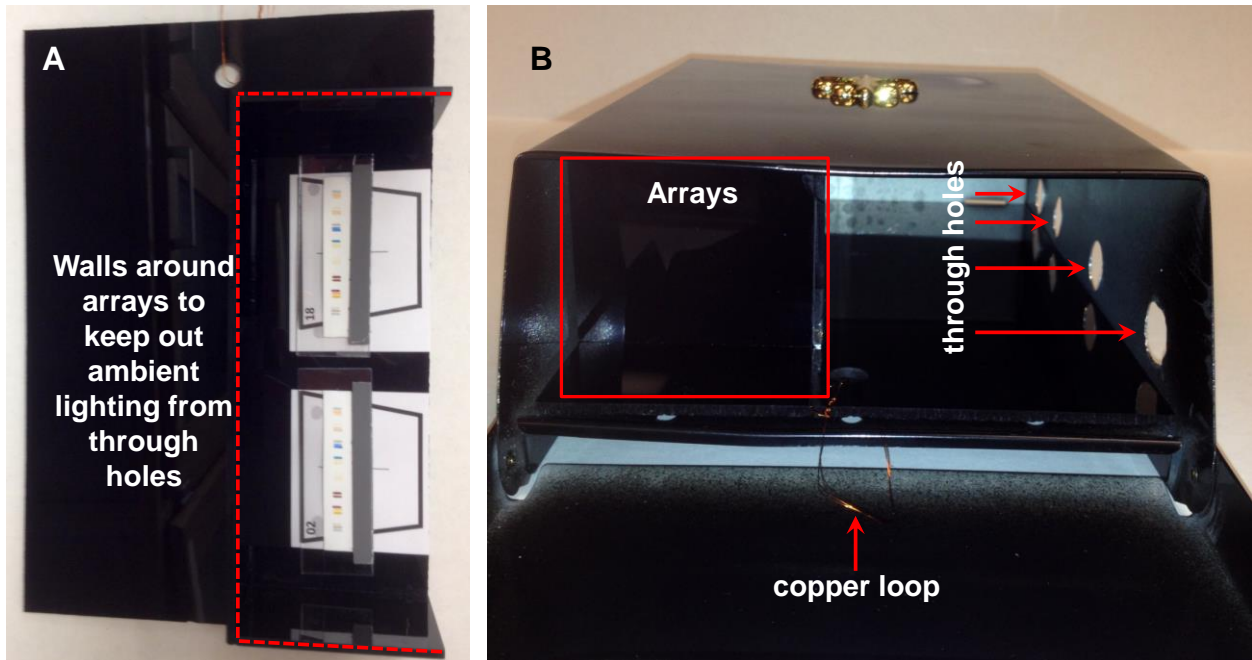


Figure 4.36 Photographs of gallery boxes placed discretely around the exhibition gallery. (a) Platform for mounting the arrays and (b) inside view of the gallery box with array mount inserted. Through holes were machined out of the side of the box to promote air flow to the sensor spots.

4.5.2 Beijing Exhibition

Figure 4.37 gives a floor plan showing placement of art pieces and gallery boxes around the Beijing gallery space. Also shown is the name of the piece, a number used as an identifier for each piece (DFL.##.###), the date each piece was produced and the materials used in each piece.

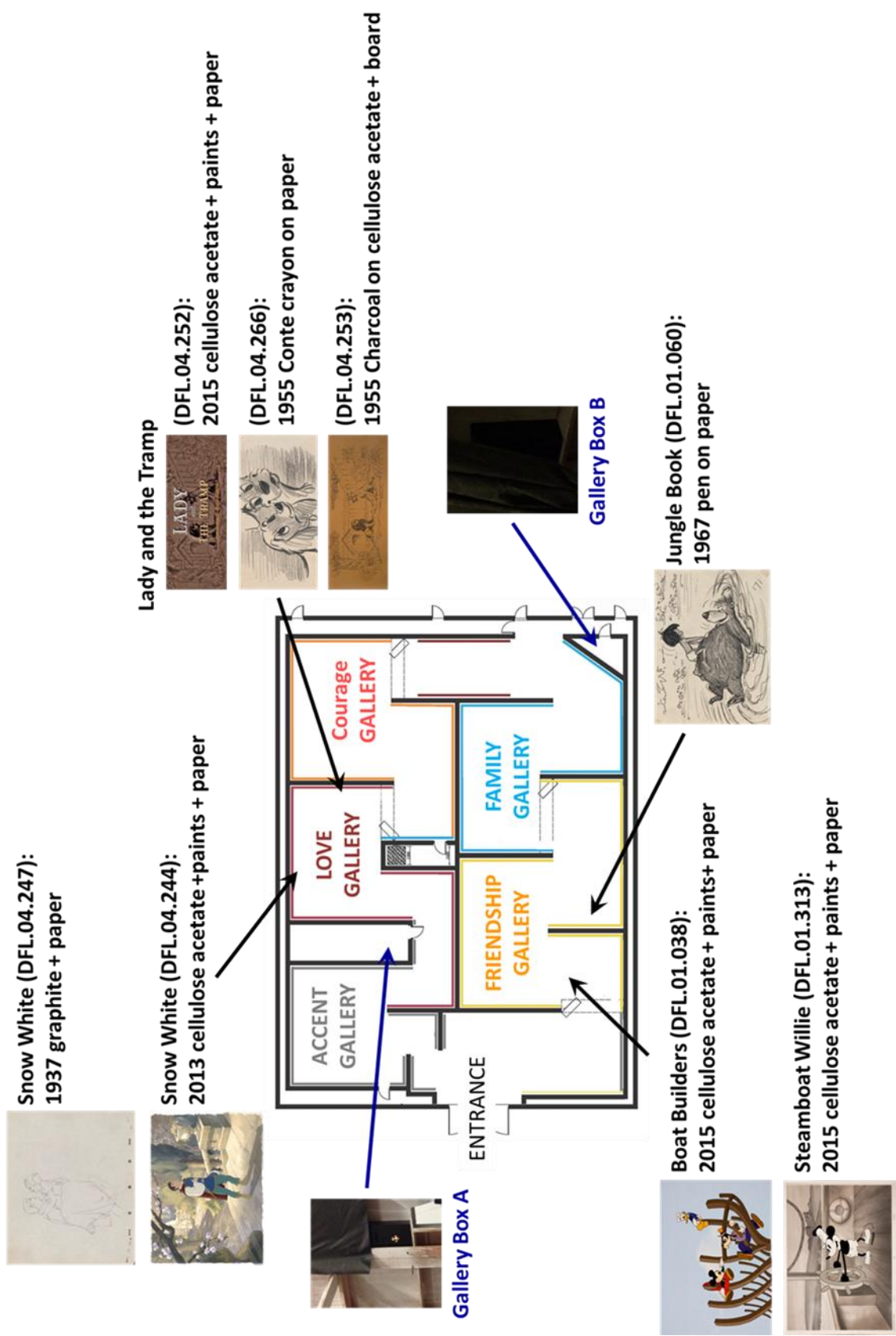


Figure 4.37 Floorplan with locations of artwork and gallery boxes within the Beijing exhibition space, the name of the piece, a number used as an identifier for each piece (DFL.##.###), the date each piece was produced and the materials used in each piece. © Disney

In comparing the magnitude of color change from arrays mounted on the inside of the passepartout versus the outside of the passepartout it is clear that the passepartout material is very effective in keeping pollutants from the ambient atmosphere from interacting with the art pieces (**Figure 4.38**).

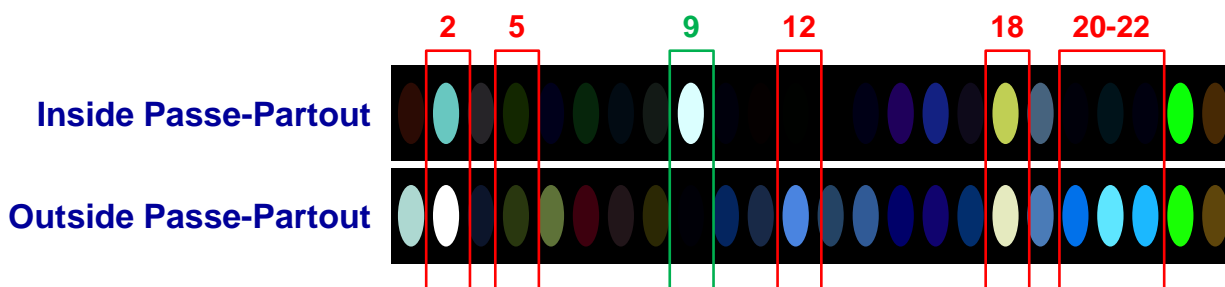


Figure 4.38 Difference maps for arrays mounted on the (top) inside and (bottom) outside of a passepartout which encased an animation drawing. Array response is representative of exposure to the environment in the Beijing gallery over a 77 day period (from when the array was mounted in LA to the end of the Beijing Exhibition). We see multiple spot responses that are much greater (shown in red) for the sensor array outside of the passepartout than for the sensor inside (#2, 5, 12, 18, 20-22). The reverse is true (shown in green) for the sulfide sensitive spot (#9).

Figure 4.39 shows the response of spots sensitive to each class of pollutants from the date the arrays were mounted in LA to their arrival at the Beijing Exhibition up to the conclusion of the exhibition. Consistent with our previously stated results, the environment inside the passepartout has a higher sulfide level than the outside environment. This is likely due to the buildup of sulfides emitted from the acrylic glass within the closed microenvironment inside the passepartout packaging. The lower response of the oxidant and acid-sensitive spots however does support the effectiveness of the passepartout packaging at preventing these pollutants in the gallery space from coming into contact with the art pieces. Aldehyde response appears to be similar between arrays mounted to the outside and inside of the passepartout packaging thus indicating that the presence of aldehydes in these environments is not significant.

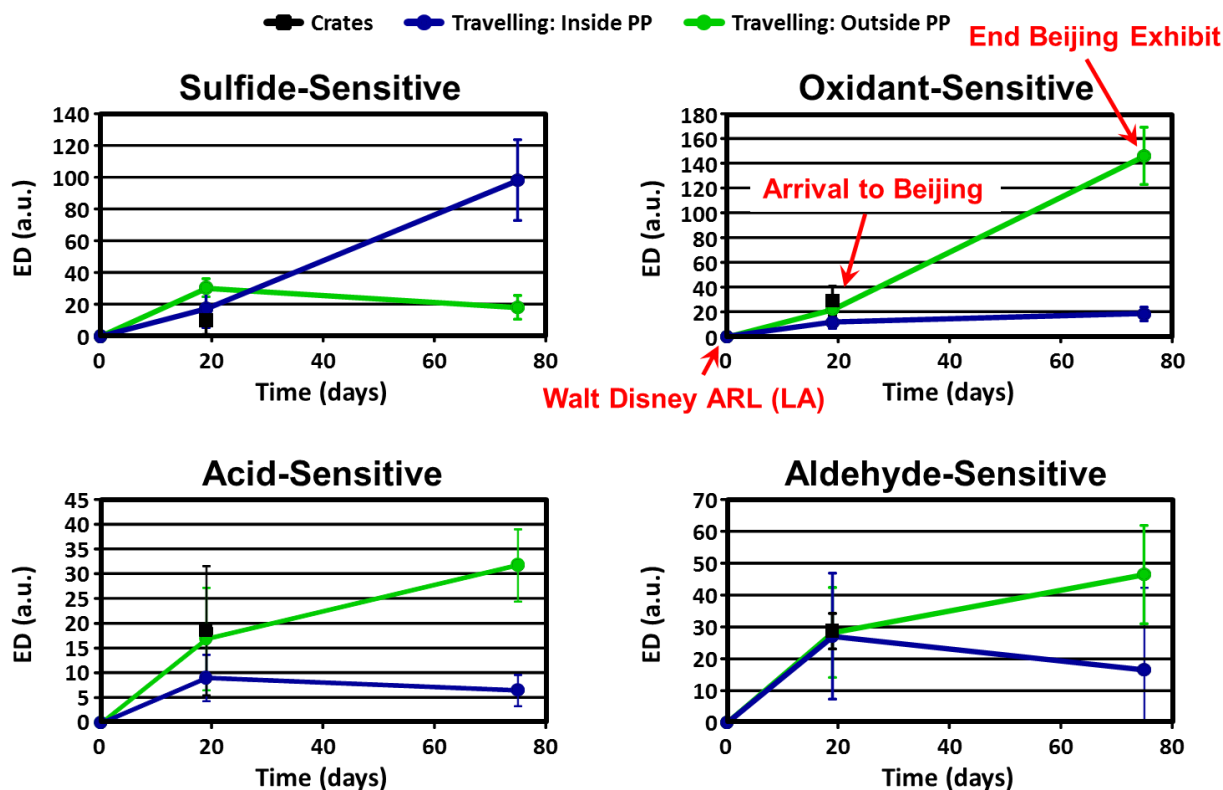


Figure 4.39 Response profiles (ED vs. time) for (top-left) sulfide, (top-right) oxidant, (bottom-left) acid and (bottom-right) aldehyde sensitive spots from arrays mounted on the crates and the inside and outside of the passepartout packaging. Data was obtained from images taken when arrays were mounted at the Walt Disney ARL in LA, upon arrival to the Beijing Exhibition and at the End of the Beijing Exhibition.

The euclidean distance values from **Figure 4.39** were then used to determine time weighted daily exposure (ppb*days) during the trip to Beijing (daily exposure calculated from 19-21 day exposure period) and over the course of the Beijing Exhibition (daily exposure calculated from 52-57 day exposure period).

Daily exposure to sulfides (**Figure 4.40**) for arrays mounted to the outside of the passepartout is greater in the trip to Beijing than over the course of the Beijing Exhibition. This is likely due to the fact that the crate acts as small microenvironment where sulfide emission from the Acrylic glass is allowed to build up during the time the art pieces are stored within the crates. The effect of moving the pieces to the larger gallery environment can be seen in the decrease in daily exposure values for the outside arrays from 200 ppb*days in the crates versus 25 ppb*days over the course of the Beijing Exhibition. All other values are as expected, considering the source of sulfide emission comes from the passepartout materials so it makes sense that the Gallery boxes see a negligible amount of sulfide.

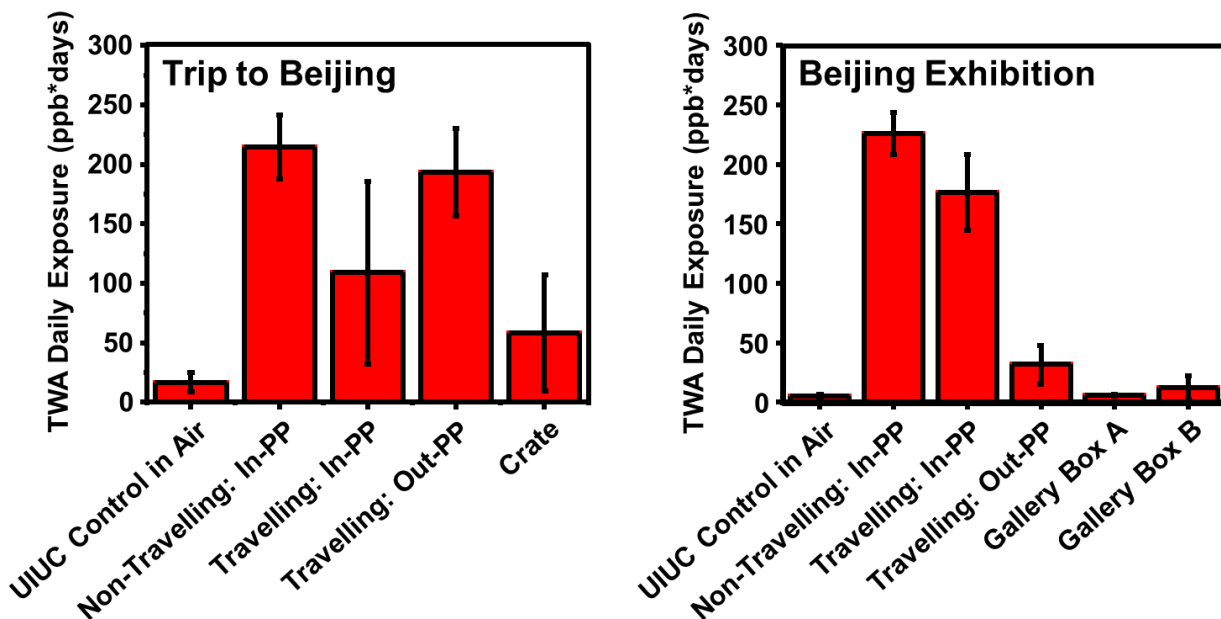


Figure 4.40 Sulfide exposure, in time-weighted average daily exposure (ppb*days), during the (left) trip to Beijing and (right) Beijing Exhibition for each of the environments monitored. Dosage (ppb*days) normalized to 19-21 day exposure period from the time sensors were mounted to arrival in Beijing for “Trip to Beijing” data and 52-57 day exposure period from arrival to and departure from Beijing for “Beijing Exhibition” data. **In-PP**: arrays mounted to the inside passé-partout, **Out-PP**: arrays mounted to the outside of the passé-partout.

In taking our analysis of sulfide exposure a step further, we found that arrays mounted on the inside of a passepartout encasing a cellulose acetate cel (whether it was a reproduction or an original) were exposed to a lower average daily dosage of sulfide than arrays inside a passepartout encasing an animation drawing (**Table 4.6**). The pieces with the green designation are those that are paper based drawings (i.e., graphite on paper, conte crayon on paper, pen on paper) and those with the red designation are those printed on cellulose acetate cels. One possible explanation is that the cellulose acetate material is absorbing some of this sulfide and doing so more effectively than the paper drawings.

Table 4.6 Time weighted average (TWA) concentration of sulfide environment inside passepartout containing (**red**) cellulose acetate cels and (**green**) animation drawings.

Piece Identifier	TWA Concentration (ppb*days)
DFL.01.038	80
DFL.04.244	100
DFL.04.252	80
DFL.04.253	80
DFL.01.060	150
DFL.04.247	120
DFL.04.266	150

Daily exposure to aldehydes (**Figure 4.41**) seems to be statistically similar in each environment. As discussed in **Section 4.5.1.3**, with one exception, the crate arrays were exposed to a higher daily concentration of aldehydes in the trip to Beijing than those mounted to the art pieces possibly due to the close proximity to the wood materials used to make each crate. In comparing daily exposure during the trip to Beijing versus exposure during the Beijing Exhibition, while daily exposure to aldehydes appears to be higher during the trip to Beijing, it is unclear how much of this response is due to a higher concentration of aldehyde in the crate environment and how much is due to aging of the aldehyde-sensitive spots; the UIUC control arrays yield a ~200 ppb*days daily exposure response.

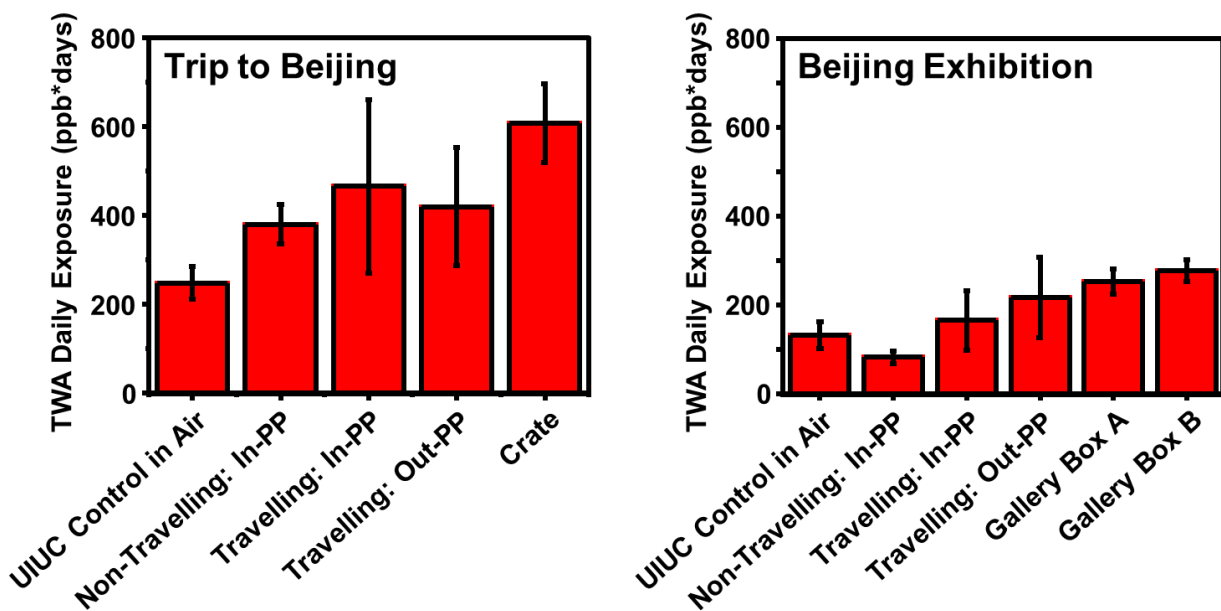


Figure 4.41 Aldehyde exposure, in time-weighted average daily exposure (ppb*days), during the **(left)** trip to Beijing and **(right)** Beijing Exhibition for each of the environments monitored. Dosage (ppb*days) normalized to 19-21 day exposure period from the time sensors were mounted to arrival in Beijing for “Trip to Beijing” data and 52-57 day exposure period from arrival to and departure from Beijing for “Beijing Exhibition” data. **In-PP**: arrays mounted to the inside passé-partout, **Out-PP**: arrays mounted to the outside of the passé-partout.

Daily exposure to oxidants (**Figure 4.42**) during the trip to Beijing is likely a false positive response due to aging of the oxidant-sensor spots as the UIUC control arrays give a similar response. The difference between oxidant exposure of the arrays mounted to the outside of the passepartout over the course of the Beijing exhibition does appear to be statistically significant. This reaffirms that the passepartout is effective in preventing oxidants from the environment outside the passepartout from building up within the passepartout. While it is surprising that the gallery boxes due not yield a similar response to the outer passepartout arrays, upon examining images of the placement of the gallery boxes within the Beijing gallery space the validity of the exposure measurements taken from these arrays is called into question because the through holes machined into the side of the gallery box (see **Figure 4.35**) were mistakenly pushed up against a wall, thus preventing proper ventilation.

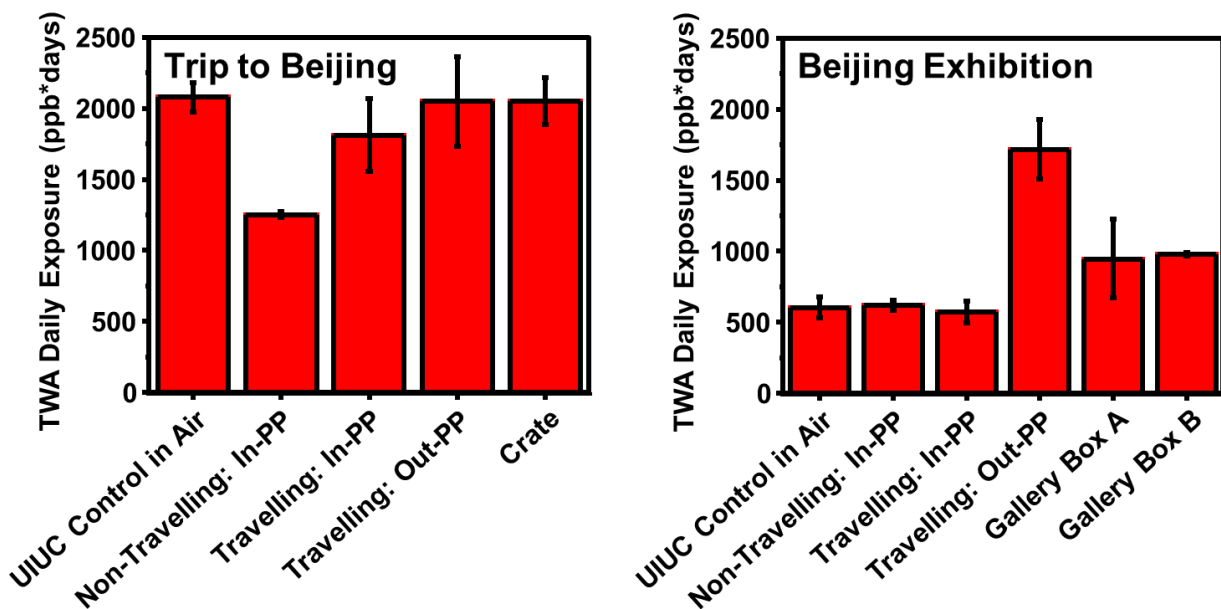


Figure 4.42 Oxidant exposure, in time-weighted average daily exposure (ppb*days), during the (left) trip to Beijing and (right) Beijing Exhibition for each of the environments monitored. Dosage (ppb*days) normalized to 19-21 day exposure period from the time sensors were mounted to arrival in Beijing for “Trip to Beijing” data and 52-57 day exposure period from arrival to and departure from Beijing for “Beijing Exhibition” data. **In-PP**: arrays mounted to the inside passé-partout, **Out-PP**: arrays mounted to the outside of the passepartout.

4.6 Conclusions and Outlook

A colorimetric sensor array of cumulative (dosimetric) sensors has been developed. A system for exposing these arrays in both an active and passive environment has been used to determine dosimetric sensitivity and provide calibrations for calculating time-weighted average concentrations of pollutants in the museum environment. A new imaging method and sensing platform that relies on an iPhone 4S digital camera has been created for periodic remote imaging of colorimetric sensor arrays and has proven acceptable for field use. Using this array and imaging set-up, we were able to calculate time-weighted average daily exposure (in ppb*days) to sulfides, oxidants and aldehydes in a variety of environments to monitor factors that influence the composition of the environment surrounding these valuable pieces of art. We also were able to determine the effectiveness of the passepartout packaging in protecting artwork from these harmful pollutants as well as determine the source of emission of sulfides from the passepartout materials themselves.

Future plans include, making alterations to the 1st generation array (e.g., developing additional sensing spots specifically for targeting acids), testing the effect of interferences on array response and taking the necessary steps to further automate this process to make it more accessible to museum professionals.

4.7 References

1. Feng, L.; Musto, C. J.; Kemling, J. W.; Lim, S. H.; Zhong, W.; Suslick, K. S., Colorimetric sensor array for determination and identification of toxic industrial chemicals. *Analytical chemistry* **2010**, 82 (22), 9433-9440.
2. Askim, J. R.; Li, Z.; LaGasse, M. K.; Rankin, J. M.; Suslick, K. S., An optoelectronic nose for identification of explosives. *Chemical Science* **2016**, 7 (1), 199-206.
3. Askim, J. R.; Mahmoudi, M.; Suslick, K. S., Optical sensor arrays for chemical sensing: the optoelectronic nose. *Chemical Society Reviews* **2013**, 42 (22), 8649-8682.
4. Lim, S. H.; Feng, L.; Kemling, J. W.; Musto, C. J.; Suslick, K. S., An optoelectronic nose for the detection of toxic gases. *Nature chemistry* **2009**, 1 (7), 562-567.
5. Janzen, M. C.; Ponder, J. B.; Bailey, D. P.; Ingison, C. K.; Suslick, K. S., Colorimetric sensor arrays for volatile organic compounds. *Analytical chemistry* **2006**, 78 (11), 3591-3600.
6. Carey, J. R.; Suslick, K. S.; Hulkower, K. I.; Imlay, J. A.; Imlay, K. R.; Ingison, C. K.; Ponder, J. B.; Sen, A.; Wittrig, A. E., Rapid identification of bacteria with a disposable colorimetric sensing array. *Journal of the American Chemical Society* **2011**, 133 (19), 7571-7576.
7. Zhang, C.; Bailey, D. P.; Suslick, K. S., Colorimetric sensor arrays for the analysis of beers: a feasibility study. *Journal of agricultural and food chemistry* **2006**, 54 (14), 4925-4931.
8. Zhang, C.; Suslick, K. S., Colorimetric sensor array for soft drink analysis. *Journal of agricultural and food chemistry* **2007**, 55 (2), 237-242.
9. Askim, J. R.; Suslick, K. S., Hand-Held Reader for Colorimetric Sensor Arrays. *Analytical chemistry* **2015**, 87 (15), 7810-7816.
10. Kireyko, A.; Veselova, I.; Shekhovtsova, T., Mechanisms of peroxidase oxidation of o-dianisidine, 3, 3', 5, 5'-tetramethylbenzidine, and o-phenylenediamine in the presence of sodium dodecyl sulfate. *Russian Journal of Bioorganic Chemistry* **2006**, 32 (1), 71-77.

11. Pankratov, A. N.; Shchavlev, A. E., Semiempirical quantum chemical PM3 computations and evaluations of redox potentials, basicities, and dipole moments of the diphenylamine series as analytical reagents. *Canadian Journal of Chemistry* **1999**, *77* (12), 2053-2058.
12. Josephy, P. D., Oxidative activation of benzidine and its derivatives by peroxidases. *Environmental health perspectives* **1985**, *64*, 171.
13. Oldfield, L. F.; Bockris, J. O. M., Reversible Oxidation-Reduction Reactions of Aromatic Amines. *The Journal of Physical Chemistry* **1951**, *55* (7), 1255-1274.
14. Alexy, M.; Hanko, M.; Rentmeister, S.; Heinze, J., Disposable optochemical sensor chip for nitrogen dioxide detection based on oxidation of N, N'-diphenyl-1, 4-phenylenediamine. *Sensors and Actuators B: Chemical* **2006**, *114* (2), 916-927.
15. Meskath, S.; Urban, G.; Heinze, J., A new optochemical chlorine gas sensor based on the application of amphiphilic co-networks as matrices. *Sensors and Actuators B: Chemical* **2011**, *151* (2), 327-332.
16. Meskath, S.; Urban, G.; Heinze, J., Nanophase separated amphiphilic polymer co-networks as efficient matrices for optical sensors: Rapid and sensitive detection of NO₂. *Sensors and Actuators B: Chemical* **2013**, *186*, 367-373.
17. Druzik, C. M.; Grosjean, D.; Van Neste, A.; Parmar, S. S., Sampling of Atmospheric Carbonyls with Small DNPH-Coated C18 Cartridges and Liquid Chromatography Analysis with Diode Array Detection. *International Journal of Environmental Analytical Chemistry* **1990**, *38* (4), 495-512.
18. Gibson, L.; Kerr, W.; Nordon, A.; Reglinski, J.; Robertson, C.; Turnbull, L.; Watt, C.; Cheung, A.; Johnstone, W., On-site determination of formaldehyde: A low cost measurement device for museum environments. *Analytica chimica acta* **2008**, *623* (1), 109-116.
19. Robins, J. H.; Abrams, G. D.; Pincock, J. A., The structure of Schiff reagent aldehyde adducts and the mechanism of the Schiff reaction as determined by nuclear magnetic resonance spectroscopy. *Canadian Journal of Chemistry* **1980**, *58* (4), 339-347.
20. Haynes, W. M., *CRC handbook of chemistry and physics*. CRC press: 2014.
21. Craig, P. J.; Bartlett, P. D., The role of hydrogen sulphide in environmental transport of mercury. *Nature* **1978**, *275* (5681), 635-637.
22. Allain, L. R.; Sorasaene, K.; Xue, Z., Doped Thin-Film Sensors via a Sol-Gel Process for High-Acidity Determination. *Analytical chemistry* **1997**, *69* (15), 3076-3080.

23. Koncki, R.; Wolfbeis, O. S., Composite films of Prussian Blue and N-substituted polypyrroles: fabrication and application to optical determination of pH. *Analytical chemistry* **1998**, *70* (13), 2544-2550.
24. Haswell, S., *Practical guide to chemometrics*. CRC Press: 1992.
25. Johnson, R. A.; Wichern, D. W., *Applied multivariate statistical analysis*. Prentice hall Englewood Cliffs, NJ: 1992; Vol. 4.
26. Hair, J. F.; Black, W. C.; Babin, B. J.; Anderson, R. E.; Tatham, R. L., *Multivariate data analysis*. Pearson Prentice Hall Upper Saddle River, NJ: 2006; Vol. 6.